AEDC-TDR-64-105

[redacted]

G.2

BASIC PROCESSES OF ION BEAM TERMINATION

By

J. D. Trolinger, J. I. Shipp, and A. E. Lennert
Experimental Research Group
Office of the Chief Scientist
ARO, Inc.

TECHNICAL DOCUMENTARY REPORT NO. AEDC-TDR-64-105

August 1964

Program Element 62405184/6950, Task 695003

(Prepared under Contract No. AF 40(600)-1000 by ARO, Inc., contract operator of AEDC, Arnold Air Force Station, Tenn.)

ARNOLD ENGINEERING DEVELOPMENT CENTER

AIR FORCE SYSTEMS COMMAND

UNITED STATES AIR FORCE

NOTICES

Qualified requesters may obtain copies of this report from DDC, Cameron Station, Alexandria, Va. Orders will be expedited if placed through the librarian or other staff member designated to request and receive documents from DDC.

When Government drawings, specifications or other data are used for any purpose other than in connection with a definitely related Government procurement operation, the United States Government thereby incurs no responsibility nor any obligation whatsoever; and the fact that the Government may have formulated, furnished, or in any way supplied the said drawings, specifications, or other data, is not to be regarded by implication or otherwise as in any manner licensing the holder or any other person or corporation, or conveying any rights or permission to manufacture, use, or sell any patented invention that may in any way be related thereto.

BASIC PROCESSES OF ION BEAM TERMINATION

By

J. D. Trolinger, J. I. Shipp, and A. E. Lennert

Experimental Research Group

Office of the Chief Scientist

ARO, Inc.

a subsidiary of Sverdrup and Parcel, Inc.

August 1964

ARO Project No. NW2210

AF - AEDC
Arnold AFS Tenn

ABSTRACT

Theoretical and empirical information necessary for the design of an electrical propulsion test facility collector system complex is compiled. Design considerations, which include sputtering, beam accommodation, secondary emission, and less serious secondary effects, are considered in some detail.

A theoretical model is presented which accounts for the energy dependence of the sputtering phenomena first at low ion energies and secondly in the region where the Bohr screening parameter is of the order of unity. Based on these functions obtained from the theoretical model in the two regions, an asymptotic empirical relation for the sputtering ratio as a function of ion energy is found to give a satisfactory account of available data. In addition, equations are developed to evaluate the effects of sputtered particles upon vacuum chamber pressure, the amount of flux leaving the target that returns to the engine, and the time required for the target to become saturated with beam particles. Two different collectors, the solid metallic type and a liquid metal system, are evaluated. The advantages and limitations of each are discussed.

PUBLICATION REVIEW

This report has been reviewed and publication is approved.

Eules L. Hively
Acting Chief, Propulsion Division
DCS/Research

Donald R. Eastman, Jr.
DCS/Research

CONTENTS

TABLES

ILLUSTRATIONS

NOMENCLATURE

A_b	Area of beam (cross sectional)
A_c	Area of chamber
a	Constant
a_h	Bohr radius
a_s	Bohr screening constant
a_t	Accommodation coefficient at target
B_A	Flux caused by reflected beam
b	Accommodation coefficient for beam molecule
C, c	Constant
D	Constant
d_{12}	Average diameter of colliding spheres
E	Energy of sputtered particles
$\bar{E}$	Average energy of ion
E_i	Ion energy
E_p	Energy of primary displaced atom
$\bar{E}_p$	Mean energy of primary displaced atom
E_t	Displacement energy for lattice atom
e	Natural logarithm base
e_i	Atomic number of ion times electron charge ($Z_i\epsilon$)
e_t	Atomic number of target times electron charge ($Z_t\epsilon$)
f	Sticking fraction
H	Linearly extrapolated threshold for sputtering, $2\ E_t/\gamma$
I	Ionic current to target
J	Ionic current density
$\bar{K}$	Function of mass ratio of ion and target particles
K	Proportionality constant
k	Collection efficiency
ℓ	Normalizing factor, Eq. (16)

M_e	Mass of electron
M_i	Mass of ion
M_t	Mass of target atom
N	Number of nuclei per unit volume
N_o	Avogadro number
N_{out}	Number of primary displaced atoms that escape from the target
N(x)	Number of primary displaced atoms per unit ion path length
P_b	Pressure contribution attributed to the beam particles
P_d	Net probability of a displacement collision
P_{d1}	Probability for a displacement collision by particles of type one
P_{d2}	Probability for a displacement collision by particles of type two
P_n	Pressure contribution in chamber caused by nth collision
P_s	Pressure contribution attributed to the sputtered particles
p	Distance traveled by displaced atom
Q	Source of efflux
q	Quantity of material collected by a target
q_s	Quantity of material collected by a target at saturation
R	Range of a particle in a medium
R_h	Rydburg energy constant
R_p	Range of primary displaced atom
r	Radial distance
S	Sputtering coefficient (ratio)
$S_A(X)$	Angular distribution function of sputtered particles
S_L	Sputtering coefficient (low energy)
S_{max}	Maximum sputtering coefficient
$S_R(X)$	Functional dependence of sputtering ratios on angle of incidence

S_s	Sputtering coefficient (self-sputtering)
$S(\theta)$	Angular distribution function
s	Accommodation coefficient for sputtered particles
t	Time
u	Potential energy
$\bar{V}$	Average velocity of residual gas particles
V_o	Initial velocity of ions
$\bar{V}_s$	Average velocity of sputtered particles
V(x)	Velocity of ion at a point x in stopping medium
W	Weight increase of target
x	Distance
y	Distance
Z_i	Atomic number of ion
Z_t	Atomic number of target
α	Secondary electron emission coefficient
β	Flux
$\Gamma(n)$	Gamma function of argument n
γ	Energy transfer factor, $\frac{4\ M_i M_t}{(M_i + M_t)^2}$
Δ	Incremental change
ϵ	Electronic change
η	Number of residual gas particles per unit volume
θ	Angle (Fig. 6)
κ	Wave mechanics parameter
Λ	Re-emission rate
λ	Scattering mean free path
μ	Reduced mass
ξ	Screening parameter
ρ	Mass density
σ	Cross section for collision
σ_d	Displacement cross section

χ	Angle of incidence
ψ_b	Angular distribution function of beam particles
ψ_s	Angular distribution function of sputtered particles
$\psi_{1,2}$	Mass dependent functions
Ω	Solid angle
ϕ	Mass flow

1.0 INTRODUCTION

To establish a ground test program for long-term testing of electrical propulsion systems, one of the major problems to be resolved is that of adequate ion beam collection. Although not a problem in flight testing, adequate beam collection is essential in the ground test facility complex to ensure accurate simulation of space (Refs. 1 and 2).

An efficient collector system is required to accommodate any new material and its associated energy introduced into the chamber from the exhaust of an operating electrical propulsion system. Means must also be furnished to isolate the engine proper from any external phenomena foreign to its actual space environment such as sputtering effects caused by beam-target interaction and secondary electron emission. The importance of these depends on (1) the duration of the test, (2) the ion current density, (3) the ion energy, (4) the ion-target material combination, and (5) the degree of space simulation required.

The purpose of this report is to furnish information necessary for the design and evaluation of a collector system complex.

2.0 SUMMARY OF SPUTTERING EXPERIMENTS

2.1 INTRODUCTION

When a target material is placed in the path of a positive ion beam which has been accelerated through a small potential, no erosion effects are observed. As the accelerating voltage is increased, a threshold value is reached and target atoms become dislodged from the surface. The threshold value depends on the target and ion beam combination (Ref. 3). This phenomenon is known as sputtering. The number of target atoms knocked off or eroded per incident ion is defined as a sputtering ratio or yield. In general, the sputtering ratio increases with increasing ion energy up to a maximum value, levels off, and then decreases with a further increase in ion energy. For low molecular weight ion beams, this maximum value occurs at a relatively low energy, and a sharp decrease in sputtering yield is noted immediately after maximum value is obtained (Refs. 4, 5, 6, and 7). With heavier molecular weight ion beams, the maximum value generally occurs at higher energies, remains constant with energy over a much longer range, and finally decreases slowly with increasing ion energy (Ref. 7). Figure 1 is a schematic diagram of a

Manuscript received May 1964.

typical yield curve. Several variables are known to affect the yield curve, such as the residual pressure in the test container, the angle and energy at which the beam material strikes the target surface, and the nature and crystalline structure of the target for a given beam material.

2.2 BACKGROUND PRESSURE VERSUS YIELD

Several authors have investigated the effect of residual gas pressure on the sputtering yield (Refs. 8, 9, and 10). It is generally concluded that at relatively high pressures the sputtering ratio is smaller than at lower pressures. For a given current density, the sputtering ratio increases with decreasing pressure and finally reaches a constant value (Fig. 2). Wehner has explained this in terms of contamination of the target surface by the residual gas (Ref. 8). According to Wehner's argument, this pressure dependency would be observed at much lower pressures than is shown in Fig. 2 if the rate of surface contamination by the residual chamber gases were comparable to the rate of surface erosion by the impinging ions. The condition for the sputtering yield to be independent of the chamber pressure can therefore be written

$$\frac{1}{4}\,\eta\,\bar{V}\,f << \frac{SJ}{\epsilon}$$

Yonts noted a pressure dependency at 5×10^{-5} torr (Ref. 10), using a current density of only 0.1 ma/cm^2. Figures 2 and 3 are experimentally determined curves showing yield versus pressure and current density, respectively. These observations coupled with Yont's findings seem to substantiate Wehner's contamination hypothesis. Also, it should be noted that back diffusion of the sputtered particles plays an important role in reducing the number of sputtered particles when the mean free path of the residual gas is much smaller than container dimensions.

2.3 CRYSTALLINE STRUCTURE OF TARGET

The crystalline structure of the target has been found to have an important role in the sputtering process. Rol and his colleagues under Kistemaker studied the sputtering rate of single copper crystals by 20-kev argon ion bombardment (Ref. 11). At normal incidence and a current density of 0.5 ma/cm^2, they found the yield of 6.4 for polycrystalline copper, 8.2 for a (111) copper surface, and 4 atoms/ion for a (100) copper surface. Yields for the single crystal samples as a function of the angle of incidence were found to show maximum and minimum points.

These peaks indicate that sputtering yields have maximum values in the direction in which the beam "sees" a large density of projected lattice points and a minimum where the crystal shows the highest transparency. Although the study of single crystal sputtering offers a greater insight to basic collision phenomena, the present work is concerned only with polycrystalline targets.

2.4 THE STATE OF SPUTTERED PARTICLES

In addition to the rate of production of free particles by the sputtering process, it is desirable to know the state, energy, and angular distribution of these particles so that the appropriate steps may be taken to accommodate all material added to the system.

A number of investigations have substantiated the fact that sputtered particles are individual atoms which are largely neutral, some being in a metastable state. One of the more recent and more comprehensive of these studies, made by Fogel (Ref. 12), found that the positive ion sputtering coefficient rises with incident ion energy until it reaches a narrow maximum in the neighborhood of 20 to 30 kev and then decreases. For the particular cases which he considered (noble gases colliding with molybdenum), the value of the positive ion coefficient never rose above 0.01 percent in the energy range up to about 50 kev. No detection of negative ions of the target species was reported by any of the authors reviewed. For every case considered here, over 95 percent of the sputtered particles were neutral atoms.

2.5 EFFECT OF IMPACT ANGLE

The effect of the angle of impact of a beam with the target material is another item of importance in facility design. The following two basic aspects are to be considered on oblique incidence of the beam with the target:

1. The sputtering ratio increases with increasing angle from the target normal for practically all materials until a critical value is obtained where a decrease in intensity becomes noticeable (Figs. 4a through c). Figures 4d through f indicate a similar trend; however, the experiments were not carried out throughout the entire range to indicate a critical maximum value, and subsequent decrease, in intensity.

   Wehner observed for low energies that materials exhibiting low normal sputtering ratios, such as scandium, titanium, and vanadium, exhibit a marked angular dependency, while

materials exhibiting a high normal sputtering ratio, such as copper, silver, and gold, show a less pronounced effect. Almén and Bruce report the absence of this distinction at high energies (Fig. 4f).

2. The angular distribution of sputtered particles is significantly changed by oblique incidence of the beam at low ion energies only. At low ion energies (below a few kev), the distribution exhibits a definite persistence in the forward direction (Ref. 13) as opposed to the symmetric distribution resulting in normal sputtering. Wehner and Rosenberg illustrate this effect in the distribution curves depicted in Fig. 5. At ion energies in the kilovolt range or greater, the angular distribution of sputtered particles becomes less dependent upon the angle of incidence of the beam (see section 2.6.1 and Figs. 6 and 7).

2.6 ANGULAR AND ENERGY DISTRIBUTION OF SPUTTERED PARTICLES

2.6.1 Neutral Particles

Angular distribution of sputtered particles has been measured by several investigators (Refs. 5, 12, 13, and 14). Considering the complexity of such a measurement, the correlation between investigators is exceptionally good, and the following general conclusions can be made: (1) For low energy normally incident particles (below 3 kev), an under cosine distribution has been observed (Figs. 8a, b, and c). (2) For intermediate energies (approximately 3 to 5 kev), the distribution is very nearly a cosine distribution for all angles of incidence (Fig. 9). (3) For higher energies (above 5 kev), the distribution is seen to become more concentrated in the direction normal to the target regardless of the incident angle (Fig. 9).

Figures 8a, b, and c give the angular distribution for a number of low energy cases of interest in electrical propulsion system design. Unfortunately, no equivalent high energy data is available for these cases.

Measurements of the energy of sputtered particles have also been extensively reported (Refs. 9, 11, 15, 16, 17, and 18), and recent measurements are in favorable agreement. Some of the most elaborate measurements of energy distributions for low energy ions have been made by Wehner where several methods were used to measure the complete energy distribution of these particles. The following conclusions are evident: The energy distributions are closely approximated by a Maxwellian distribution for low energy sputtering and deviate slightly from a Maxwellian

distribution at higher ion energies. The average energy of sputtered neutral particles varies only slightly (5 to 10 ev) with impingement energy up to approximately 3 kev and rises to a value of 30 to 40 ev for 50-kev impingements. The average energy of sputtered ions is slightly higher than that of neutrals (Ref. 29).

The velocity distribution for a number of particular cases can be seen in Fig. 10. Average velocity is plotted against ion energies in Fig. 11.

2.6.2 Re-emitted Beam Particles

In addition to the sputtering phenomenon, a target can become saturated with beam material and in equilibrium re-emit beam material at a rate equal to that of the beam impingement upon the target. Very little work has been conducted concerning the re-emitted beam material. Recent studies concerning this phenomenon indicate that a large majority of material re-emitted from such a target comprises neutral atomic particles. The more reliable measurements of the degree of ionization of these particles indicate a concentration of ionized particles, both positive and negative, of less than one percent. Based on previous discussion and information from other sources (Refs. 19, 20, 21, and 22), it is believed that if the ions strike the target at (or near) normal incidence, the energy of re-emitted beam particles having lost most of their energy in collisions with the lattice atoms will lie between that corresponding to the localized target temperature and that of the sputtered particles. If this theory is correct, because of the randomizing collisions with lattice atoms, the angular distribution of such particles should be in the form of a cosine. At oblique incidences, however, a significant amount of the primary beam is re-emitted with a considerable amount of energy, indicating very few thermalizing collisions. This effect is especially pronounced when ions in the primary beam are of lower molecular weight than target molecules (Ref. 21).

In addition to re-emitted beam material and sputtered target material, sputtered contaminant materials from the surface of the target have been noted by most investigators. Both negative and positive ions have been observed and offer a method for detecting what contaminants are on a given metallic surface (Ref. 12). Coefficients for the production of such material are usually less than 3 to 4 percent and should be of negligible importance, especially when targets are under long-term bombardment under high vacuum.

2.6.3 Reflected Beam Material

A number of investigators have conducted studies with the so-called reflected beam molecules (Refs. 23, 24, 25, and 26). A closer definition

of the term is desirable to discern the difference between the reflection and re-emission. Obviously, any molecule which strikes the surface must remain there for at least the finite time duration involved in a single collision with a target molecule before it leaves the surface. Therefore, in the strictest sense, all molecules leaving the target surface are re-emitted; however, reflection is a useful term to apply to those beam particles that make only one collision before leaving the target. In this case, the reflected particle energy is relatively very high.

The studies of reflection of normal beams indicate that very few particles are reflected for incident ion energies greater than a few hundred electron volts. Most of the studies were concerned with metastable atoms and ions because of the ease of detection. The following characteristics are generally observed for reflected particles:

1. The mean energy is relatively higher than that of emitted materials. (This feature actually follows from definition.)
2. The angular distribution is cosine in nature. This property is apparent since the de Broglie wavelength of an incident molecule is much smaller than the irregularities of the surface of any solid at room temperature, leading to diffuse reflection from the surface.
3. The values for reflection coefficients increase with energy to a maximum of 3 to 4 percent at 30 to 40 kev and decrease with further increase in energy.
4. Normal reflection can occur only for the case in which the striking molecule has a smaller mass than the target molecule.

Conceivably, this phenomenon could become an important one for the collector system design for beams of high current density. The oblique incidence of a beam increases reflection of ion beams, especially where the ion-target mass ratio is less than unity. Although several investigators have noted this effect, no qualitative data have been found in the literature.

2.7 SECONDARY ELECTRON EMISSION

In addition to the ejection of atomic particles from a target under ion bombardment, the phenomenon of secondary electron emission has been observed. There are two basic types of secondary electron emission: (1) electron induced and (2) ion and neutral particle induced. The first is more conducive to experimental and theoretical analysis and has been under extensive study for many years. A number of books and journals cover this phenomenon in detail (Refs. 26, 27, and 28), and values of the

secondary electron emission coefficient have been extensively tabulated. The importance of this phenomenon in collector system design work will depend upon the nature of the beam electrons to be collected. Under normal circumstances, electrons in the beam of an ion engine are relatively low in energy so that electron-induced secondary electron emission may be relatively unimportant in collector system design.

The second process, ion-induced secondary electron emission, can be expected to be more important for this application. Experimental data for low energy ion beams in the ranges from 0.2 to 1 kev have been given in Refs. 28, 29, 30, 31, and 32 and for higher energies in Refs. 16, 33, and 34. Some of these data are reproduced in Fig. 12 for cesium impinging on various targets. Here it is shown that the secondary emission coefficient (α) increases from 0.01 electrons per incident ion with energies of a few hundred ev to values of the order of unity and higher for energies up to 20 to 30 kev. Values for α are plotted for other alkali metals in Fig. 13. The general trend seen in Figs. 12 and 13 holds for all cases of ion-target combinations found in the literature. It is widely accepted that the secondary electron emission (α) is an order of magnitude higher than positive or negative ion emission coefficients.

An increasing target temperature results in a decrease in α. Most investigators explain that this effect (shown for cesium on nickel in Fig. 14) is caused by the change in surface condition. A cleaner surface usually exhibits lower values of α. Surface condition has been shown to be an important factor in all of the emission coefficients; for example, it is well known that the work function of an oxide-coated tungsten surface is lower than that of a clean tungsten surface, resulting in higher emission currents. The effects of secondary emission must be considered when any electrical measurements are taken at the target. Since the incident energy of the ion beams is expected to be in the kilovolt range, the secondary electron emission coefficient can be expected to be the order of unity or greater. The necessity for electrical isolation of the collector from the test article is apparent but will not be considered here.

2.8 EFFECT OF VARIOUS IONS ON YIELD AT HIGH ENERGY

Almén and Bruce (Ref. 9) used a wide variety of ion beams to acquire further insight into the effects of sputtering. Figure 15 contains the data obtained by these authors using 70 different ion species impinging upon tantalum, copper, and silver targets at an incoming energy of approximately 45 kilovolts. Sputtering yield is plotted versus the atomic number of the ion beams. From this figure it is seen that sputtering phenomena at this energy are not simply mass dependent but exhibit an atomic group periodicity.

3.0 SUMMARY OF SPUTTERING THEORIES

Several theories have been advanced to describe sputtering phenomena (Refs. 35 through 41). These theories generally fall into two major classes: (1) that of macroscopic evaporation caused by local thermal spikes and (2) microscopic collision theories. The evaporation theories have been discredited because of their inability to account for (1) the invariance of the sputtering ratio with target temperature, (2) the ion mass dependence of the sputtering ratio, and (3) secondary emission caused by ion bombardment being considerably less than would be expected from thermionic emission at the surface.

An earlier victory for the evaporation theories stemmed from the Knudsen angular distribution of sputtered particles that was observed in experiments. Wehner has recently shown that the cosine distribution holds only for ions of intermediate energies. An "under" cosine distribution is generally noted for low energy bombardment while an "over" cosine distribution (heavier concentration is found in the normal direction) is witnessed at higher energies (Ref. 13).

A low and intermediate energy range sputtering equation has been developed by Keywell (Ref. 35), based upon a neutron cooling model. The validity of the development is difficult to ascertain from experimental data. However, the assumption of a random walk phenomenon does not appear valid because of the persistence of velocity effect; that is, random walk theory assumes that there is no preferred direction of motion after collision. The same shortcoming is evident in other theoretical developments which assume the applicability of the diffusion equation (Ref. 38).

Rol (Ref. 36) has finessed the problem of predicting the number of displaced particles that are able to escape the target surface by assuming that the sputtering ratio is proportional to the number of particles created at the surface. In his treatment all ion collisions after the first were assumed negligible. No theoretical basis exists for such an assumption. Langberg (Ref. 37) developed a low energy sputtering equation assuming a Morse-type interaction potential between neighboring atoms. He also concluded that a rigid-sphere-type potential between collision partners is invalid at low energies; this conclusion tends to contradict Bohr's work (Ref. 42).

Several authors have treated the problem of high energy sputtering of low molecular weight particles (Refs. 38, 39, and 40). These developments are generally made considering Rutherford-type collisions and are concerned only with the portion of the yield curve that decreases with increasing energy. Since the Rutherford-type phenomenon generally

occurs at energies higher than is of interest to electrical propulsion collector system design, except for very light collision partners, no further mention will be made of the above works.

Bohr (Ref. 42) has extensively treated the penetration of atomic particles through matter. Since a single model of the penetration phenomena covering the entire energy spectrum could not be readily attained, he defined two parameters which may be used to ascertain the appropriate model that will best approximate the collision mechanism for the energy range of interest. These parameters are:

$$\kappa = 2 Z_i Z_t \left(\frac{R_h M_i}{E M_e}\right)^{1/2} \tag{1a}$$

$$\xi = \frac{2 Z_i Z_t R_h M_i a_h}{E \mu a_s} \tag{1b}$$

Equation (1a) is the ratio of the collision diameter to the de Broglie wavelength of the incident particle; hence, its value dictates whether or not the wave properties of the particles can be neglected and a classical approach used. For values of $\kappa \gg 1$, the de Broglie wavelength is negligibly small and the use of classical mechanics is completely justified. This approximation is valid even for interactions involving low molecular weight ion-target combinations, such as helium and beryllium, for energies extending to 1 mev. Thus the wave mechanical approach is not required for a collector design and will be disregarded.

When an ion* interacts with a target atom, the electron clouds of each tend to overlap and screen the fields of the two nuclei. To describe the interaction, Bohr has suggested use of a potential function of the following form:

$$u(r) = \frac{e_1 e_2}{r} e^{-\frac{r}{a_s}} \tag{2a}$$

The factor a_S in the above equation is a screening constant given by

$$a_s = \frac{a_h}{\left(Z_1^{2/3} + Z_2^{2/3}\right)^{1/2}} \tag{2b}$$

Equation (1b) is the ratio of the collision diameter to the above screening constant. If the parameter of Eq. (1b) is very much less than unity, the screening is weak, and Rutherford-type scattering may be employed (provided $\kappa >> 1$). If on the other hand, $\xi \gg 1$ the phenomenon approaches a rigid sphere interaction in which the scattering of the ions approaches spherical symmetry in the center of mass reference frame. Figure 16 is a schematic diagram of the logarithms of Eqs. (1a) and (1b). The

*Although it is generally felt that the impinging ions are neutralized before actual surface contact is made, the bullet particle will be alluded to as an ion.

region in the upper left hand quadrant with horizontal hatching is that in which the screening is weak wherein classical mechanics may be used. The region having vertical hatching, which includes the two lower quadrants and a portion of the upper right hand quadrant, is the region which must be described in terms of wave mechanics. Bohr has used approximate methods to describe the phenomena in this region. The open area is a region in which exact wave mechanic treatment must be used. In the region above the 45-deg line indicated by dots, the scattering of the ion can be treated classically and is the rigid sphere region, at least down to points near the origin. In the following analysis the sputtering phenomenon is treated only in this region.

4.0 ANALYSIS OF SPUTTERING PHENOMENA

4.1 DERIVATION OF SPUTTERING EQUATION

In view of the uncertainties and limitations inherent with existing theories, a theoretical model is developed in the following to evaluate the effects of sputtering on collection system design. Consider the distribution function f(p)dp, which is defined as the probability that a primary displaced particle with initial energy E_p will come to rest between p and p + dp. The mean range of the particle may then be defined as the following:

$$R_p = \bar{p} = \int_0^\infty p\, f(p)\, dp \tag{3}$$

which assumes that the range is very much less than the thickness of the material through which the particle is traversing. The probability g(p) that a particle will travel a distance p or greater before coming to rest may be calculated from the above distribution function.

$$g(p) = \int_p^\infty f(p')\, dp' \tag{4}$$

The probability that a displaced particle will escape the surface starting at a distance x from the surface of the plate pictured in Fig. 17 may be written as follows:

$$W(x) = 2\pi \int_0^{\pi/2} g\left(\frac{x}{\cos\theta}\right) S(\theta)\, d\theta \tag{5}$$

where S (θ) is defined as the angular distribution of particles with a velocity component in direction of the surface. The 2π arises from the fact that the scattering is assumed to be symmetric about the incident direction. The above distribution function will in general be dependent upon

the mass of the ion and target materials. The total number of primaries that are able to escape the target may then be written as follows:

$$N_{out} = \int_0^\infty N(x)\ W(x)\ dx \tag{6}$$

The number of primary displaced atoms per unit path length of the incident ion N(x) is defined as the displacement cross section times the number of target nuclei per unit volume. For a rigid sphere-type interaction, the displacement cross section is given by the following expression:

$$\sigma_d = \pi d_{12}^2 \left[1 - \frac{E_t}{\gamma E(x)}\right] \tag{7}$$

The quantity in brackets represents the probability of a displacing event occurring per collision and πd_{12}^2 is the collision cross section. Since the energy of the incoming ion will vary with path length, the number of particles produced per unit path length is dependent upon x, the depth of penetration. Although E(x) is not generally known, the displacement cross section as a function of x may be obtained by dividing the beam flux into two separate groups: (1) the ions which have yet to make their first scattering collision and (2) the ions which have made at least one collision with the target lattice. The probability of a displacement collision for the first type particle is given by

$$P_{d_1} = 1 - \frac{E_t}{\gamma E_i} \tag{8}$$

The probability of displacing an atom per collision for the second type of ion may be written as follows:

$$P_{d_2} = 1 - \frac{E_t}{\gamma \bar{E}} \tag{9}$$

where

$$\bar{E} = \int_0^{E_i} E\ \frac{dE}{E_i} = \frac{E_i}{2}$$

since the probability of finding a group 2 particle in the energy range dE is dE/E_i for rigid sphere encounters. The total probability of a displacement collision per ion-target impact may be obtained by weighting each of the above probabilities by the fraction of ions in each group.

$$P_d = \left[1 - \frac{E_t}{\gamma E_i}\right] e^{-x/\lambda} + \left[1 - \frac{2E_t}{\gamma E_i}\right]\left[1 - e^{-x/\lambda}\right] \tag{10}$$

$$= 1 + \frac{E_t}{\gamma E_i}\left(e^{-x/\lambda} - 2\right)$$

where the exponential term is the probability that an ion will make a collision between x and x+dx (Ref. 53). Thus N(x) is obtained by multiplying Eq. (10) by $N\pi d_{12}^2$. Equation (6) may now be evaluated using Eq. (10).

$$N_{out} = (2\pi)\,\pi\,d_{12}^2\,N\left[\int_0^{\pi/2}\int_0^{\infty} d\theta\;dy\;g(y)\,S(\theta)\,\cos\theta\right.$$

$$-\frac{2E_t}{\gamma E_i}\int_0^{\pi/2}\int_0^{\infty} d\theta\;dy\;g(y)\,S(\theta)\,\cos\theta \qquad (11)$$

$$\left.+\frac{E_t}{\gamma E_i}\int_0^{\pi/2}\int_0^{\infty} d\theta\;dy\;e^{-\frac{y\cos\theta}{\lambda}}\;g(y)\,S(\theta)\,\cos\theta\right]$$

where

$$y = \frac{x}{\cos\theta}$$

The first two terms of Eq. (11) may be evaluated without a knowledge of the distribution function g(y). For brevity let

$$\psi_1 = 2\pi\int_0^{\pi/2} S(\theta)\,\cos\theta\,d\theta \qquad (12)$$

Integrating the first two terms of Eq. (11) by parts (the y dependency) and noting that $\frac{\partial g}{\partial y} = -f(y)$, we obtain

$$N_{out} = \pi\,d_{12}^2\,N\left\{\psi_1\left[\int_0^{y} y\;f(y)\;dy - \frac{2E_t}{\gamma E_i}\int_0^{\infty} y\;f(y)\,dy\right]\right.$$

$$\left.+\frac{E_t}{\gamma E_i}\int_0^{\infty}\int_0^{\pi/2} d\theta\;dy\;e^{-\frac{y\cos\theta}{\lambda}}\;g(y)\,S(\theta)\,\cos\theta\right\} \qquad (13)$$

The first two integrals appearing in Eq. (13) are simply R_p defined by Eq. (3). Equation (13) can therefore be written as

$$N_{out} = \pi\,d_{12}^2\,N\left[\psi_1\,R_p\left(1-\frac{2E_t}{\gamma E_i}\right)+Z(E_i)\right] \qquad (14)$$

where $Z(E_i)$ represents the last term of Eq. (13).

To evaluate $Z(E_i)$, a knowledge of g(y) is mandatory. One would expect the distribution function defined by Eq. (4) to have a maximum value at the surface x = 0 or y = 0 since primaries produced at that point will, in general, be much more energetic and hence will have a maximum probability of traveling a distance y or greater. For increasing values of x, the distribution function is expected to approach zero, since primary displaced atoms produced at a considerable depth within the solid

material have on the average very little energy, and hence their probability of reaching the surface decreases with increasing depth of origin. A distribution function having these general characteristics ($y > 0$) is:

$$g(y)\,dy = \frac{\left(y + \frac{n}{a}\right)^n e^{-a\left(y+\frac{n}{a}\right)} dy}{\int_0^\infty \left(y + \frac{n}{a}\right)^n e^{-a\left(y+\frac{n}{a}\right)} dy} \tag{15}$$

$$= \frac{a^{n+1}}{\Gamma(n+1)}\left(y + \frac{n}{a}\right)^n e^{-a\left(y+\frac{n}{a}\right)} dy$$

The range distribution function may be obtained by taking the negative derivative of Eq. (15). This is seen to be

$$f(y)\,dy = \ell\, a\, y\, e^{-a\left(y+\frac{n}{a}\right)}\left(y + \frac{n}{a}\right)^{n-1} dy \tag{16}$$

where ℓ is a normalizing factor.

Figure 32 compares the function above with data obtained by Davies and Sims (Ref. 43) for xenon on an aluminum target. The correlation is satisfactory. Using the above distribution function for g(y), $Z(E_i)$ of Eq. (14) may then be evaluated (setting n = 2). Upon integrating over y, $Z(E_i)$ becomes:

$$Z(E_i) = \frac{e^{-2} E_t}{\gamma E_i \Gamma(3)} \int_0^{\pi/2} d\theta\, S(\theta) \cos\theta \left[ab + (ab)^2 + (ab)^3\right] \tag{17}$$

where

$$b = \frac{\lambda}{\cos\theta}$$

and

$$a = \frac{18}{5}\,\frac{1}{R_p} \tag{18}$$

The relationship between a and R_p may be obtained from Eq. (16) and evaluating Eq. (3).

The mean range of particles through matter has been theoretically evaluated by Davies and Sims (Ref. 43), who extended Nielsen's derivation (Ref. 44). The expression they developed is

$$R_p = \left[\frac{\bar{K}\, 1.19\, M_t^2}{M_t + M_i}\right]\left[\frac{\left(Z_i^{2/3} + Z_t^{2/3}\right)^{1/2}}{\rho\, Z_i\, Z_t}\right] E \tag{19}$$

where $\bar{K}$ is a function of the mass ratio only. The values of $\bar{K}$ were calculated by Monte Carlo techniques, and its value for particles of equal mass is approximately 1.55×10^{-6}. For primary displaced particles moving in

the target, Eq. (19) reduces to:

$$R_p = \frac{1.19\,\bar{K}\,M_t\,(2\,Z_t)^{1/3}\,\bar{E}_p}{2\,Z_t^2\,\rho} = K\,\bar{E}_p \tag{20}$$

The average energy of the primary particle in Eq. (20) may be written in terms of the incident ion energy. For isotropic scattering in the center of mass system, the relation, neglecting E_t, is

$$\bar{E}_p = \int_0^{\gamma E_i} E\,\frac{dE}{\gamma E_i} = \frac{\gamma E_i}{2} \tag{21}$$

Equation (17) may be written in terms of the incident ion energy with the aid of Eqs. (18), (20), and (21) as follows:

$$Z(E_i) = \frac{e^{-2}\,E_t}{\Gamma(3)} \int_0^{\pi/2} S(\theta)\,\cos\theta \left[\frac{36}{5}\,\frac{b}{K\gamma^2 E_i^2} + \frac{\left(\frac{36}{5}\,b\right)^2}{K^2\gamma^3 E_i^3} + \frac{\left(\frac{36}{5}\,b\right)^3}{K^3\gamma^4 E_i^4}\right] d\theta \tag{22}$$

Each term on the right hand side of Eq. (22) depends inversely on powers of E_i and will take part in shaping the initial portion of the yield curve (note the initial bend in Fig. 1). These terms will rapidly approach zero in the energy range of interest.

Since the range of any secondary particles produced by the primary displacements is significantly less than that of the primary particles themselves, it is assumed that the number of secondary displaced atoms escaping the target boundary is negligible. Thus, the number of particles escaping the target per incident ion, which is defined as the sputtering ratio, is given approximately by N_{out} (Eq. (14)).

By combining Eqs. (14) and (20), it is possible to obtain an expression for the sputtering ratio as a function of incident ion energy (neglecting the contribution made by $Z(E_i)$):

$$S_L = \pi\,d_{12}^2\,N\,\psi_1\,K\,\frac{\gamma}{2}\left[E_i - H\right] \tag{23}$$

where

$$H = \frac{2\,E_t}{\gamma}$$

Since Eq. (23) was developed for the case of $E_i >> E_t$, the threshold energy H corresponds to the linearly extrapolated threshold (Fig. 1). Equation (23) predicts a linear dependency of the sputtering ratio for incident ion energies well above the threshold but still within the domain of validity of rigid sphere collisions. This linear dependency has been substantiated experimentally (Ref. 45).

As the energy of the incoming ion beam is increased, Eq. (1b) indicates that the screening parameter approaches unity. In this region, Bohr pointed out (Ref. 42) that the major portion of the deflections take place in the potential field of the inverse square type. Assuming a field of this nature, the collision cross section takes the following form:

$$\sigma = \frac{\pi \xi a_s}{e} \tag{24}$$

The displacement cross section may then be obtained by multiplying Eq. (24) by the probability of a displacement collision. However, at energies much greater than the threshold energy, the probability is essentially unity. Again, neglecting secondary particles escaping the boundary, the displacement cross section, as a function of depth of penetration x, in the energy range $\xi \sim 1$ is obtained by considering molecules that have made at least one collision separately from those that have not. The total displacement cross section is then given by weighting the cross section for each type event by the fraction of particles within each group. Substituting for ξ from Eq. (1b) into Eq. (24) yields

$$\sigma = \frac{2\pi e_i e_t a_s (M_i + M_t) R_h a_h e^{-\frac{x}{\lambda}}}{e M_t E_i} + \frac{4\pi e_i e_t a_s (M_i + M_t) R_h a_h}{e \gamma M_t E_i}\left(1 - e^{-\frac{x}{\lambda}}\right) \tag{25}$$

simplifying Eq. 25

$$\sigma = \frac{2\pi e_i e_t a_s (M_i + M_t) R_h a_h}{e M_t E_i}\left[\frac{2}{\gamma} - e^{-\frac{x}{\lambda}}\left(\frac{2}{\gamma} - 1\right)\right] \tag{26}$$

Thus the sputtering ratio at $\xi \sim 1$ may be obtained from Eqs. (26) and (6) and the condition that $N(x) = N\sigma$. The maximum value of the sputtering ratio may be readily obtained since S decreases with increasing ion energy in the Rutherford region. Again neglecting inverse powers of E_i,

$$S_{max} = \frac{2\pi d_{12}^2 N \psi_2}{M_t \gamma e}\left[4\pi e_i e_t a_s (M_i + M_t) R_h a_h\right] K \tag{27}$$

where the function ψ_2 has been introduced to allow for the possibility of a different angular distribution function in this energy region.

Equation (27) predicts that the sputtering ratio is independent of energy within the energy range where ξ is of the order of unity. From the model that has been developed, as ξ varies from a very large positive quantity to the order of unity, the asymptotes of the sputtering ratio may be obtained from Eqs. (23) and (27). Thus, the sputtering ratio

begins with essentially a linear rise beyond the initial bend and peaks out at some maximum value where ξ is of the order of unity. It has been found that throughout the transition region, the sputtering ratio may be represented by the following equation:

$$S = S_{max} \left[1 - e^{-C(E_i - H)} \right] \tag{28}$$

where S_{max} is the sputtering ratio obtained from Eq. (27). By expanding Eq. (28) in a Taylor series, S approaches a linear function of (E - H) at low energies as required by Eq. (23). Also at high energies, S approaches a constant value, S_{max}, as predicted by Eq. (28).

Without a prior knowledge of ψ_1 and ψ_2, absolute values of S_{max} and C cannot be calculated. However, to expedite the solution of the collector problem, S_{max} and C have been considered as experimental constants. Values of these constants for materials of interest are tabulated in Table 1.

Figures 18 and 19 illustrate the fit of Eq. (28) to experimental results of other workers. Note that the curves are essentially linear for low energies and approach a constant value for ξ on the order of unity, as predicted by Eq. (28).

4.2 TARGET SATURATION

When an energetic ion beam impinges upon a target, sputtering is accompanied by other phenomena which result in additional requirements for the successful beam accommodation. For example, the target will rapidly become saturated with beam material and subsequently will become a source of free molecules of both the target and beam species that rebound into the system. These molecules then advance to other points in the system where they are ultimately collected. This section describes the effects of these phenomena upon test chamber conditions.

Analytical treatments to determine the effect of terminating an energetic ion beam on test chamber conditions have been presented by other investigators (Refs. 46 to 48), but unfortunately none of these have proved successful. Richley and Cybulski (Ref. 47) adopted a model developed by Mickelsen and Childs and added two additional assumptions: (1) they assumed that the effects of sputtering could be neglected and (2) that a near unity collection efficiency existed at a target.* While either assumption is valid in a specific ion energy range, neither is generally valid in

*Collection efficiency is defined as:

$$\left[1 - \frac{\text{No. particles leaving target/sec}}{\text{No. particles striking target/sec}} \right]$$

the range of interest. The second assumption is valid only during the first few milliseconds of the operation of an ion beam and is in direct contradiction with the findings of Almén and Bruce (Refs. 9 and 49) and of Brown and Davies (Refs. 15 and 19), who noted saturation of the target. From the observations made by these investigators, a description of the phenomenon of saturation may be formed. In the presence of sputtering, the target collects essentially 100 percent of the ion beam of energy above approximately 3 kev at the initial application of the beam. This can be shown by using Fig. 20 (Ref. 9) together with Fig. 21 (Refs. 9, 19, and 50). As can be seen in these figures, the collection efficiency decreases continuously from a maximum value of unity at the initiation of the beam collection to a minimum of zero at a time when the target becomes saturated with beam material. At this time any new molecule striking the target travels to some finite depth, depending upon its initial energy, where it reaches a plane of very high density. Finding no empty site in which to be trapped, it is either reflected, subsequently diffusing back from the target, or it replaces an already trapped molecule which diffuses back from the target. Re-emission of the "striking" molecules after saturation as opposed to re-emission of already trapped molecules is indicated for noble gases in the saturation studies of Brown and Davies.

The observed changes in range distribution of collected molecules in the noble-gas-bombarded targets suggests that self-sputtering of these molecules does not occur (Fig. 22); they are simply driven deeper into the target (Ref. 50); that is, the governing mechanism for re-emission appears to be collision with target and collected ions as opposed to sputtering by incoming ions. This follows from the previously cited observation on re-emission.

Unfortunately, no such experimental observation has been made for other ions. From the available information, a slight difference is evident for other ions in which a stronger bond occurs between the ion and lattice, for example, Cs^+ on Cu. It is believed that for such combinations the density distribution of collected ions in the saturated target would exhibit a higher concentration of trapped ions near the target surface*, resulting in a combination of self-sputtering, ion-target sputtering, and ion re-emission. In such a distribution, a high concentration of collected molecules is in a situation that is favorable to self-sputtering (Fig. 22). This suggests that the sputtering ratio for a given ion-target combination changes continuously until the target is saturated, thereafter becoming constant and

*It is important to note that the actual range distribution for all molecules has the same form even in the saturated target. The final distribution of trapped molecules in the saturated target is the property which is variant in form.

representative of the ion-target mixture as opposed to the target-ion beam combination alone. This effect has been noted by Almén and Bruce.

To explain the previous observations, a simplified model can be developed. For a given target, assume that a finite number of sites exists wherein an ion can be collected, the average number depending upon the depth to which the ion can penetrate. Assuming that the distribution of these sites is such that the probability of the occupation of a site by an incoming ion is dependent only upon the total remaining number of sites available to it, the collection rate of beam material can be expressed by:

$$\frac{dq}{dt} = k\phi = \phi f - \Lambda \tag{29}$$

$$\phi = \frac{M_i I}{\epsilon} \tag{30}$$

Further, assume that

$$\Lambda = Dq \tag{31}$$

where D is dependent upon the diffusion capabilities of the trapped molecule and, where self-sputtering occurs, on the value of S_S.

The sticking fraction f is obtained from:

$$f = c\left(1 - \frac{q}{q_s}\right) \tag{32}$$

where q_s is the saturation value of target (gm).

Combining Eqs. (29), (31), and (32)

$$\frac{dq}{dt} + \left(D + \frac{\phi c}{q_s}\right) q = \phi c \tag{33}$$

and therefore

$$q = \frac{\phi c}{D + \frac{\phi c}{q_s}}\left[1 - e^{-\left(D + \frac{\phi c}{q_s}\right)t}\right] \tag{34}$$

leading to

$$q = \frac{1}{\frac{1}{q_s} + \frac{D}{\phi c}}\left[1 - e^{-\phi c\left(\frac{D}{\phi c} + \frac{1}{q_s}\right)t}\right] \tag{35}$$

Equation (35) may be used to explain most of the saturation phenomena reported in the experiments of Almén and Bruce as shown in Fig. 20. This treatment is similar to that of adsorption phenomena. The important

difference can be recognized, however, by comparing the magnitude of the sticking probability, accommodation coefficient, and saturation value. The first two are usually smaller for surface phenomena, whereas the third is invariably smaller by a factor of 2 to 1,000 or more, depending, of course, upon the degree of penetration of the target by the beam particles. Since the range of an ion is a linear function of energy over a wide range of application (Refs. 9, 19, 50, and 51), the saturation value can be expected to be a linear function of energy in view of the model adopted; that is, the number of sites available to an array of impinging ions is proportional to their mean depth of penetration. This phenomenon is also reported by Almén and Bruce. In comparing Eq. (35) with the experimental data available, the value of c was found to vary only slightly from unity. Saturation values for various targets of interest for application to electrical propulsion test facilities are plotted in Fig. 23. Almén and Bruce have shown that Λ, the re-emission of collected atoms, in Eq. (29) is effectively zero for most ion target combinations at room temperature when the energy of bombardment is above approximately 2 kev. By using radioactive ions as a tracer, Λ was measured by setting ϕ equal to zero after a given bombardment and checking specific radioactivity of the target as a function of time. Observations lasting up to 10 days showed no substantial decrease in specific radioactivity for a large number of combinations which usually included the heavier ions as beam material. Such targets are considered permanent in nature. As would be expected, the re-emission rate and therefore the diffusion coefficient D increase with temperature. Various constants and values applicable to Eq. (34) have been tabulated in Table 2. By use of these constants, certain useful calculations are possible. For example, the time required for a target to reach 98 percent of its saturation value is equal to four time constants, $4\Big/\left(D + \frac{\phi c}{q_s}\right)$ of Eq. (34), which is attained almost immediately after starting the ion engine.

4.3 BEAM COLLECTION

Below a certain critical energy, it appears likely that an unlimited quantity of any solid element might be retained on the surface of a saturated target. This phenomenon, covered in some detail by Almén and Bruce, occurs only in the presence of what they called "zero sputtering".* They proposed three basic requirements for "zero sputtering": (1) the self-sputtering ratio, that is, the sputtering ratio of ions on the same

*This term is meant to imply zero target material sputtering. Sputtering of the collected material may continue to occur with some sputtering ratio less than unity.

target material, must be less than unity, (2) the initial sputtering of the target must not be too large, and (3) the target temperature must be sufficiently low to avoid evaporation of the deposit. In view of the above treatment, one basic requirement which comprises all of the above three can be made. The collection efficiency for the beam must be greater than its self-sputtering ratio. Where this is true, the situation then proceeds as follows: Initially, sputtering occurs at the target in a normal way; however, the target becomes saturated and a deposit of the ion species forms on the surface of the target. The target will then gain in weight according to the following:

$$\frac{dq}{dt} = \phi (k - S_s) \tag{36}$$

If $k > S_S$, the saturation of the target seemingly never occurs, and since the deposit eventually grows out from the target face, the original target has an infinite lifetime and remains undamaged after its initial exposure to the beam. (A finite time is required for the target saturation and surface deposition by material of the ion species.)

Self-sputtering measurements are available in a number of references, but specific cases of interest are not available at this time. The use of the zero sputtering concept in the resolution of problems depends upon the ability of propellant-target combination to support the proposed phenomena. This in turn will require some form of beam decelerating system to reduce the ion energy to the necessary magnitude such that $k > S_S$.

In the event that "zero sputtering" does not occur, saturation of a target results. When saturation is obtained, continual target impingement results in self-sputtering, diffusion, or a mixture of the two as a mechanism for re-emission of molecules of the ion species in addition to sputtering of the target species.

4.4 THE TARGET AS A SOURCE OF PARTICLES

Based on the results of the previous discussion, if $k < S_S$, an analytical treatment for the accommodation of an ion beam except for very short tests will deal only with the phenomena occurring after target saturation. Where $k < S_S$, the target now acts as a source of mass given by

$$Q = \frac{I}{\epsilon} (M_i + S M_t) \tag{37}$$

If $k > S_S$, the source after initial target saturation and deposition of a few layers of beam material will be given by

$$Q' = \phi \left[S_s + (1 - k) \right] \tag{38}$$

The former case will be considered first, although the method developed is directly applicable to either case. The importance of the source given by Eq. (37) depends upon the size of the ion engine and duration of the test. Figure 24 is a plot of Eq. (37) for a number of values of anticipated engine test conditions. The source given by Eq. (37) must be completely accommodated for the continuous operation of a facility to prevent contamination of the test cell.

Of particular importance, for example, is the flux of particles in the direction of the engine thruster or chamber instrumentation. Reference to Fig. 25 gives the geometry for the following expression for the number sputtered per incident ion in the direction of the engine:

$$S(\chi) = S_o \left[S_A(\chi)\right] \left[S_R(\chi)\right] \tag{39}$$

Available data indicate that in the energy range from a few kev to ten kev and for values of χ up to 70 deg

$$S_A(\chi) = \cos(\chi) \tag{40}$$

$$S_R(\chi) = \frac{1}{\cos^n(\chi)} \tag{41}$$

where $n > 0$.

Thus,

$$S(\chi) = \frac{S_o}{(\cos\chi)^{n-1}} \tag{42}$$

The following conclusions can now be drawn. If the product $S_A S_R > 1$, a tilted target cannot be justified. This is the case up to at least ten kev. But as mentioned previously, at higher energies S_A becomes more concentrated in the normal direction. Therefore, if the effect is found great enough, the majority of the flux can be aimed at a suitable spot in the collector. However, at the present time no such data are available to justify this technique. It should be noted that certain exceptions to Eqs. (40) and (41) exist, but all exceptions, such as platinum, reported in the literature at this time are impractical for use in testing.

For angles χ less than 70 deg and energies above a few kev the angular distribution of re-emitted beam particles has been shown to be cosine. Assuming direct line of flight from the target to the engine thruster, an approximation of flux impingement on the thruster can be made by assuming that the target is a point source and that a uniform distribution over the engine subtends a solid angle $\Delta\Omega$. Neglecting any secondary sputtering and all but direct line of flight particles, the flux impingement can be expressed as (Fig. 25)

$$\beta = S_A(\chi) S_R(\chi) \frac{I S_o}{\epsilon} \frac{\Delta\Omega}{2\pi} + \frac{I}{\epsilon} \frac{\Delta\Omega}{2\pi} \cos(\chi) \tag{43}$$

The first term results from sputtered particles, whereas the second results from the beam. Finally, the critical parameter for the operational system is the collection efficiency for β on vital parts of the thruster where failure might result.

4.5 PRESSURE INCREASE CAUSED BY ENGINE EFFLUX

To this point, material added to the system has been characterized only by the number of molecules and their mass. For certain applications this would be sufficient and necessary parameters could be determined experimentally. However, to determine the system's ability to accommodate such material, it sometimes becomes necessary to consider also the mean velocity of particles and the effect of reflection from various points in the collector. One such approach is to determine the equivalent pressure increase in a chamber caused by the new material which emerges from the target upon the introduction of an ion beam into the system. One important result of this treatment is that it displays the relative importance of the beam and the sputtered particles on test chamber conditions. The method of Mickelsen and Childs was modified and extended for this application. To summarize their method, an equilibrium situation is assumed wherein the total momentum transfer to the walls of the collector is given as a summation over n collisions, n being the number required for the condensation of beam material on a cold collector surface. If the pressure experienced at the target is neglected, the pressure contribution within the test chamber by particles making the nth collision is given by

$$\Delta P_n = \frac{\phi V_o}{2 A_c}\left[1 + (1 - k)(1 - a)^{1/2}\right]\left[(1 - k)(1 - a)^{1/2}\right]^n \tag{44}$$

where the zeroth collision is that made on the target. Since the accommodation coefficient and collection efficiency will in most cases of interest be very near unity, only the first few collisions are of importance; that is, the series converges very rapidly. For this reason, it is easily shown that very little error is introduced by allowing n to approach infinity. Hence,

$$\Delta P_b = \frac{\phi_b V_o}{2 A}\left[1 + (1 - k)(1 - a)^{1/2}\right]\sum_{n=1}^{\infty}\left[(1 - k)(1 - a)^{1/2}\right]^n \tag{45}$$

$$= \frac{\phi_b V_o}{2 A}\left\{\frac{\left[1 + (1-k)(1-a)^{1/2}\right]\left[(1-k)(1-a)^{1/2}\right]}{1 - (1-k)(1-a)^{1/2}}\right\}$$

a random angular emission distribution results in the factor of one half.

The same result is derived if n collisions are considered and

$$\left[(1 - k)(1 - a)^{1/2}\right]^n \approx 0 \tag{46}$$

Pressure on the target face (the zeroth collision) being neglected, the summation begins with unity.

From previous discussions, it is concluded that the collision with the target cannot be considered similar to remaining collisions made with the walls of the collector for energy and saturation reasons. Interactions at points in the collector system other than at the target face will be surface interactions, whereas beam target interactions are not strictly surface interactions. In the latter case, the impinging molecules penetrate through a number of lattice layers before they are reemitted from the target; therefore, the accommodation coefficient of these beam particles is expected to be much greater at the target than at any other collision surface, and the average velocity of beam particles emerging from the target is given by

$$\bar{V} = V_o (1 - a_t)^{1/2} \tag{47}$$

The magnitude of $\bar{V}$ was discussed previously in section 2.6.2.

Modification of Eqs. (44) and (45) to consider the target itself as a source of particles leads to a different expression for the pressure contribution of the particles after leaving the target. A general angular distribution will be assumed for the present by inserting a constant factor ψ in calculations. For the nth collision, considering first the beam particles,

$$\Delta P_b = \frac{\psi_b \phi_b V_o (1 - a_t)^{1/2}}{A_c} \left[(1 - k)(1 - a)^{1/2}\right]^{n-1} \left[1 + (1 - k)(1 - a)^{1/2}\right] \tag{48}$$

A summation over n leads to

$$\sum_{n=1}^{\infty} \Delta P_b = \frac{\psi_b \phi_b V_o}{A_c} \left\{ \frac{(1 - a_t)^{1/2} \left[(1 - k)(1 - a)^{1/2} + 1 \right]}{\left[1 - (1 - k)(1 - a)^{1/2} \right]} \right\} \tag{49}$$

Until now no mention has been made of the second term of the right hand side of Eq. (37), which describes the source of the sputtered particles. Similarly, the previous treatment (Eq. 49) for primary beam particles can be applied to the sputtered particles; however, the results must be properly interpreted for each case before conclusions of any value can be made, especially for certain ion-target combinations. This is true because the collection efficiency for some of the combinations to be considered is near unity. In this case, the angular distribution of emergent

particles is very important since there is a large pressure variation in the collector; that is, the flux of material is concentrated upon a localized portion of the large vacuum chamber. For the same reason, pressure readings in such a chamber must be properly interpreted since these atoms could only be detected by a properly oriented "nude" sensing element. Such atoms would plate out on any gage tubulation before entering the electrodes and the resulting gage readings would be erroneously low. Where sticking fractions are lower, this problem is not encountered. The following additional assumptions are required to extend the theory to consider sputtered particles effects:

1. Sputtering at any point in the collector system other than at the target is considered negligible. This is true because a very high accommodation coefficient for a normally energetic beam results in low ion energies for the re-emitted particles. In the case of normal incident beams, the primary sputtered particles are so low (20 to 50 ev) that they can induce very little secondary sputtering. The same cannot be said for an obliquely incident beam. An increase in reflection of high energy particles with very little accommodation can result in secondary sputtering. Even this effect will be shown negligible, however, for angles of target rotation as high as 60 deg.

2. The remainder of the collector is not saturable. This assumption follows if the surface temperature of the collector walls is such that condensation can occur. The relatively low energies of the particles result in their condensation and accumulation.

3. Gettering can be considered separately. The possibility has been recognized that sputtering phenomena might be harnessed to augment the pumping components of the test chamber. Yonts has noted the observation of a reduction in residual gas pressure when the materials are such that gettering is possible (for example, Ca^+ on Cu). For materials not conducive to gettering, a pressure rise was noted (Ref. 32). In any event, the following treatment is independent of gettering of the residual gases, and a further study will be necessary to include this phenomenon.

Using the same treatment for primary beam particles, the following expression of pressure contributions in the nth collision for sputtered particles is obtained:

$$\Delta P_n = \frac{\psi_s \phi_b \bar{V}_s S}{A_c} \left[(1 - k)(1 - a)^{1/2}\right]^{n-1} \left[1 + (1 - k)(1 - a)^{1/2}\right] \qquad (50)$$

A summation over all collisions yields

$$\sum_{n=1}^{\infty} \Delta P_s = \frac{\psi_s \phi_b}{A_c} \frac{\bar{V}_s S [1 + (1-k)(1-a)^{1/2}]}{[1 - (1-k)(1-a)^{1/2}]} \tag{51}$$

To find the total pressure caused by the operation of an engine, add Eqs. (49) and (51).

$$\Delta P = \sum_{n=1}^{\infty} (\Delta P_s + \Delta P_b) \tag{52}$$

If it is assumed that

$$k \approx a \approx 1 \tag{53}$$

and thus

$$(1 - k)(1 - a)^{1/2} \approx 0 \tag{54}$$

assuming a cosine distribution for the total efflux, making the factor $\psi = 2/3$, the pressure in the chamber may be estimated by:

$$\Delta P = \frac{2}{3A}\left[S M_s \bar{V}_s + M_b V_o (1 - a_t)^{1/2}\right] \tag{55}$$

Equation (55) is plotted in Fig. 26 and compared with experiments conducted by Richley and Cybulski. While Eq. (55) is derived from a highly idealized model, it indicates what parameters are involved in a determination of pressure changes and how such pressure changes vary.

The relative importance of sputtered and re-emitted particles from the target may be found by comparing their contributions to the change in chamber pressure after target saturation occurs. This may be obtained by taking the ratio of Eq. (51) with Eq. (49). The sputtering ratio is obtained from Eq. (28), and it is assumed that Eq. (54) is valid for both beam and sputtered target materials. We obtained the following relationship:

$$\frac{\Delta P_s}{\Delta P_b} = \frac{S_{max}(1 - e^{-CE_i})\sqrt{M_s \bar{E}_s}}{\sqrt{M_i (1 - a_t) E_i}} \tag{56}$$

The greatest uncertainty lies in the proper value for $(1 - a_t)E_i$.

The upper and lower limits can be established based upon the following argument. Since the mechanism for re-emission of beam particles is essentially the same as that for sputtered particles, the upper limit for their energy is conceivably that of the sputtered particles. However, since these beam particles penetrate the target and are thermalized to some degree, their lower energy limit can be estimated as that energy corresponding to the localized target temperature. Until further studies

are conducted in this area the following limits are assumed:

$$\frac{3}{2} K T_t \leq (1 - a_t) E_i \leq \bar{\bar{E}}_s \tag{57}$$

Equation (56) is plotted (Fig. 27) for typical values of the limits in Eq. (57). It can be seen from Fig. 27 that the effects of sputtered particles are much greater than those caused by the re-emitted beam particles.

4.6 COLLECTOR SYSTEM PROBLEMS

The effects of the various phenomena inherent in the collection and termination of an energetic beam upon the operational capability of an electrical propulsion test facility will now be considered. For long term tests, a major problem is the lifetime of the collector system. The rate of erosion of a collector surface may be described by the following expression (assuming a uniform current distribution impinging normally upon the target):

$$\text{rate of erosion} = \frac{SJ}{N\epsilon} \tag{58}$$

Figure 28 presents a series of curves of the erosion rate per incident current density for mercury and cesium ions on aluminum, iron, copper, and nickel targets. It is clear that for long term engine tests, the conventional metallic plate collector may not be used unless modifications are made. For example, a mercury ion beam having a current density of 30 ma/cm^2 with a beam energy of 6 kv will erode approximately 2 cm of target material after 30 hr of bombardment. Electrical propulsion systems operating for extended periods of time (1,000 hrs or longer) could erode meters of target material. Considering the nature of application of electrical propulsion systems, the necessity of tests of such length is evident (Ref. 1), and the sputtering problem demands resolution before long-term test programs can be performed in ground test facilities.

For tests of a shorter duration, the erosion rate will not be an important factor. However, the particle efflux defined by Eq. (37) introduced into the chamber because of the operation of the engine will limit the degree of simulation possible by the ground test facility. In a two-fold problem for long term tests, the lifetime of the system as well as the efflux problem must be resolved before an effective collector system is achieved.

4.6.1 Solid Collectors

The solid target collector is restricted to low total ion flux tests except under one condition to be mentioned presently. Therefore, the use

of Fig. 28 lends a rough estimate of the capabilities of such a system where the unmodified beam impinges normally on such a target. Examination of the relations covered in past sections indicates that the most favorable conditions for the collector are obtained at low energies (up to a few kev) for a normally incident beam.

A search for optimum collector geometry has been conducted (Ref. 46). Some of the configurations include honeycomb-type surfaces and variously arranged fin-covered walls. Preliminary data from such arrangements indicate that very little is gained by the introduction of fins and wells such as an egg crate structure into the collector. This can be understood by examining Eq. (55). The value for area to be used in that equation must be an unshadowed area and hence can be considered to be the area of an imaginary smooth surface surrounding the target. The magnitude of such a surface cannot be increased by the addition of fins or plates because the first collision with the wall contributes by far the most to the pressure ($k \approx 1$). Such fins can only serve as cryosurfaces to reduce residual gas pressure or for beams composed of molecules which do not condense in the first few collisons. Furthermore, the use of finned or honeycombed surface targets does not prove feasible for long term tests where the beam energy is not reduced because of surface erosion problems.

4.6.2 Long Term Tests Using Solid Collectors

For long term tests, Fig. 28 illustrates that solid targets could be used in an unmodified beam only by continuously replacing targets as they are deteriorated by the beam. Replacing a large target without breaking the vacuum is quite a formidable task.

One very important phenomenon which has been observed may offer the solution to problems presented by sputtering. It was previously described as "zero sputtering" and can be controlled and employed only if the beam can be decelerated by some means to an energy level so that the collection efficiency at the target is greater than the self-sputtering coefficient. Then equilibrium conditions would be established without appreciable damage to the target for tests of any duration.

In principle, it is possible to retard the beam by having the collector at a high voltage. However, the retarding field also acts as an electrostatic lens, which causes defocusing of the beam at low energies. By using a suitably shaped collector arrangement, Elbeck, Oleson, and others have reported a solution to overcome this defocusing (Ref. 54).

For any decelerating system, a convenient method for ascertaining the desired ion energy is similar to that used by Wehner to determine

sputtering thresholds (Ref. 55) employing emission spectroscopy. When zero sputtering conditions are met and equilibrium is established, no spectral lines characteristic of the target can be detected by the spectrometer. If it is possible to achieve the phenomenon described as zero sputtering, there is little question that herein lies the solution of the sputtering problem in electrical propulsion test facilities.

Some of the criteria which must be considered in the selection of materials for collector systems are:

1. electrical conductivity
2. thermal conductivity
3. sputtering coefficient
4. secondary emission properties
5. vapor pressure at operating temperature of thruster components
6. economy

The above criteria and the data in Figs. 29a, b, c, and d (Refs. 56 and 57) on the sputtering yield of various targets by Hg^+ and Xe^+ indicate that the most favorable target materials are aluminum, nickel, and iron. The Xe^+ ion is chosen because it behaves quite similarly to Cs^+ (Ref. 20). Even though these metals do not exhibit the lowest sputtering yields, they were chosen for economy or, more important, for the high vapor pressure characteristics they exhibit at the operating temperatures of typical thruster components. For example, the components of cesium contact engines generally operate at temperatures of approximately 1400°K. Therefore, while a material such as carbon appears because of its small sputtering ratio to be favorable, its use must be avoided because its vapor pressure at 1400°K is very low (approximately 10^{-10} torr) and could cause failure by condensing on vital parts of the ion engine (for example on the ionizer). Of the three collector materials mentioned above, aluminum possesses the most favorable overall properties (note the erosion rates in Fig. 28).

4.6.3 Liquid Collector Systems

The use of a liquid metal as a collector target has been considered (Ref. 1) and appears to offer some advantages over the conventional solid system. It may, for example, eliminate collector system lifetime problems. In addition, some liquid metals have desirable characteristics when used as gettering materials. Furthermore, this suggests the possibility of collecting and reusing expended propellant by using the same type of material for the liquid metal target as is used for the propellant.

The practicality of a liquid metal system is being investigated and comparisons made with present day solid systems. Experiments are required to determine if a significant difference exists in the sputtering of a liquid and solid target. Some work has been reported at ion energies below one kev (Ref. 57) (Figs. 30 and 31); however, no precise statements can be made about sputtering ratios, distribution, or energies of sputtered particles for higher ion energies.

5.0 SUMMARY AND CONCLUSIONS

The foregoing study comprises a compilation and investigation of studies on sputtering made by numerous investigators to date. This was done with the objective of obtaining information necessary for the design of space simulation chambers for testing advanced propulsion devices for which exhaust beam termination represents a serious problem in view of its ablative action upon the target and chamber walls and its possible interaction with the system to be tested. Since no analytical treatment was found in which sputtering and saturation phenomena were accurately described over a broad energy range, a theoretical study was made.

Equations were derived leading to the sputtering ratio characteristic of two types of collision models which are applicable in different energy ranges. The resulting equations then serve as the upper and lower boundaries for a general expression throughout the two energy ranges applicable to electrostatic propulsion. The form of this equation compares favorably with experimental results obtained at other laboratories.

Also an attempt was made to establish a theoretical basis for saturation phenomena. The resulting equations are in good agreement with experimental data. Based on the above study the following conclusions are drawn:

1. To describe the sputtering phenomenon in the region of interest in ion propulsion, at least two different collision models are required.

2. The termination of an ion beam at a target can result in the addition of free target and ion beam particles into the test chamber. The amount of contamination is shown to be appreciable if a collector is not designed to accommodate this material.

3. Positive and negative ion emission from the collector is much less than secondary electron emission, which in turn is much less than neutral particle emission.

4. Under operating conditions, a solid target will become saturated with beam particles within a few milliseconds except in the presence of "zero sputtering".

5. If the energy of the ion beam can be controlled without altering operating conditions, it may be possible to collect more material than is sputtered, thus eliminating target lifetime problems.

6. It appears that xenon sputtering data can be substituted where cesium data are not available.

7. Under long term test conditions where solid targets are not adequate, the use of liquid metal targets appears feasible.

8. Experimental work is necessary in the following areas:

   a. Sputtering and saturation of solid and liquid targets by prospective propellant materials.

   b. The effect upon flight simulation of beam deceleration, sputtered particle flux, and secondary emission.

REFERENCES

1. Lennert, A. E. "Electrical Propulsion Testing Research at the Arnold Engineering Development Center." AIAA Summer Meeting, June 17 - 20, 1963, No. 63-240.

2. Keller, T. A. "NASA Electric Rocket Test Facilities." Vacuum Symposium Transactions P161 M60.

3. Stuart, R. V. and Wehner, G. K. "Sputtering at Very Low Bombarding Ion Energies." Journal of Applied Physics, Vol. 33, No. 7, 2345-2352, July 1962.

4. Harrison, D. E. and Yonts, O. C. "Survey of High Energy Sputtering Experiments." A.R.S. Paper No. 1752-61, May 3 - 5, 1961.

5. Gronlund, F. and Moore, W. J. "Sputtering of Silver by Light Ions with Energies from 2 to 12 kev." Journal of Chemistry and Physics, Vol. 32, No. 5, 1540-S, May 1960.

6. Kenknight, C., to be published, Journal of Applied Physics.

7. Bader, M., Witteborn, F. Z. and Snouse, I. W. "Sputtering by Mass Analyzed N_2^+ and N^+." NASA TRR-105.

8. Laegreid, N. and Wehner, G. K. "Sputtering Yields of Metals for Ar^+ and Ne^+ Ions with Energies from 50 to 600 ev." Journal of Applied Physics, Vol. 32, No. 3, March 1961.

9. Almén, O. and Bruce, G. "Collection and Sputtering Experiments with Noble Gas Ions." Nuclear Instruments and Methods, Vol. II, 1961, pp. 257-273.

10. Yonts, O. C. and Harrison, D. E. "Surface Cleaning by Cathode Sputtering." Journal of Applied Physics, Vol. 31, No. 9, September 1960.

11. Rol, P. K. and Fluit, J. M., Viehboech, F. P., and de Long, M. "Sputtering of Copper Monocrystals by Bombardment with 20 kev Ar^+." Procedures of the Fourth Conference on Ionic Phenomena in Gases, Uppsala, North Holland Publication Co., Amsterdam, 1959.

12. Fogel, Y. M., Slabospitskii, R. P., and Karnaukhov, I. M. "Mass Spectrometer Investigation of Secondary Positive and Negative Ion Emission Resulting from the Bombardment of an Mo Surface by Positive Ions." Zhurn. Tek. Fiz., Vol. 30, No. 7, July 1960, pp. 777-785, 824-834.

13. Wehner, G. K. and Rosenberg, D. "Angular Distribution of Sputtered Material." Journal of Applied Physics, Vol. 31, No. 1, January 1960, pp. 177-179.

14. Patterson, H., and Tomlin, D. N. "Experiments by Radioactive Tracer Methods on Sputtering by Rare Gas Ions." Proceedings of the Royal Society of London, Series A, Vol. 265, 1961-2, p. 474.

15. Stein and Hurlbut. "Angular Distribution of Sputtered Potassium Atoms." Journal of Applied Physics, Vol. 31, 1960, p. 177.

16. Wehner, G.K., Stuart, R. V., and Rosenberg, D. Annual Report on Sputtering Yields, General Mills Report No. 2356, 1962, pp. 43-69.

17. Wehner, G. K. "Force on Ion-Bombardment Electrodes in a Low-Pressure Plasma." Journal of Applied Physics, Vol. 31, August 1960, pp. 1392-97.

18. Wehner, G. K. "Velocities of Sputtered Atoms." Physical Review, Vol. 114, No. 5, June 1959, pp. 1270-1272.

19. Davies, J., Brown, F., and McCargo, M. "Range of Xe^{133} and Ar^{41} Ions of Kiloelectron Volt Energies in Aluminum." Canadian Journal of Physics, Vol. 41, No. 6, June 1963, pp. 829-843.

20. Rol, P. K., Book, E. P., Fluit, J. M., and Kistemaker, J. "Sputtering of Copper by Ion Bombardment in the Energy Range of 5-25 kev." Electrostatic Propulsion, Academic Press, New York, 1961, pp. 203-216.

21. Wehner, G. K. Private Communication, General Mills Electronics Division, Minneapolis, Minnesota.

22. Davies, J. Private Communication, Atomic Energy of Canada Limited, Chalk River, Ontario.

23. Massey, H. S. W. and Burhop, E. H. S. Electronic and Ionic Impact Phenomena. Clarendon Press, Oxford, 1952.

24. Bader, M., and Savage, H. F. "Momentum Accommodation Above the Sputtering Threshold." Proceedings of the Eighth Conference on Ionization Phenomena in Gases, Paris, 1963.

25. Arifov, U. A., Ainkhanov, KH. A. and Starodubtow, S. V. "Ion Scattering Coefficient as a Function of Colliding-Particle Mass Ratio." Soviet Physics-JETP, Vol. 6 (33), No. 4, April 1958, p. 653.

26. Hagstrum, H. D. "Reflection of Noble Gas Ions at Solid Surfaces." Physical Review, Vol. 123, No. 3, August 1961, p. 758.

27. Hachenberg, O., and Brauer, W. "Secondary Electron Emission." Advances in Electronics and Electron Physics, Vol. 11, 1959.

28. Bruining, H. Secondary Electron Emission, McGraw-Hill, New York, 1954.

29. Telkoviski, V. G. "Secondary Emission from Metals Induced by Ions and Neutral Particles." Soviet Physics-Doklady, Vol. 1, 1956, p. 334.

30. Cheney, W. L. "The Emission of Electrons by a Metal when Bombarded by Positive Ions in a Vacuum." Physical Review, Vol. 10, No. 4, 1917, pp. 325-347.

31. Jackson, W. J. "Secondary Emission from Metals Due to Bombardment of High Speed Positive Ions." Physical Review, Vol. 28, 1926, pp. 524-30, and "Secondary Emission from Mo Due to Bombardment by High Speed Positive Ions of the Alkali Metals." Physical Review, Vol. 30, 1927, pp. 473-478.

32. Kuskevics, R. C., et. al. "Ionization, Emission, and Collision Processes in the Cesium Ion Engine." Electrical Propulsion Conference, March 1962, American Rocket Society Paper.

33. Waters, Paul. "Kinetic Ejection of Electrons from Tungsten by Cesium and Lithium Ions." Physical Review, Vol. III, No. 4, 1958, pp. 1053-1061.

34. Large, L. N. "Secondary Ion-Induced Electron Emission from Tungsten." Proceedings of the Physical Society, Vol. 81, 1963, p. 1101.

35. Keywell, F. "Measurements and Collision-Radiation Damage Theory of High-Vacuum Sputtering." Physical Review, Vol. 97, No. 6, March 15, 1955, p. 1611.

36. Rol, P. K. "Sputtering of Copper by Ion Bombardment of 5-25 kev." AEC-TR-4448 ORNL, Thesis, Amsterdam, 1960.

37. Langberg, E. "Analysis of Low Energy Sputtering." Unpublished Thesis, Princeton, 1956.

38. Goldman, D. T. and Simon, A. "Theory of Sputtering by High-Speed Ions." Physical Review, Vol. III, No. 2, 383-6, July 15, 1958.

39. Pease, R. S. "Sputtering of Solids by Penetrating Ions." Rend. Scuola Intern. Fis., Enrico Fermi. Corso XIII 1959, 1960, pp. 158-65.

40. Harrison, D. E. "Extended Theory of Sputtering." Journal of Chemical Physics, Vol. 32, No. 5, May 1960, p. 1336.

41. Hippel, A. von. "Theory of Kathode Scattering." Annalen der Physik, Vol. 81, December 11, 1926, pp. 1043-1076.

42. Bohr, N. "Penetration of Atomic Particles Through Matter." Det Kgl. Danske Viden. Sel., 1948.

43. Davies, J. A., and Sims, G. A. "The Range of Na^{24} Ions of kev Energies in Aluminum." Canadian Journal of Chemistry, Vol. 39, 1961, p. 601.

44. Smith, M. L. Electromagnetically Enriched Isotopes and Mass Spectrometry. Contribution by Nielsen, K. O. "The Range of Atomic Particles with Energy About 50 kev." Butterworth, 1956, p. 68.

45. Wehner, G. K. "Sputtering Yields for Normally Incident Hg^{+}-Ion Bombardment at Low Ion Energy." Physical Review, Vol. 108, No. 1, October 1, 1957, pp. 35-45.

46. Richley, E. A. and Cybulski, R. J. "High Vacuum Condenser Design: Experimental Effects from Cesium and Mercury Ion Beams." NASA TN-D-1217, August 1962.

47. Richley, E. A., Cybulski, R. J., and Keller, T. A. "Experimental Evaluation of High Vacuum Condensers in Large Vacuum Facilities." Transactions of the Eighth Vacuum Symposium, Vol. 2, 1961.

48. Mickelsen, W. R., and Childs, J. H. "Theoretical Analysis of Ultrahigh Vacuum Condensers." The Review of Scientific Instruments, Vol. 29, 1958.

49. Almén, O., and Bruce, G. "Sputtering Experiments in the High Energy Region." Nuclear Instruments and Methods, Vol. 2, 1961.

50. Brown, F., and Davies, J. "The Effect of Integrated Flux on the Rentention and Range of Inert Gas Ions Injected at kev Energies in Metals." Canadian Journal of Physics, Vol. 41, No. 6, June 1963, pp. 844-857.

51. Davies, J. A., et. al. "The Range of Alkali Metal Ions of Kilo-electron Volt Energies in Aluminum." Canadian Journal of Chemistry, Vol. 38, 1960, pp. 1535-1546.

52. Yonts, O. C. Private Communication, Oak Ridge National Laboratory.

53. Present, R. D. Kinetic Theory of Gases, McGraw-Hill, New York, 1958, p. 29.

54. Elbeck, B., Olesen, M. C., and Skilbreid, O. "Inelastic Scattering from Separated Lutecuim Isotopes." Nuclear Physics, Vol. 10, 1959, pp. 294-305.

55. Wehner, G. K. "Sputtering Yields Data in the 100-600 ev Range." General Mills Report No. 2309, 1962.

56. Stuart, R. V., and Wehner, G. K. "Sputtering Yields at Very Low Bombarding Energies." Journal of Applied Physics, Vol. 33, 1962, pp. 2345-52.

57. Wehner, G. K. "Annual Report on Sputtering Yields." General Mills Report No. 1902, 1959.

58. Wehner, G. K., and Rosenberg, D. "Mercury Ion Beam Sputtering of Metals at Energies 4-15 kev." Journal of Applied Physics, Vol. 31, August 1960, pp. 1392-97.

TABLE 1

VALUES OF S_{max} AND C FROM EQ. (28)

Ion	Target Material	S_{max}	C (kev)$^{-1}$	H ev
Hg^+	Cu (Ref. 58)	14.0	0.179	60
Hg^+	Ni (Ref. 58)	8.0	0.218	80
Hg^+	Fe (Ref. 58)	6.0	0.179	65
Hg^+	Al (Ref. 45)	2.4	0.218	130
Cs^+	Cu (Ref. 32)	15	0.34	60

TABLE 2

SATURATION VALUES AND TIME CONSTANTS

		μgm cm^{-2}	cm^2 sec^{-1} amp^{-1} x 10^4
Ion	Target	qs (45 kev)	Calculated decay constant / current density
Kr^+	Al	5.2	1.6
	Fe	2.1	4.0
	Ni	1.6	5.2
Xe^+	Al	4.2	3.1
	Fe	1.4	9.5
	Ni	1.5	8.8

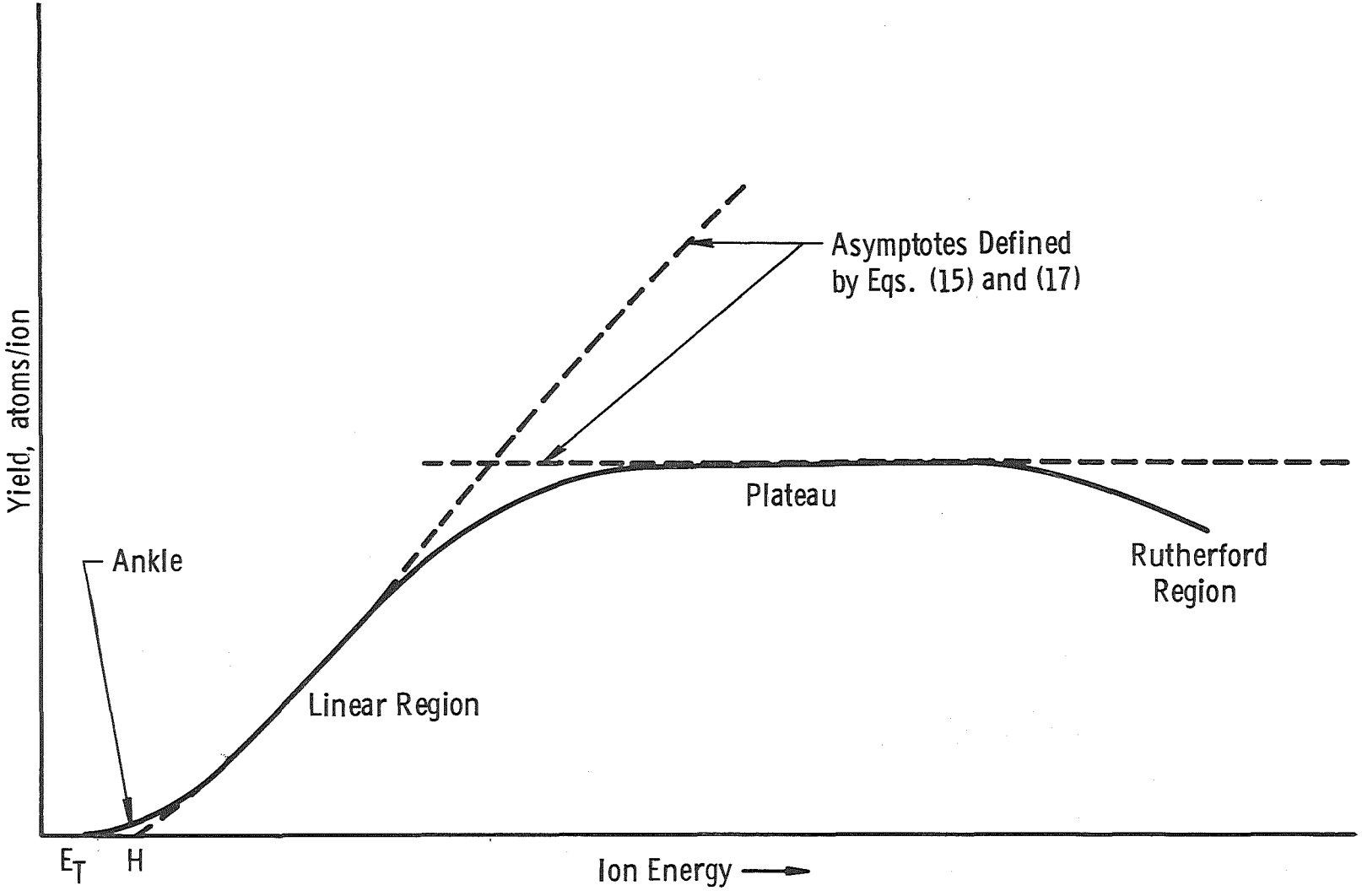

Fig. 1 Typical Sputtering Yield Curve

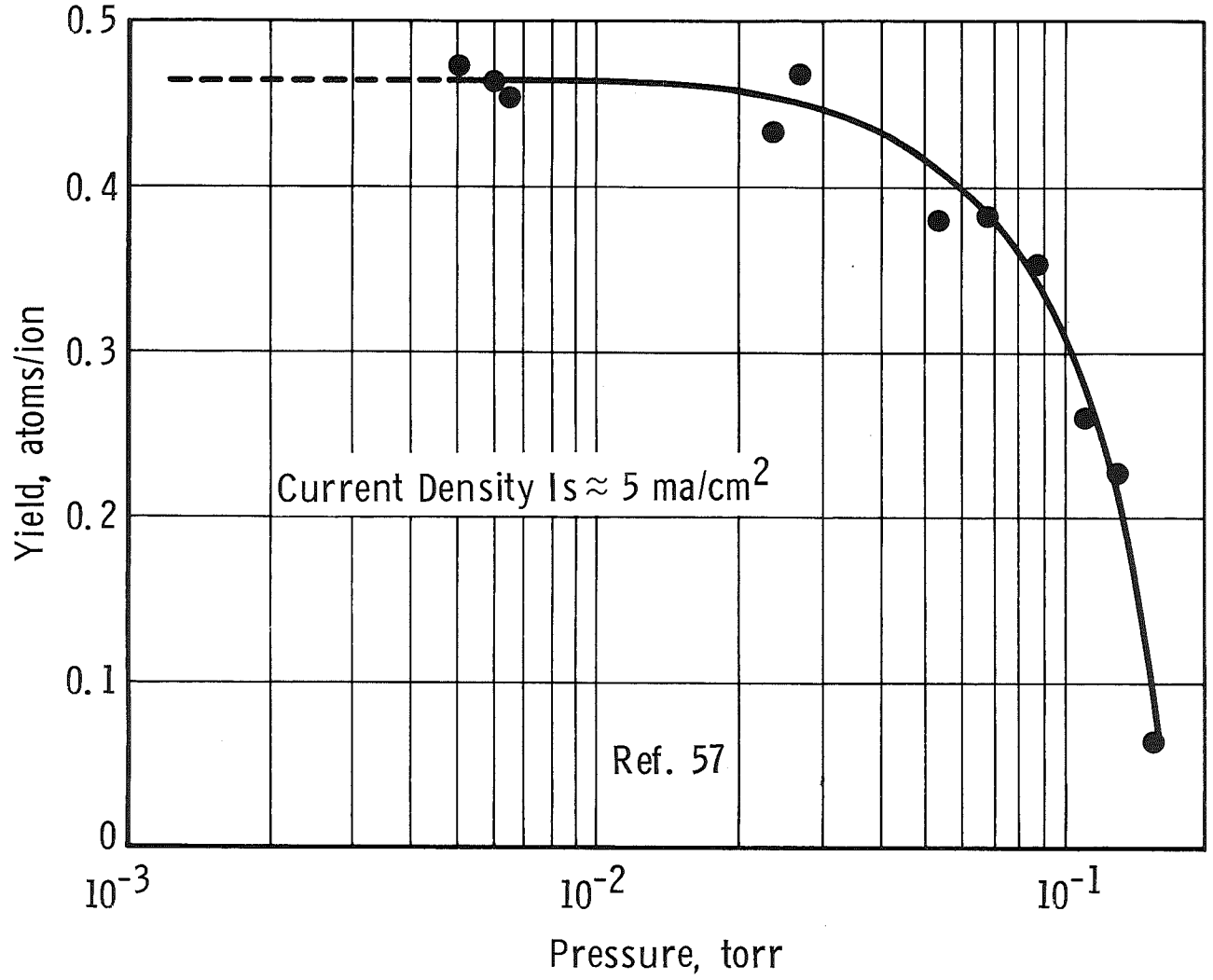

Fig. 2 Nickel Sputtering Yields at 150 ev vs Argon Pressure

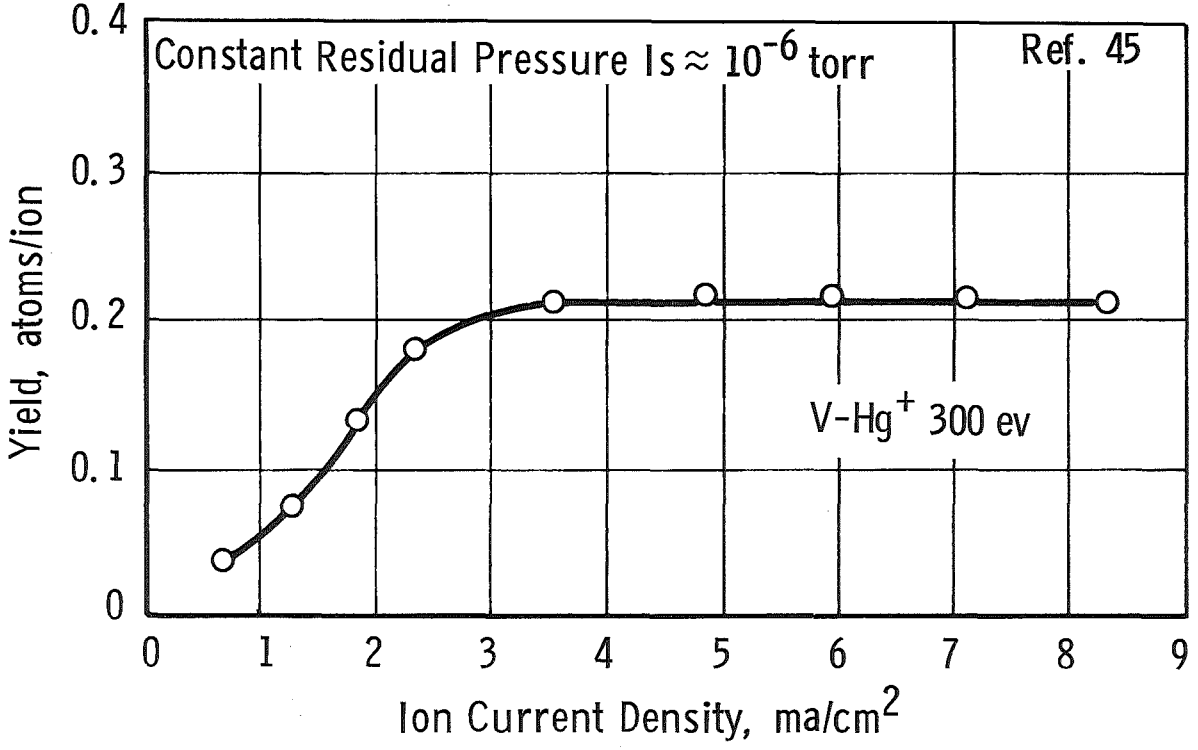

Fig. 3 Sputtering Yield of V vs Ion Current Density

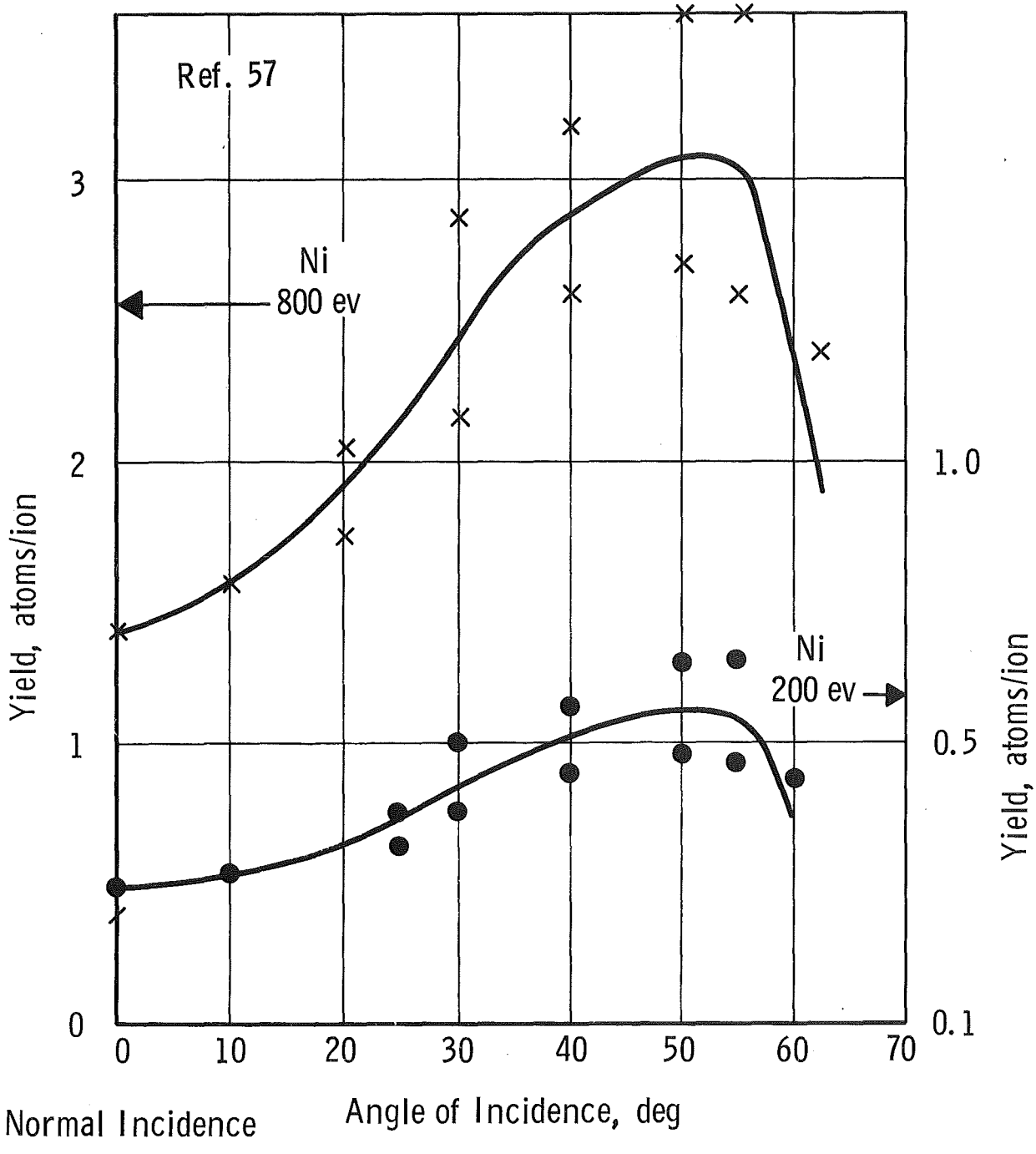

a. Ni

Fig. 4 Effect of Angle of Incidence on Sputtering Yield

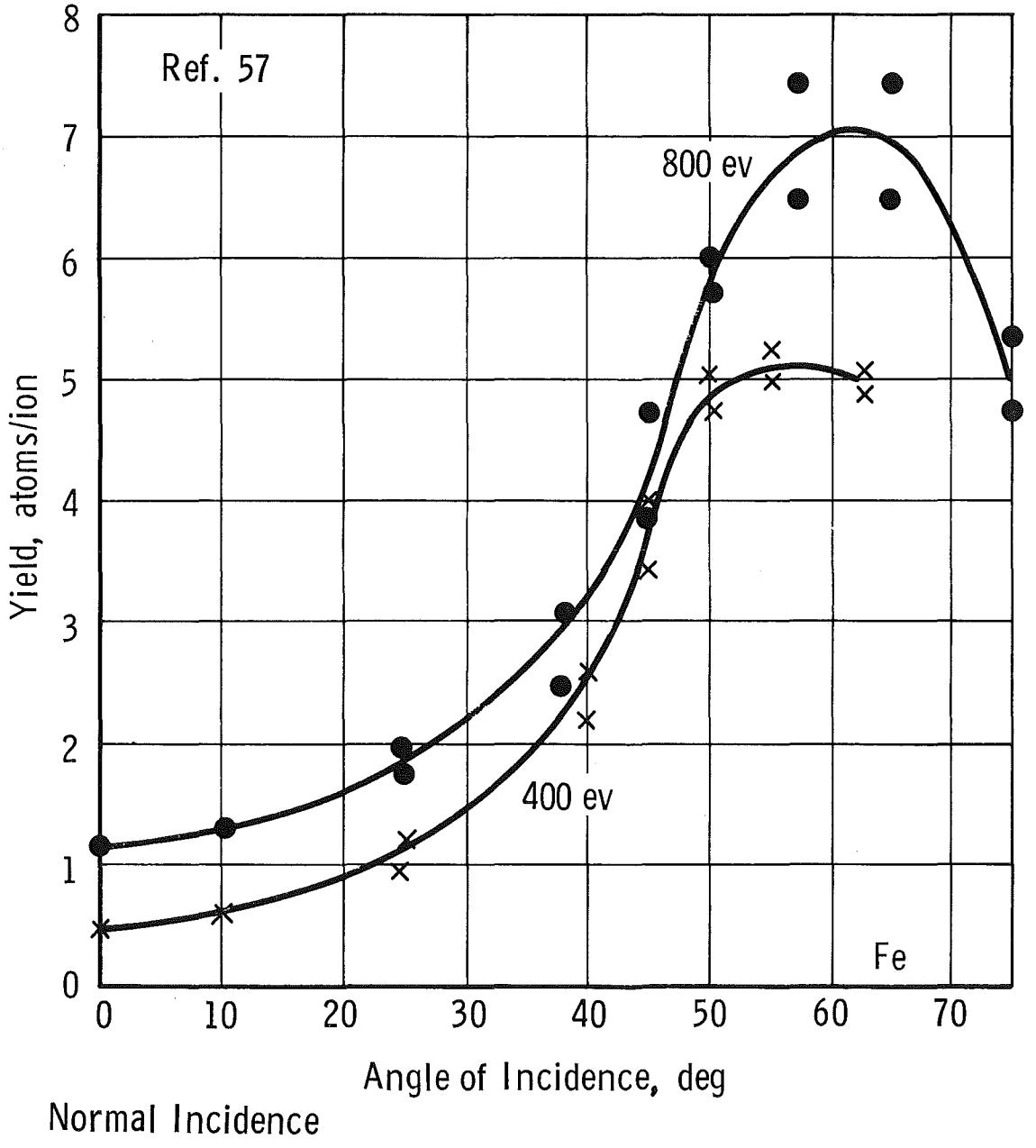

b. Fe

Fig. 4 Continued

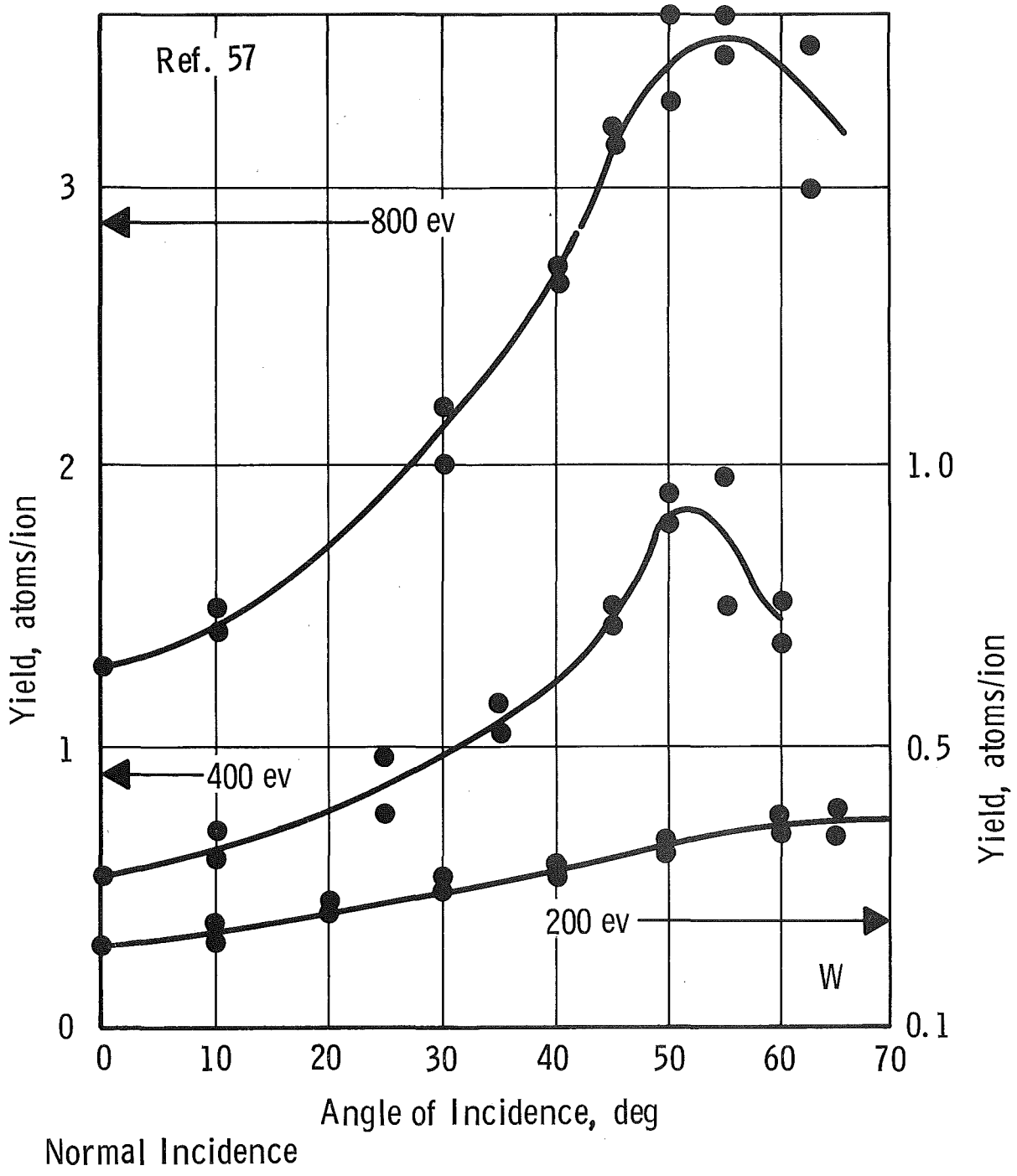

c. W

Fig. 4 Continued

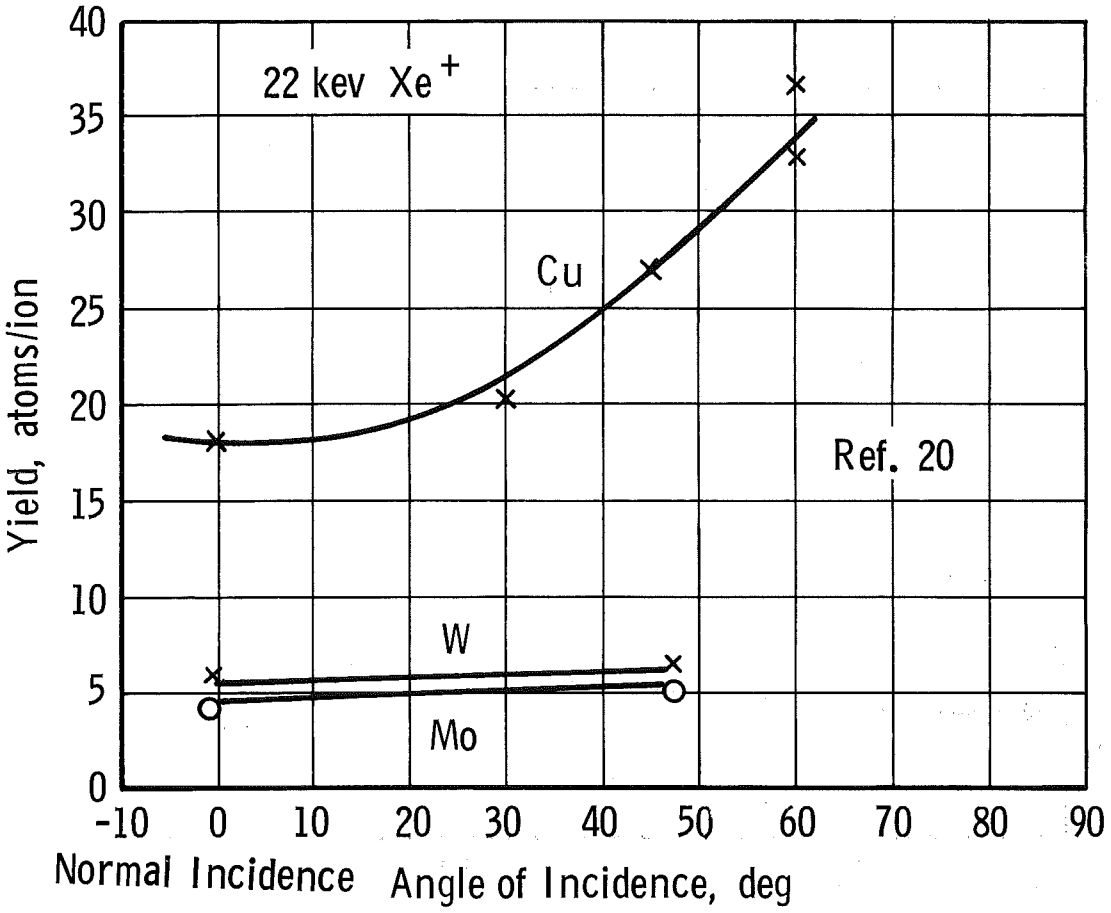

d. Cu, W, Mo

Fig. 4 Continued

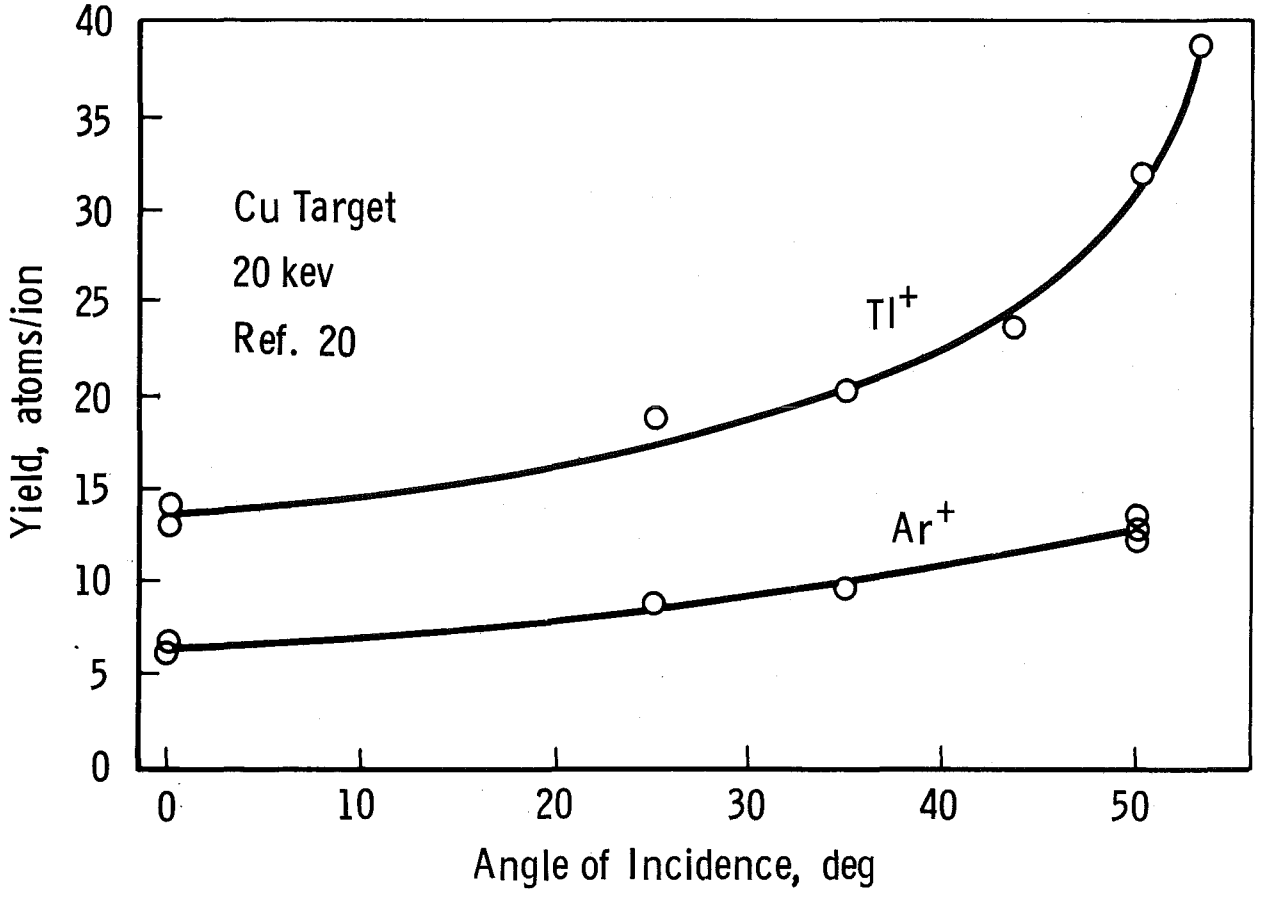

e. Cu

Fig. 4 Continued

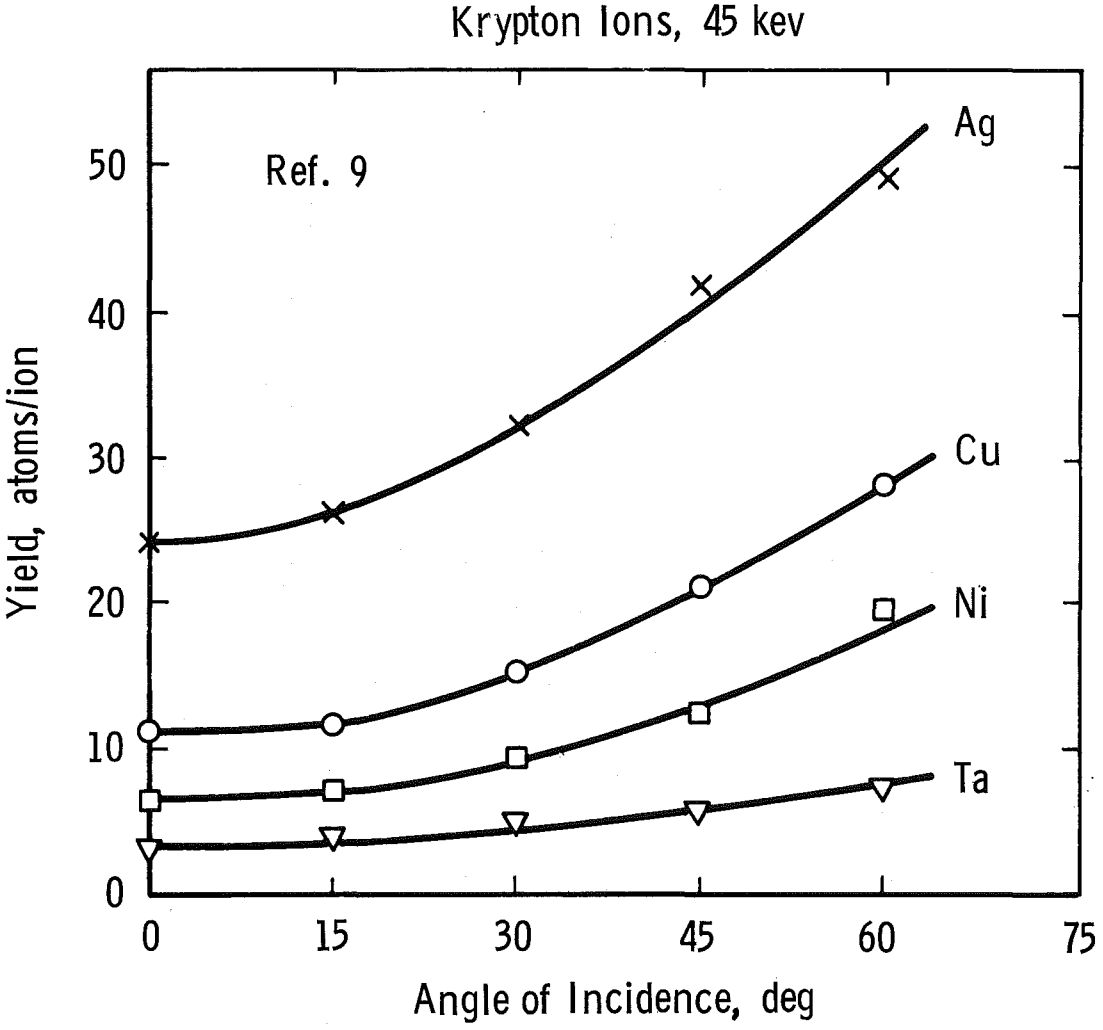

f. Ag, Cu, Ni, Ta

Fig. 4 Concluded

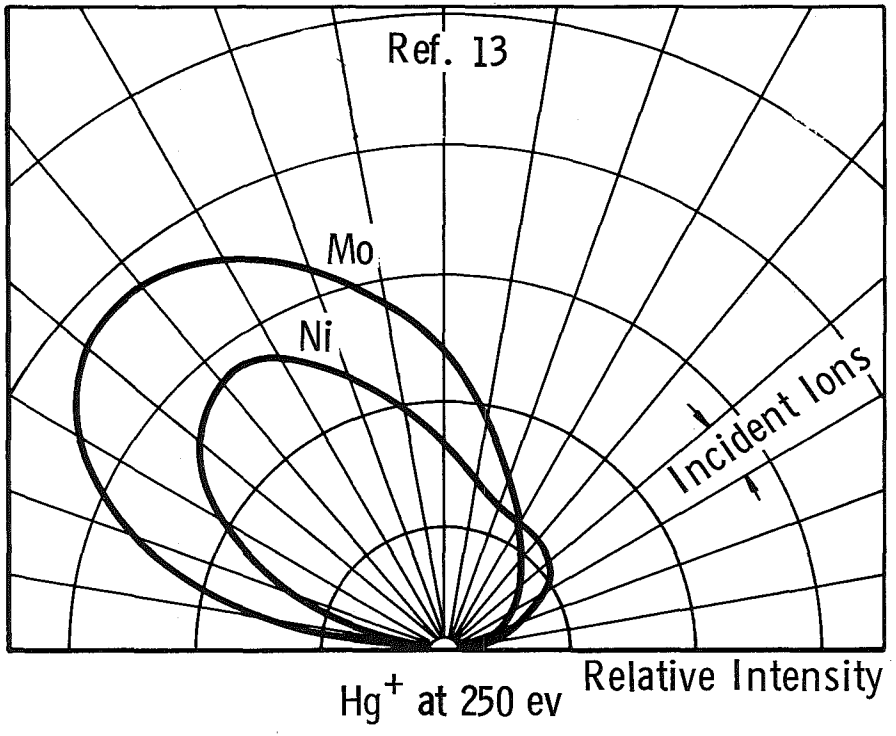

Fig. 5 Angular Distribution of Sputtered Particles at Oblique Incidence (250 ev)

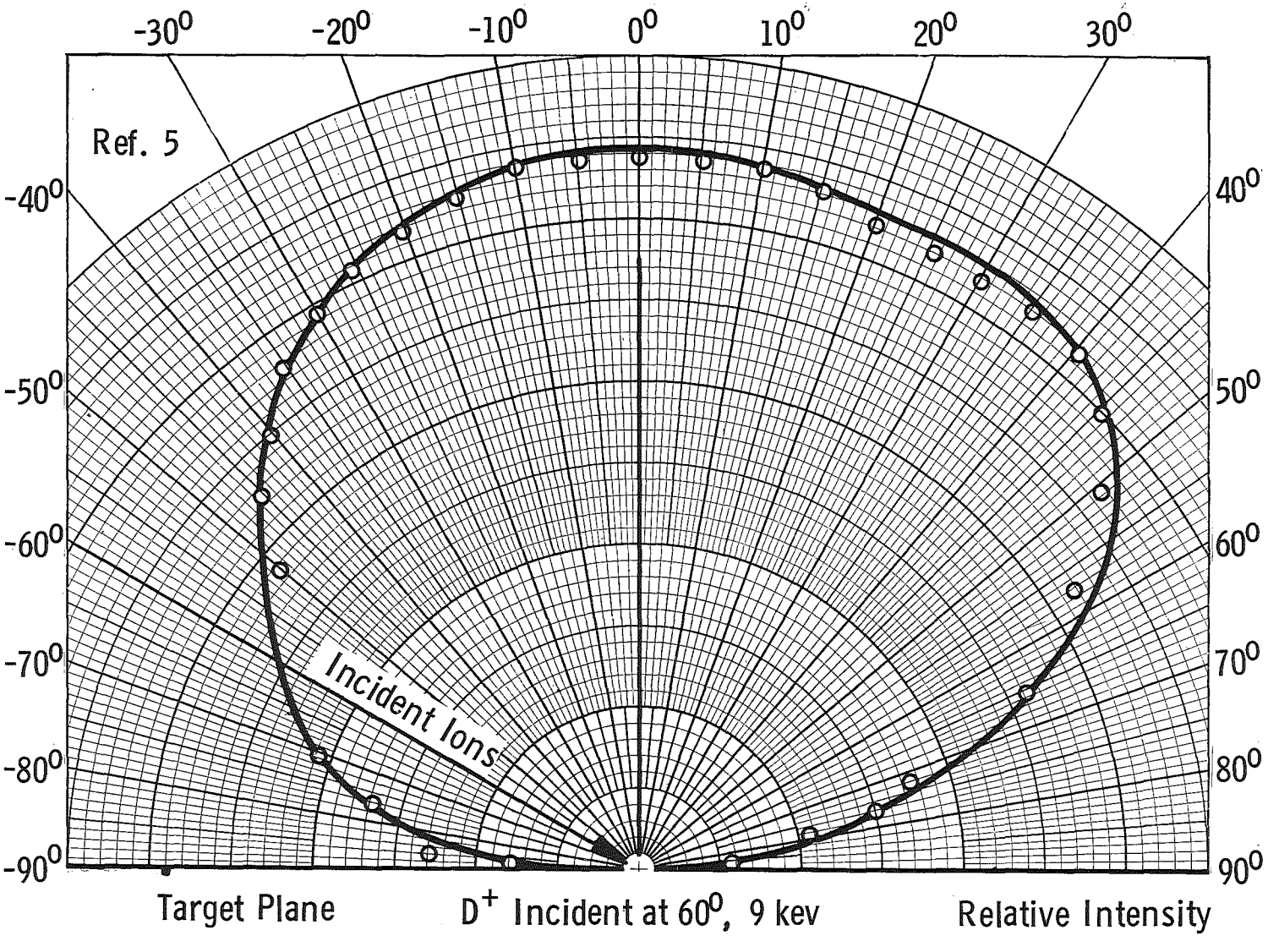

Fig. 6 Angular Distribution of Sputtered Particles at Oblique Incidence (9 kev)

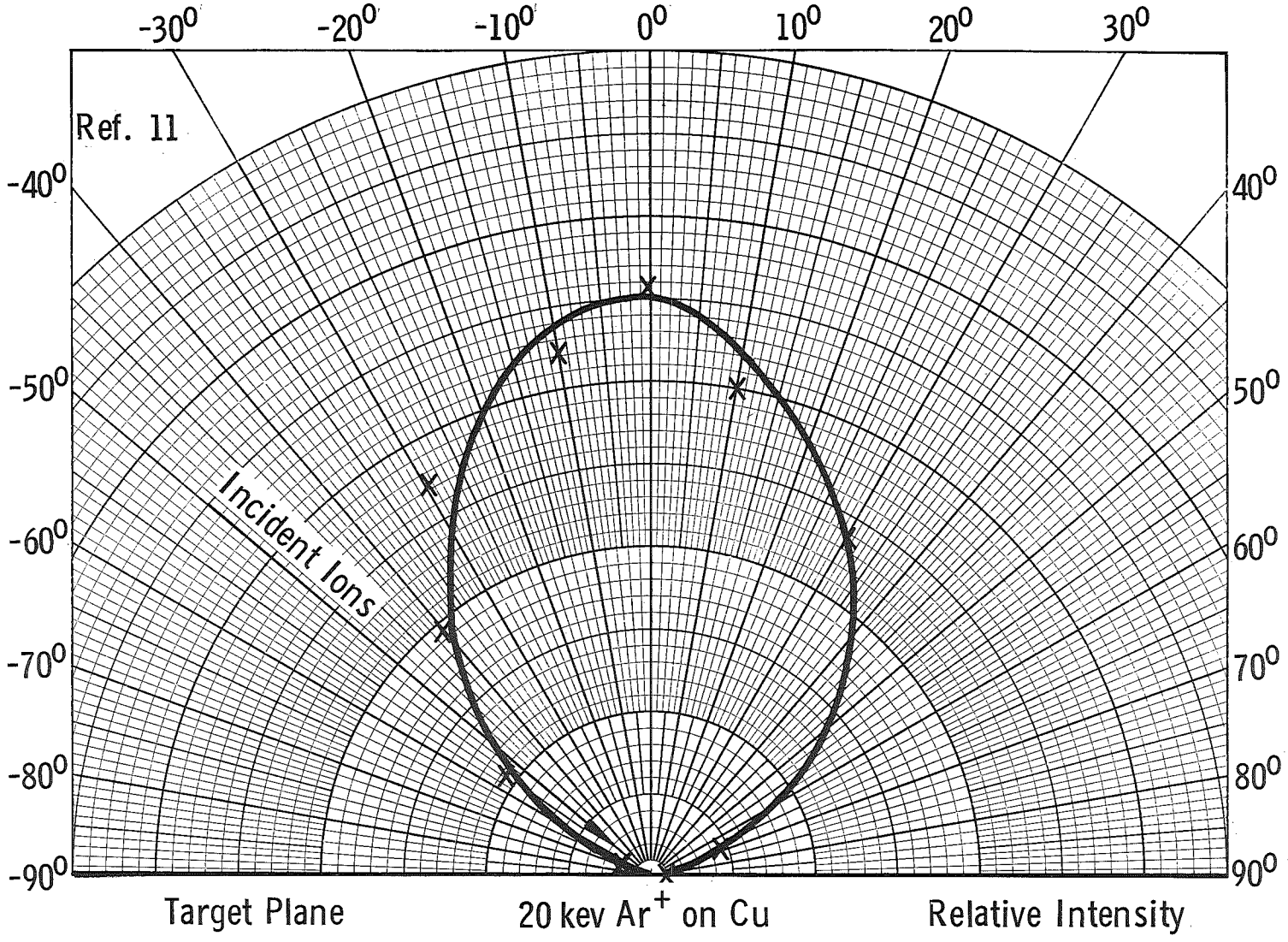

Fig. 7 Angular Distribution of Sputtered Particles at Oblique Incidence (20 kev)

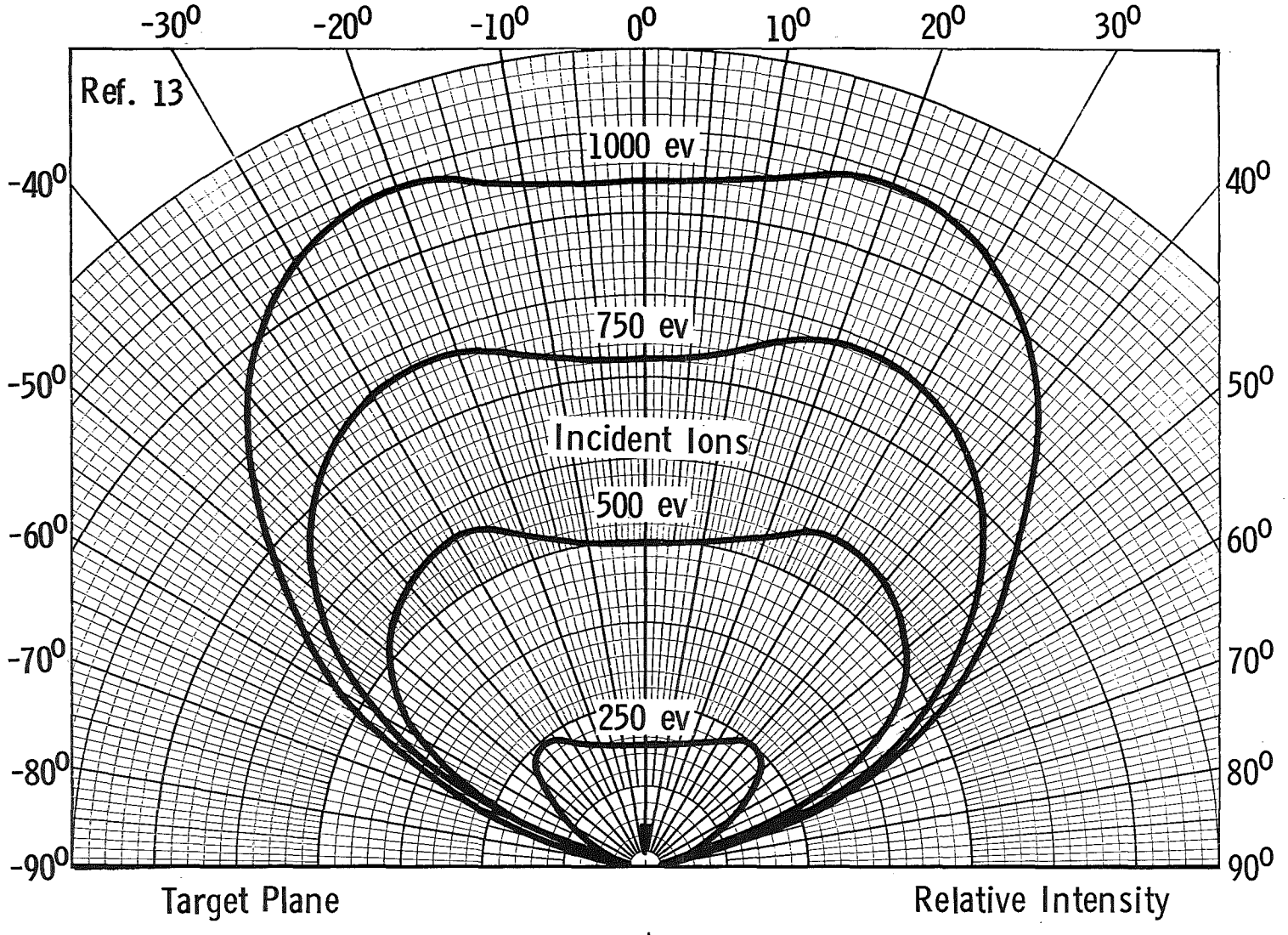

a. Hg^+ on Ni

Fig. 8 Angular Distribution of Sputtered Particles

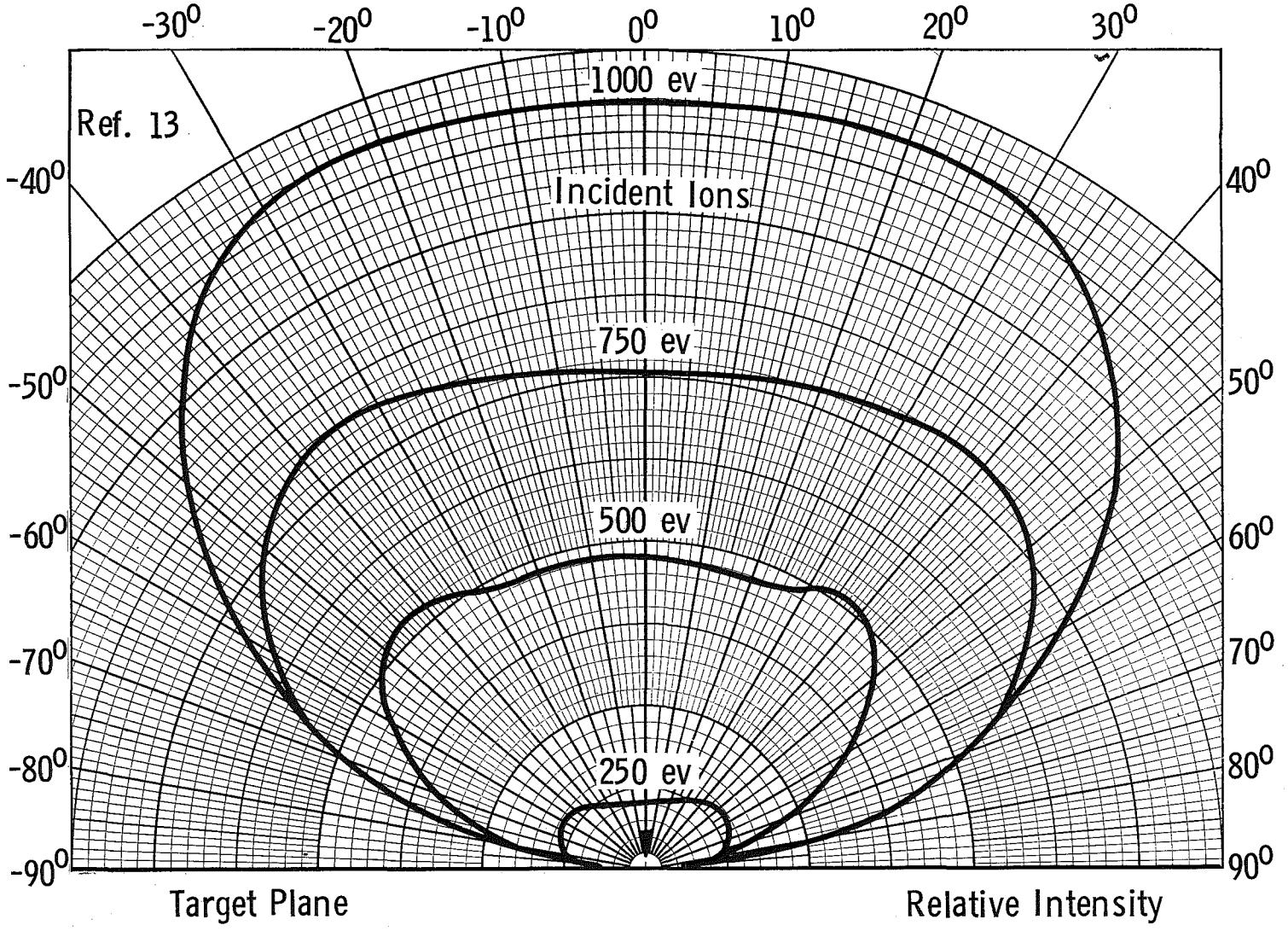

b. Hg^+ on Fe

Fig. 8 Continued

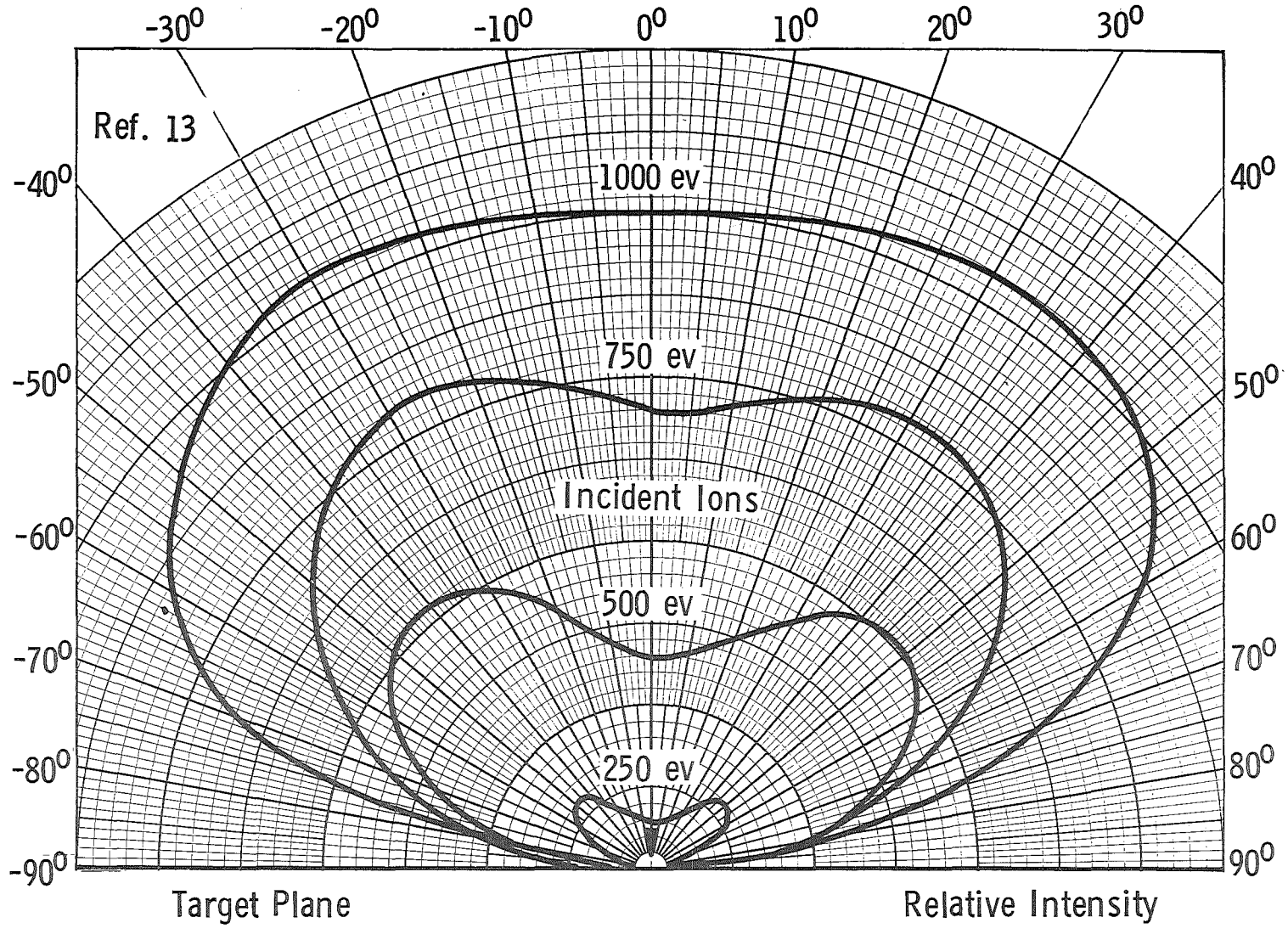

c. Hg^+ on Mo

Fig. 8 Concluded

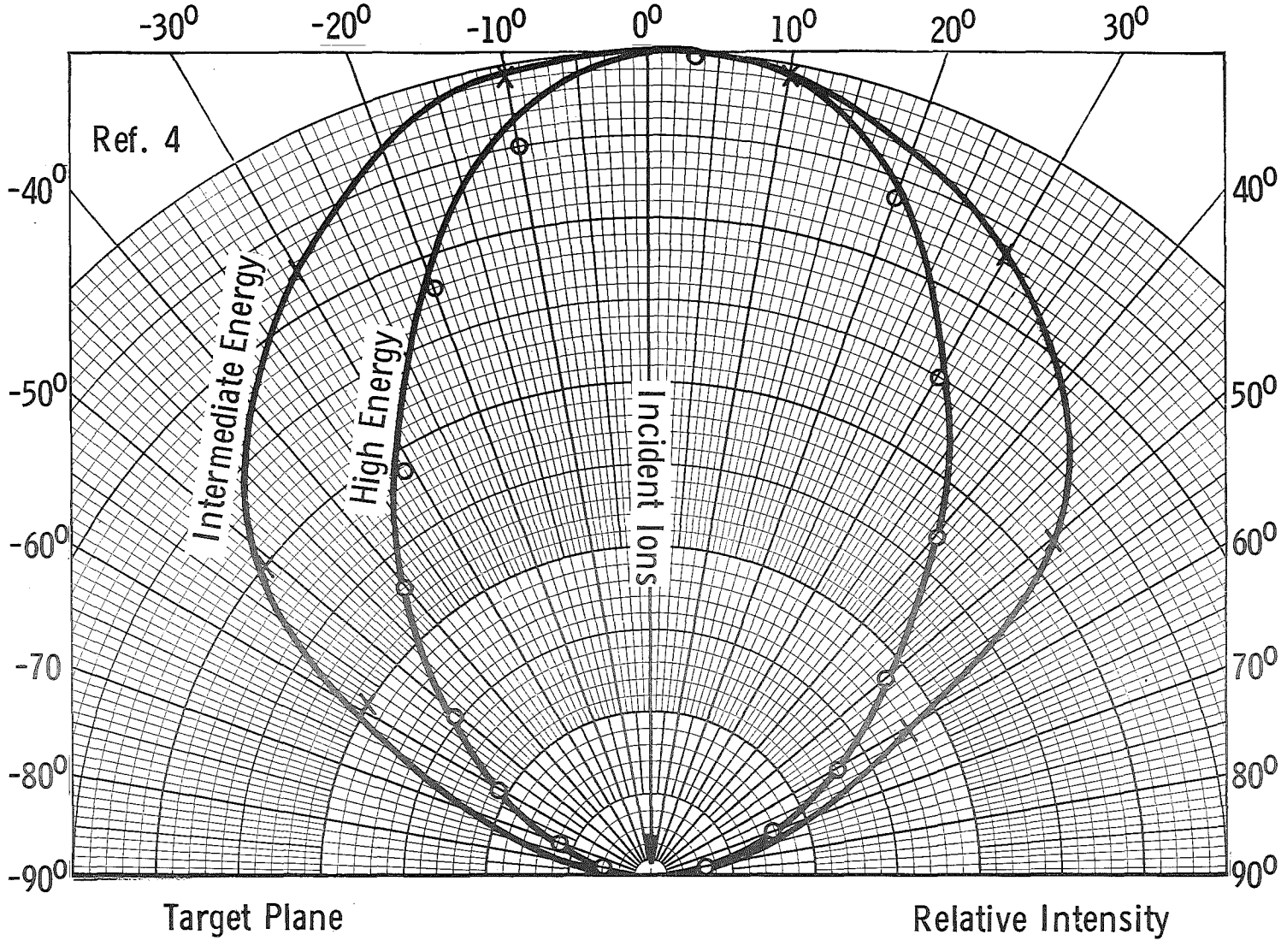

Fig. 9 Angular Distribution of Sputtered Particles

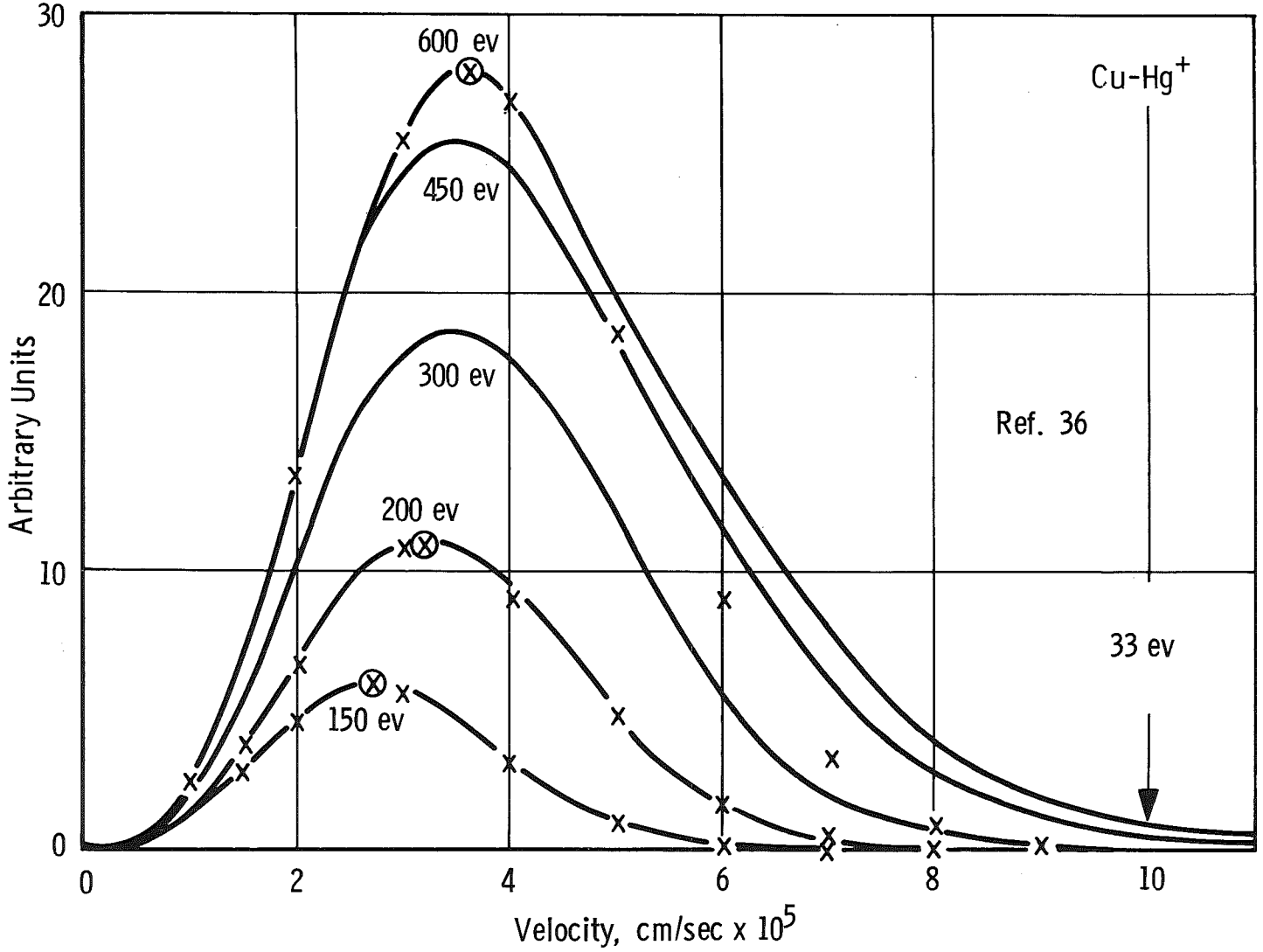

Fig. 10 Velocity Distributions of Sputtered Copper Atoms

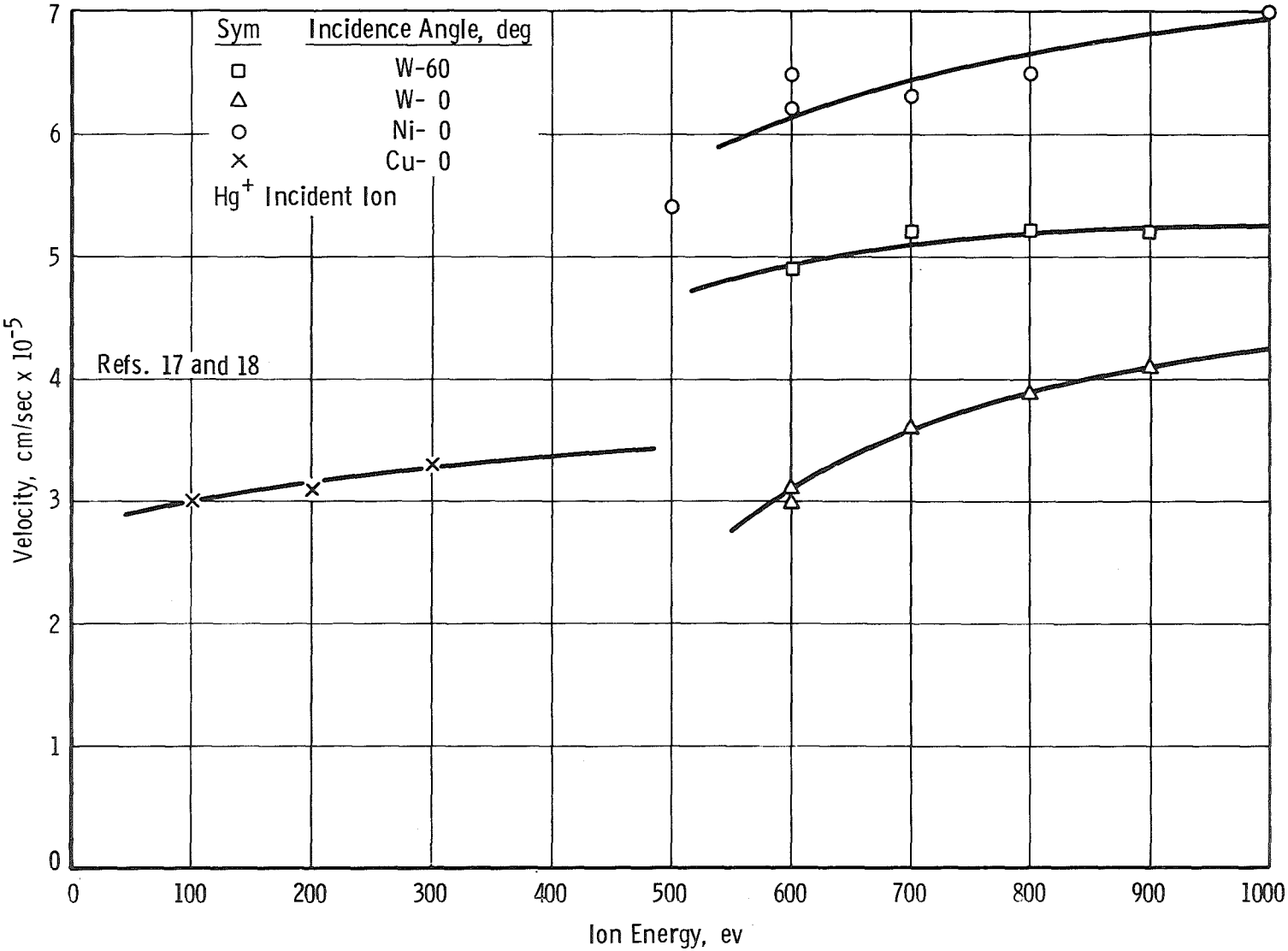

Fig. 11 Average Velocity of Sputtered Particles vs Ion Energy

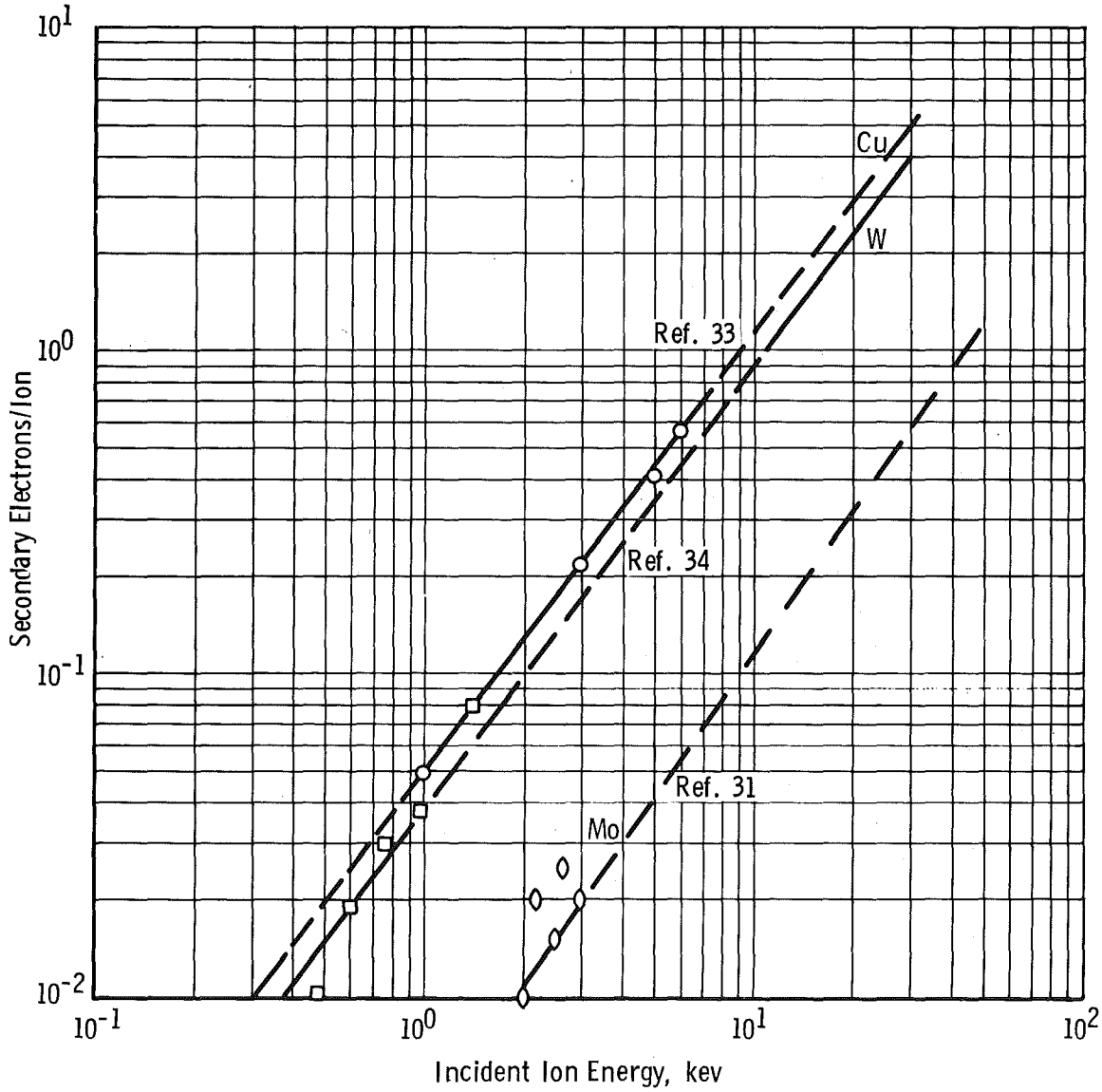

Fig. 12 Secondary Emission Coefficient vs Ion Energy (Cs^+)

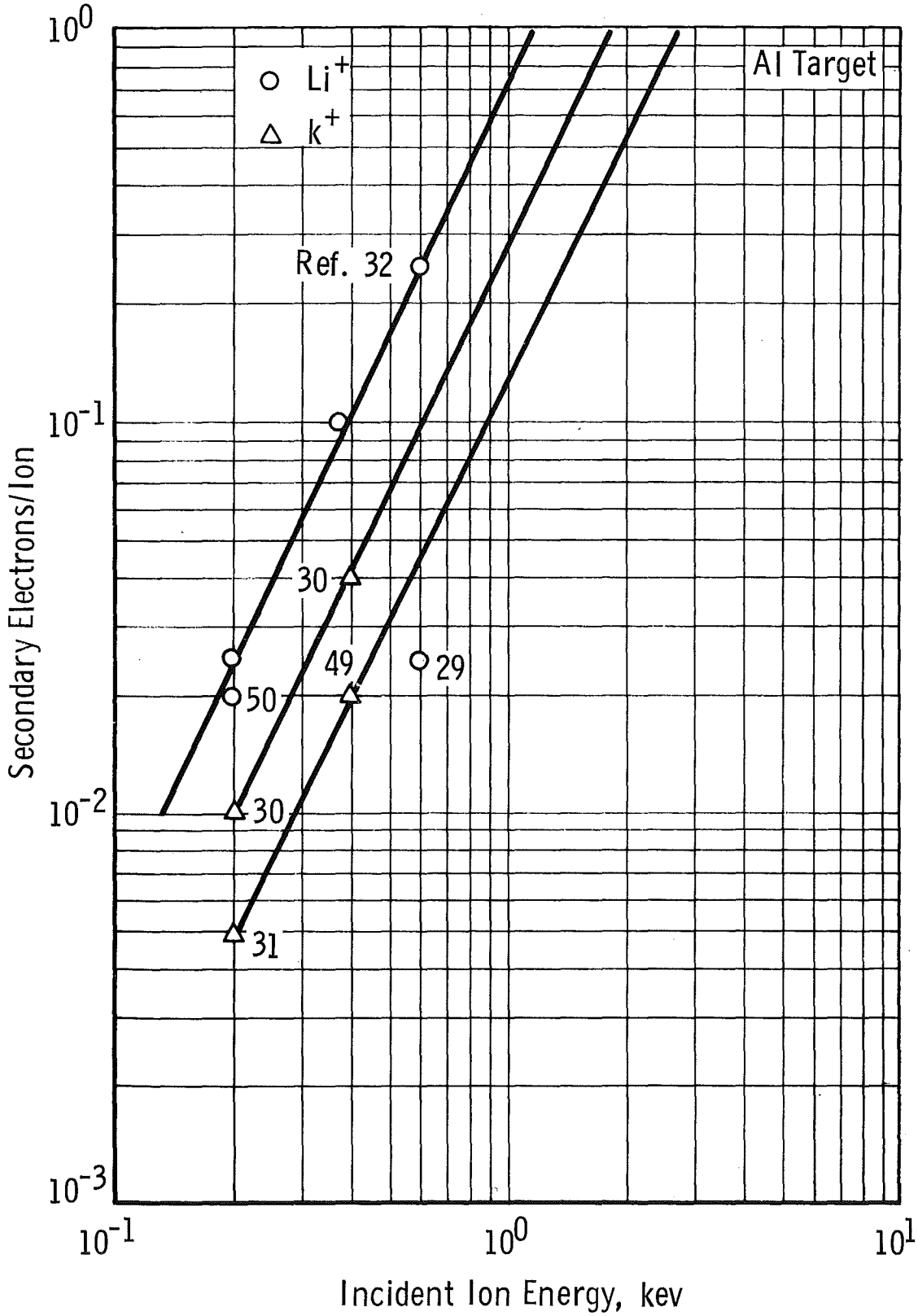

Fig. 13 Secondary Emission Coefficient vs Ion Energy (Li^+ and K^+ Ions)

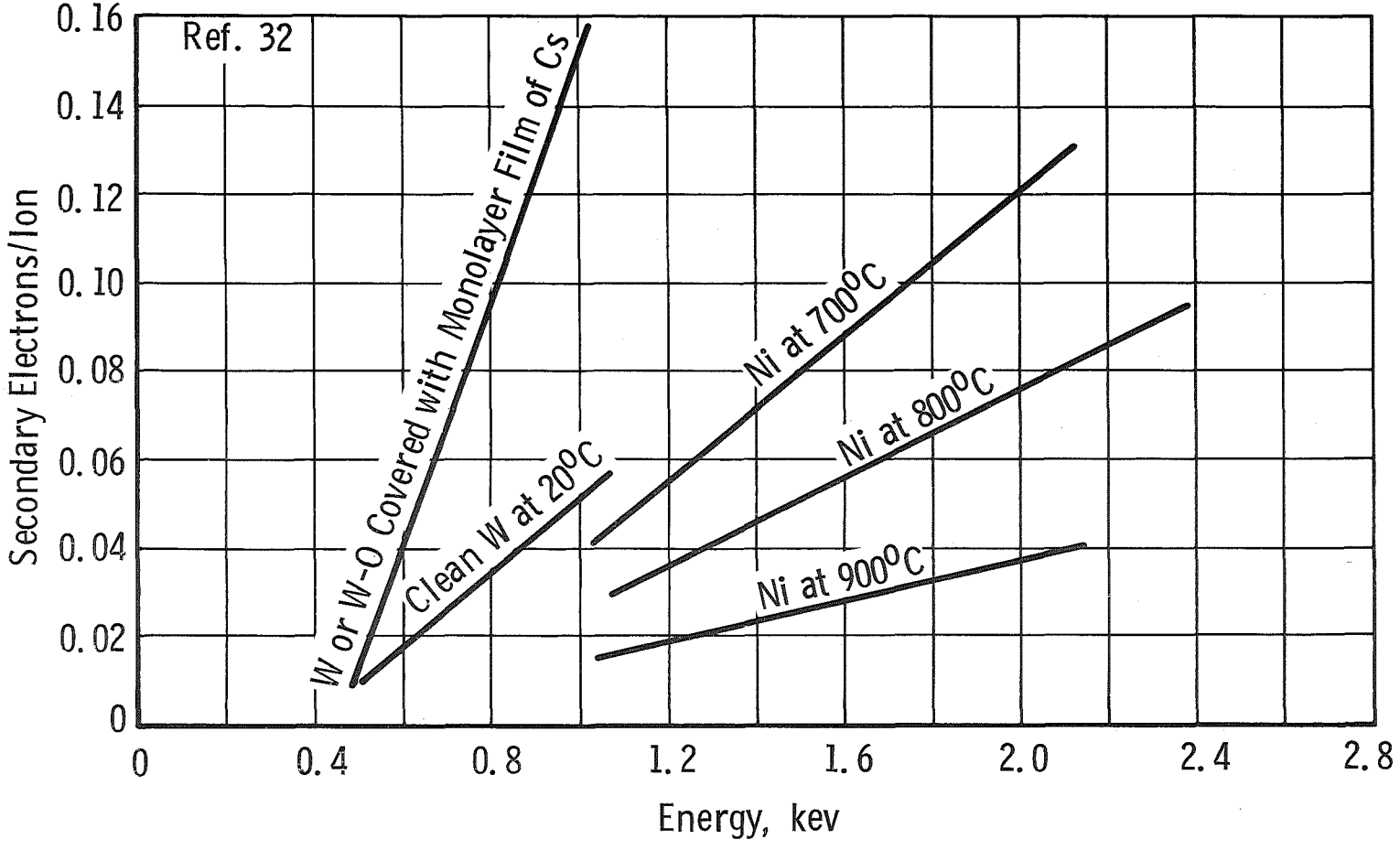

Fig. 14 Effect of Temperature and Surface Condition on Secondary Emission (Cs^+)

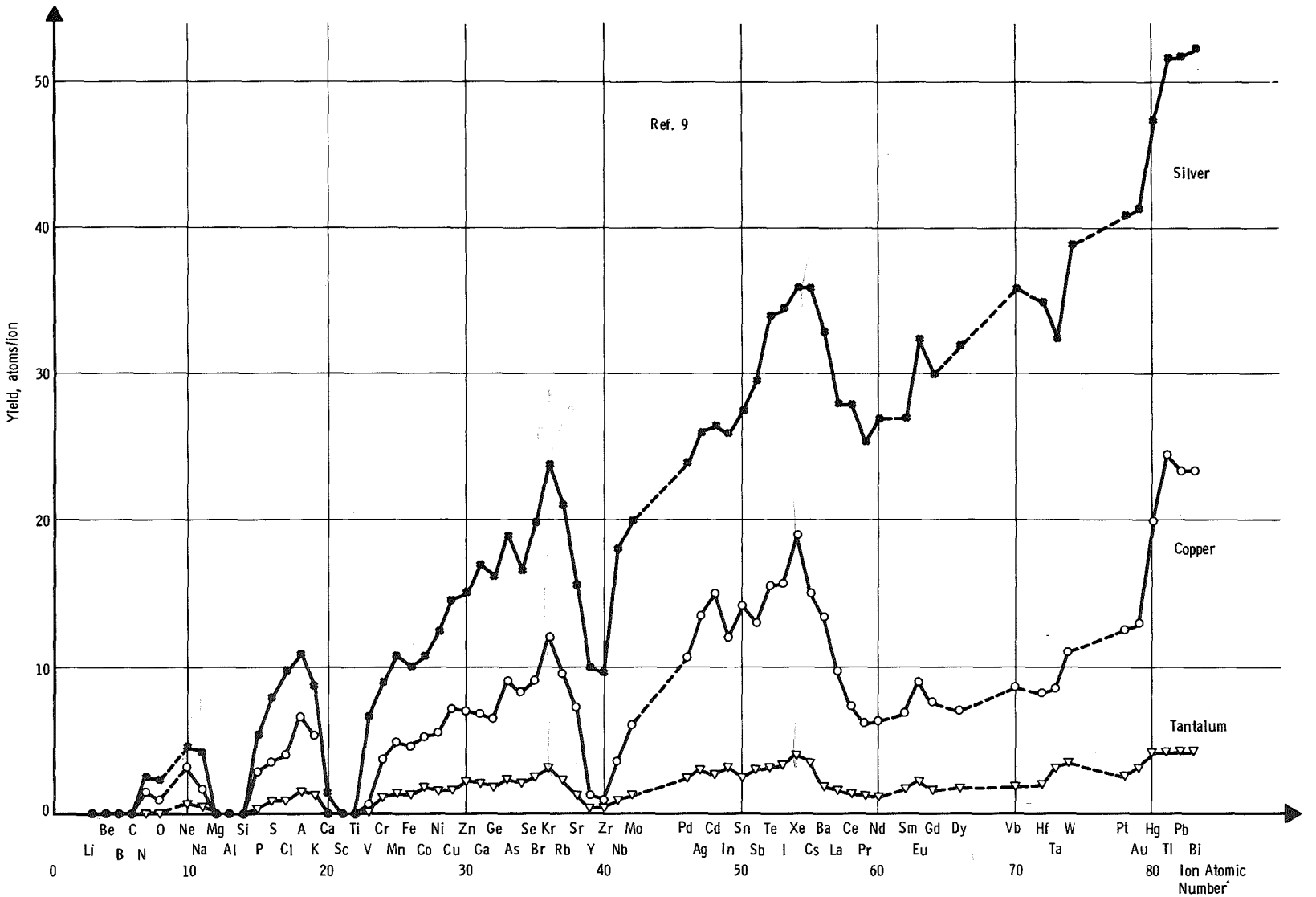

Fig. 15 Sputtering Yields for Different Ions at 45 kev

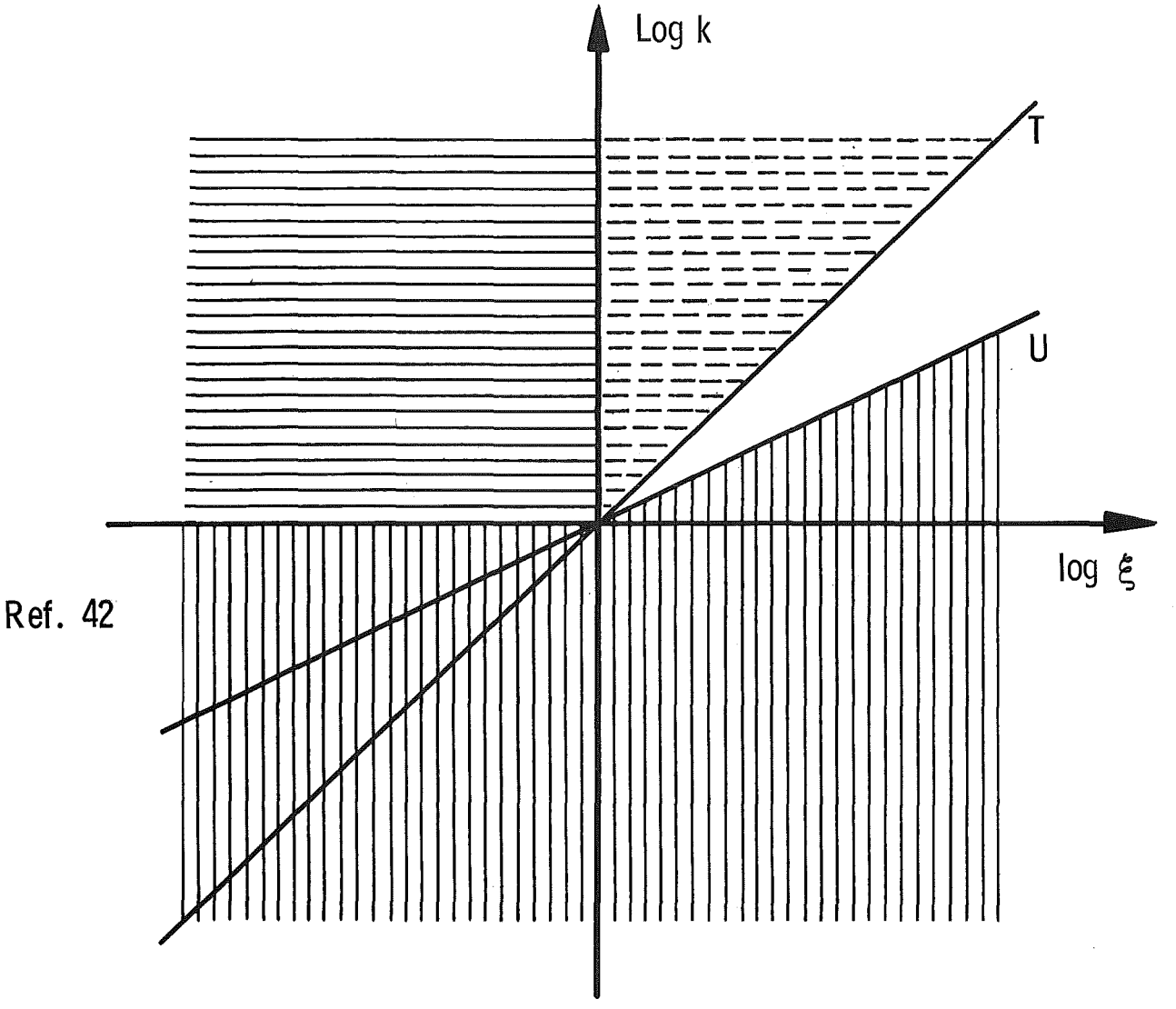

Fig. 16 Regions of Validity of Collision Models

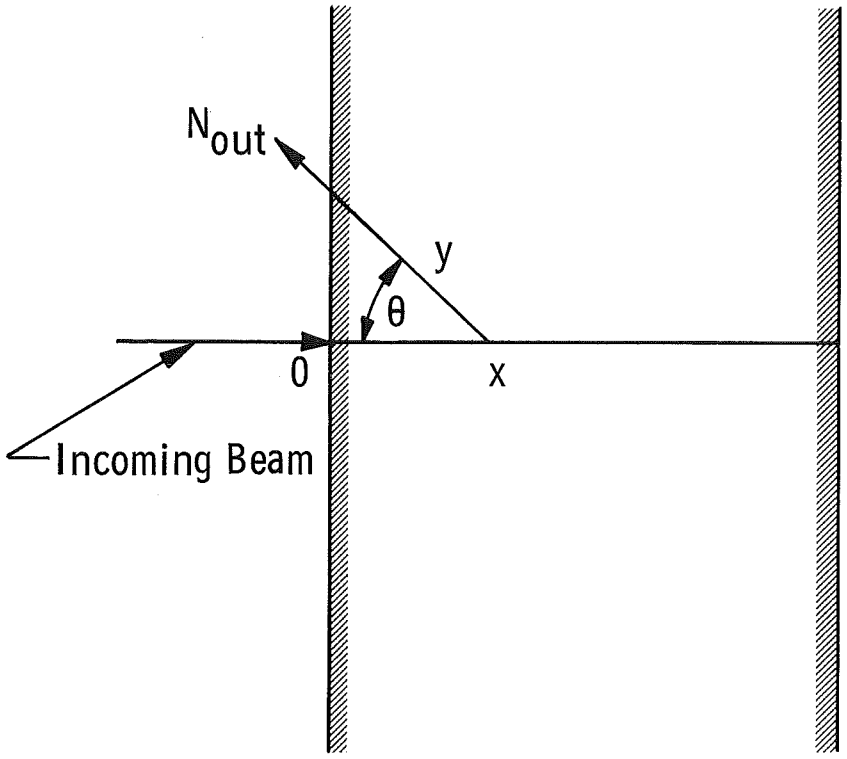

Fig. 17 The Geometry for the Escape of a Primary Displaced Particle from a Plate

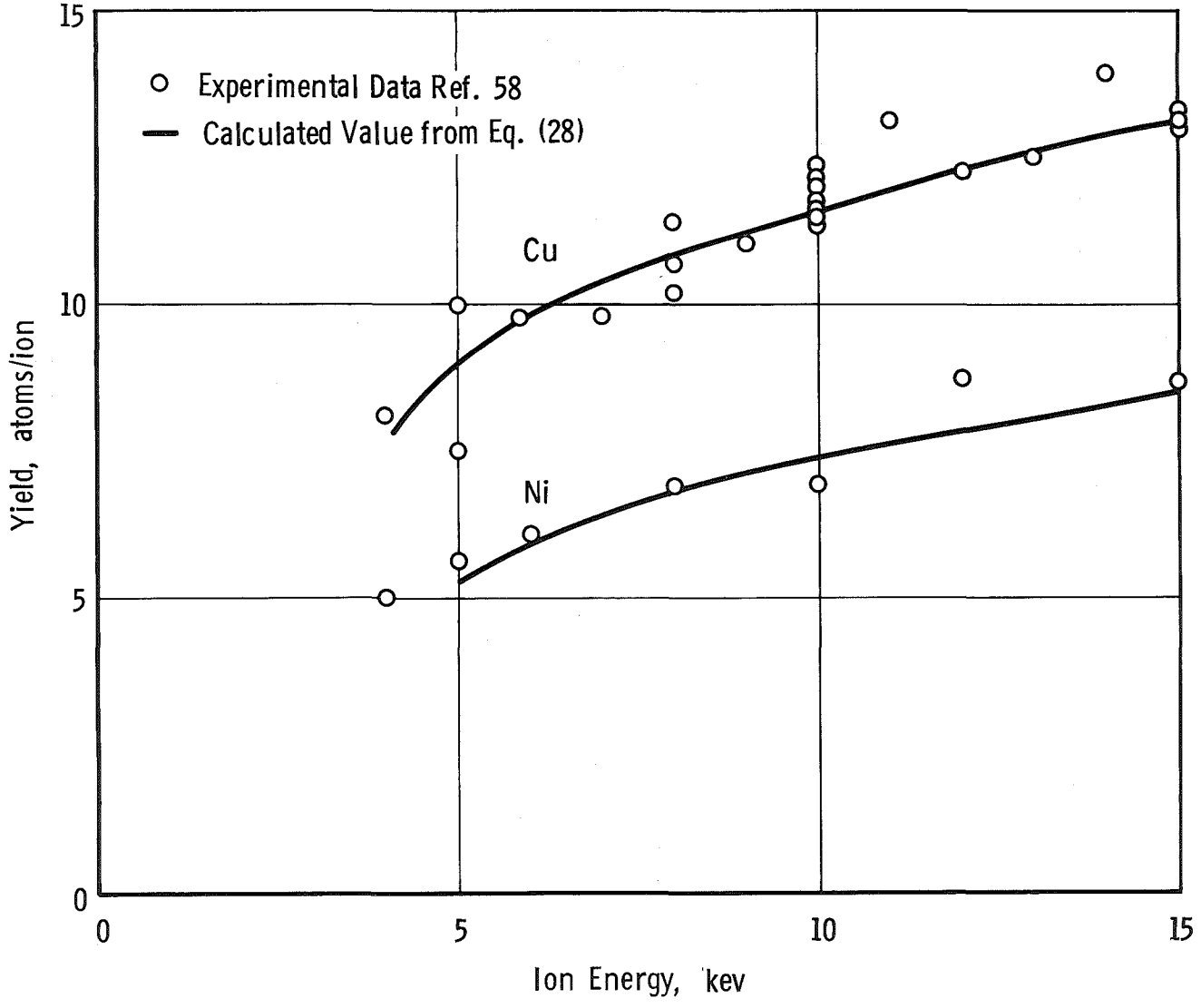

Fig. 18 Sputtering Yield vs Ion Energy (Mercury Bombarding Copper and Nickel)

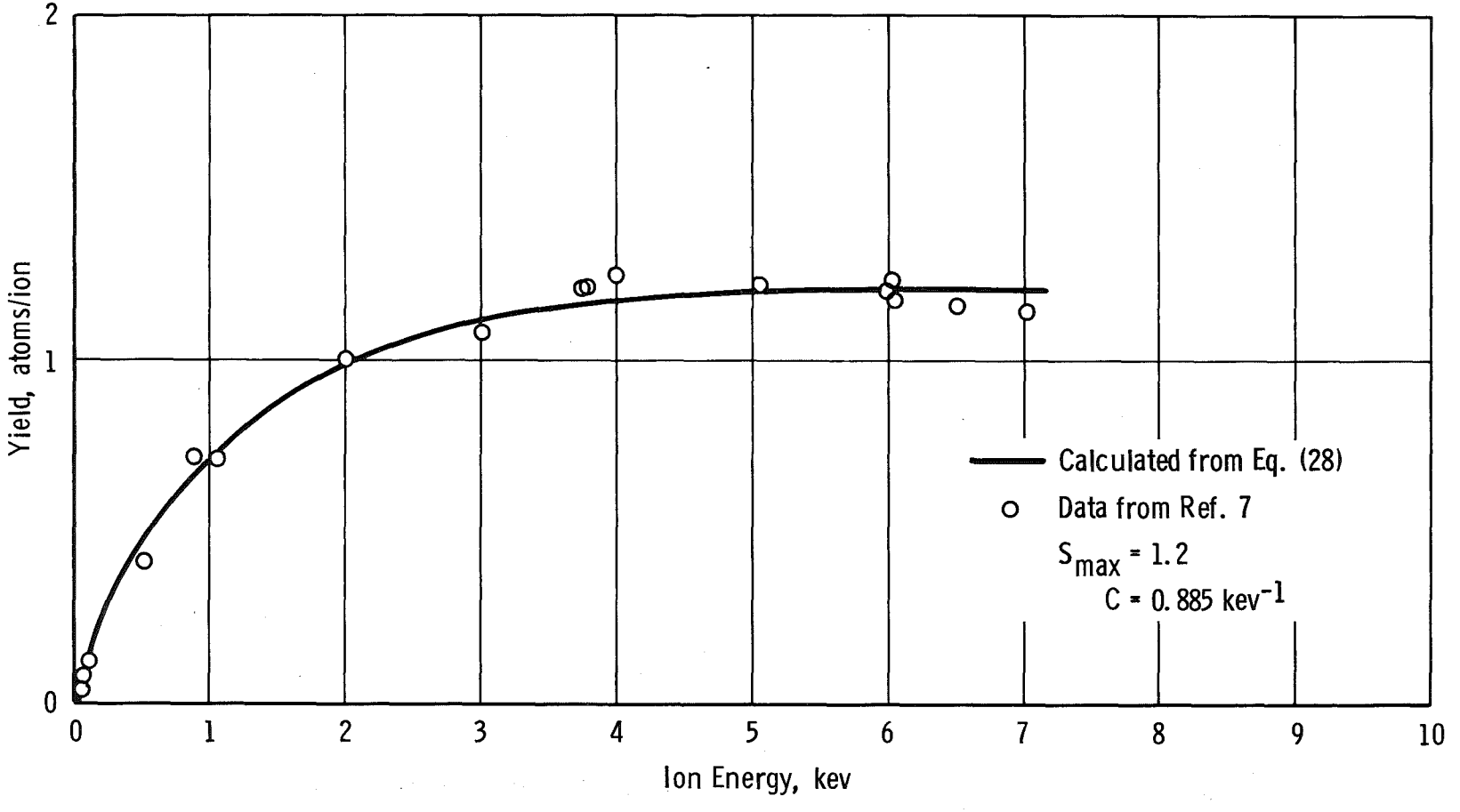

Fig. 19 Sputtering Yield vs Ion Energy (N_2^+ on Ni)

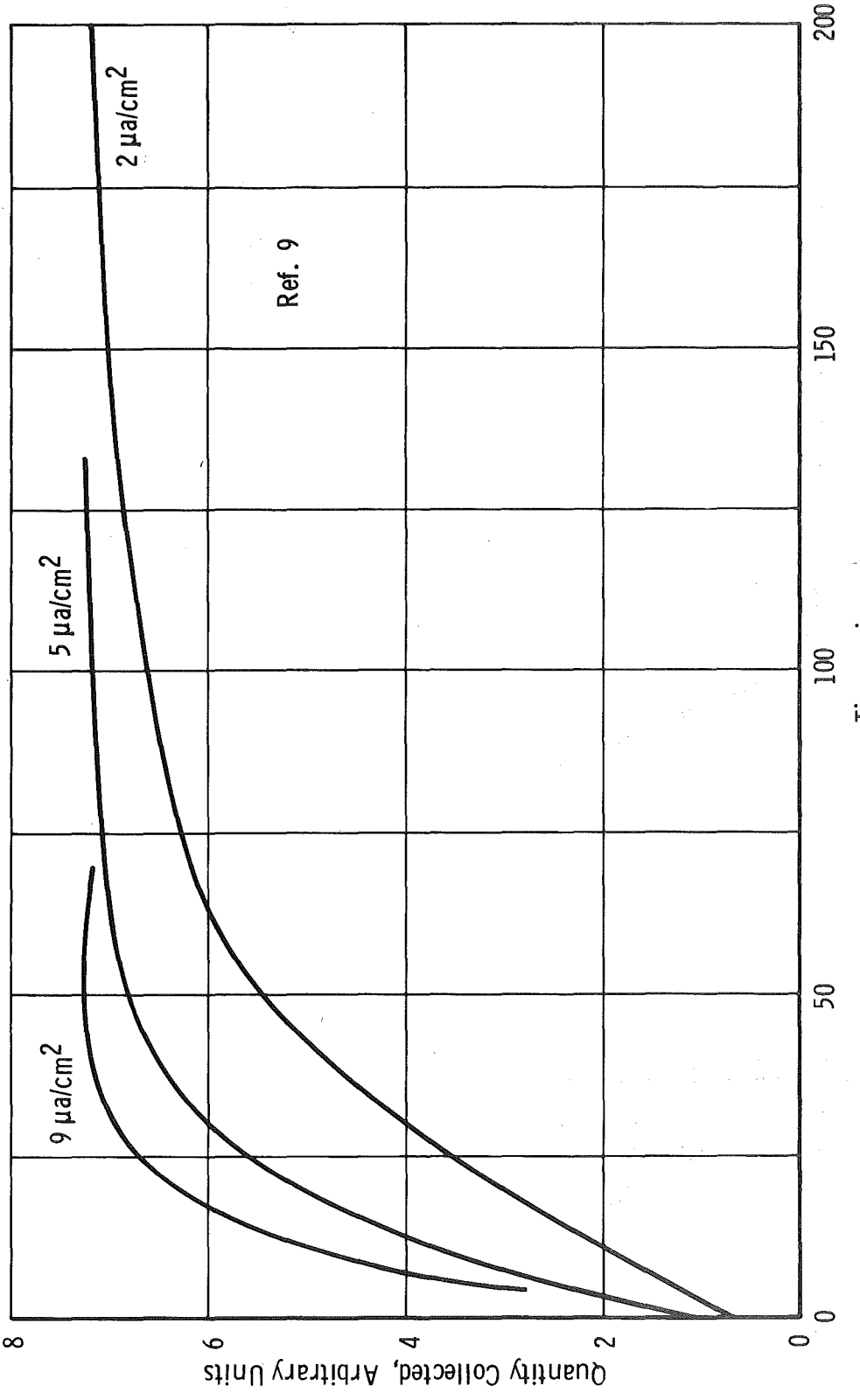

Fig. 20 Collection of Krypton by Aluminum at 45 kev

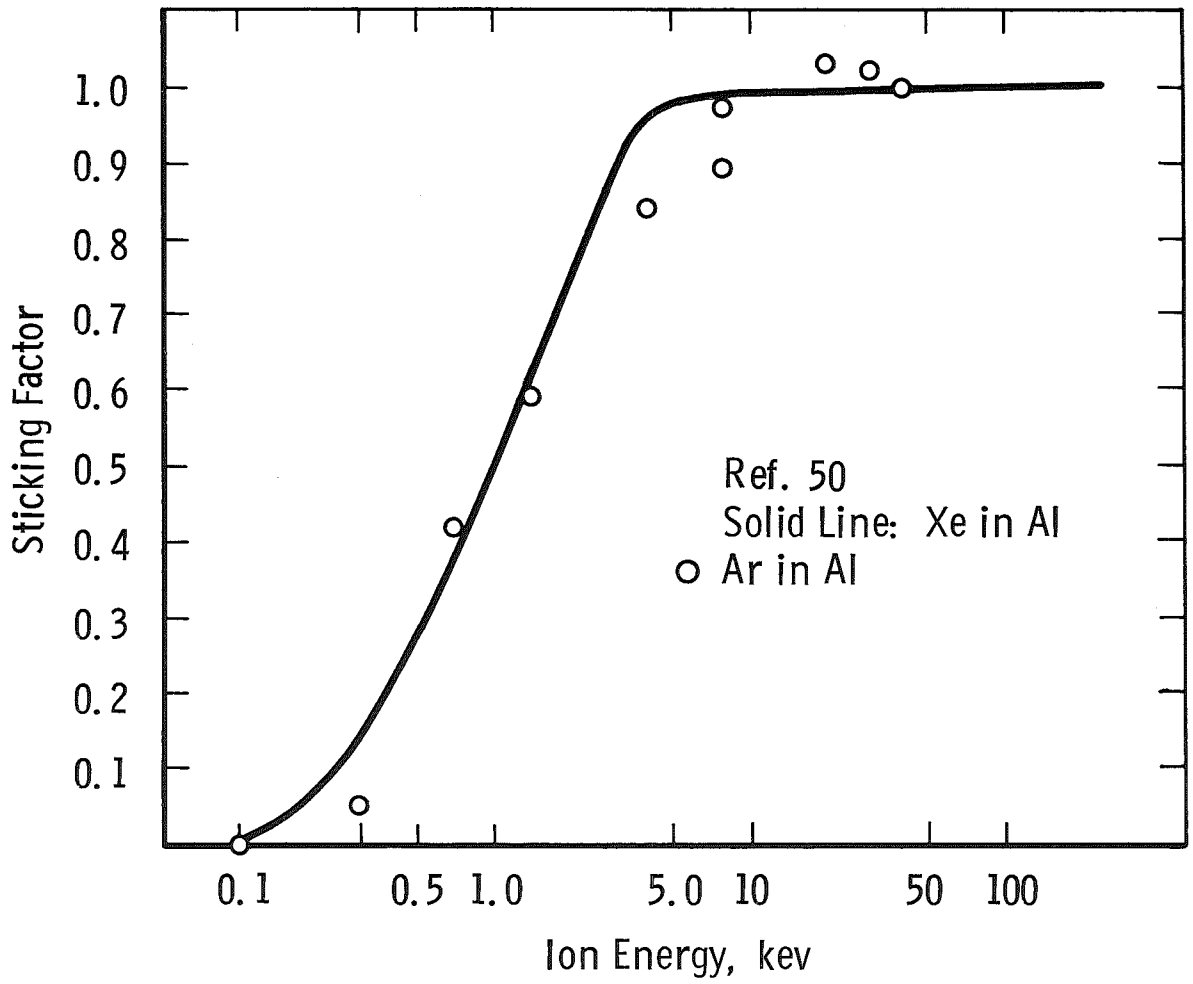

Fig. 21 Sticking Probability vs Ion Energy (Ar^+, Xe^+ on Al)

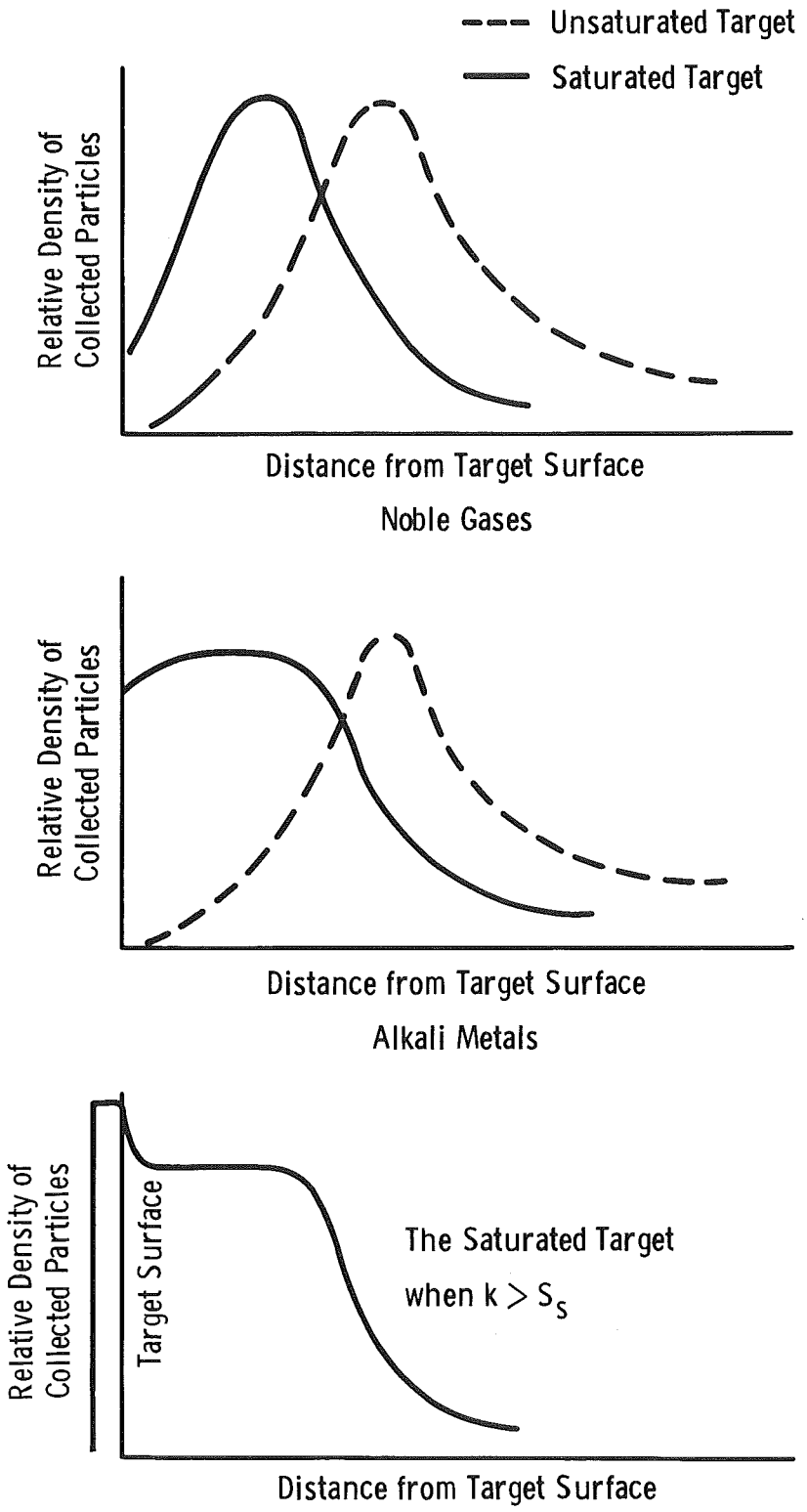

Fig. 22 Distribution of Collected Atoms

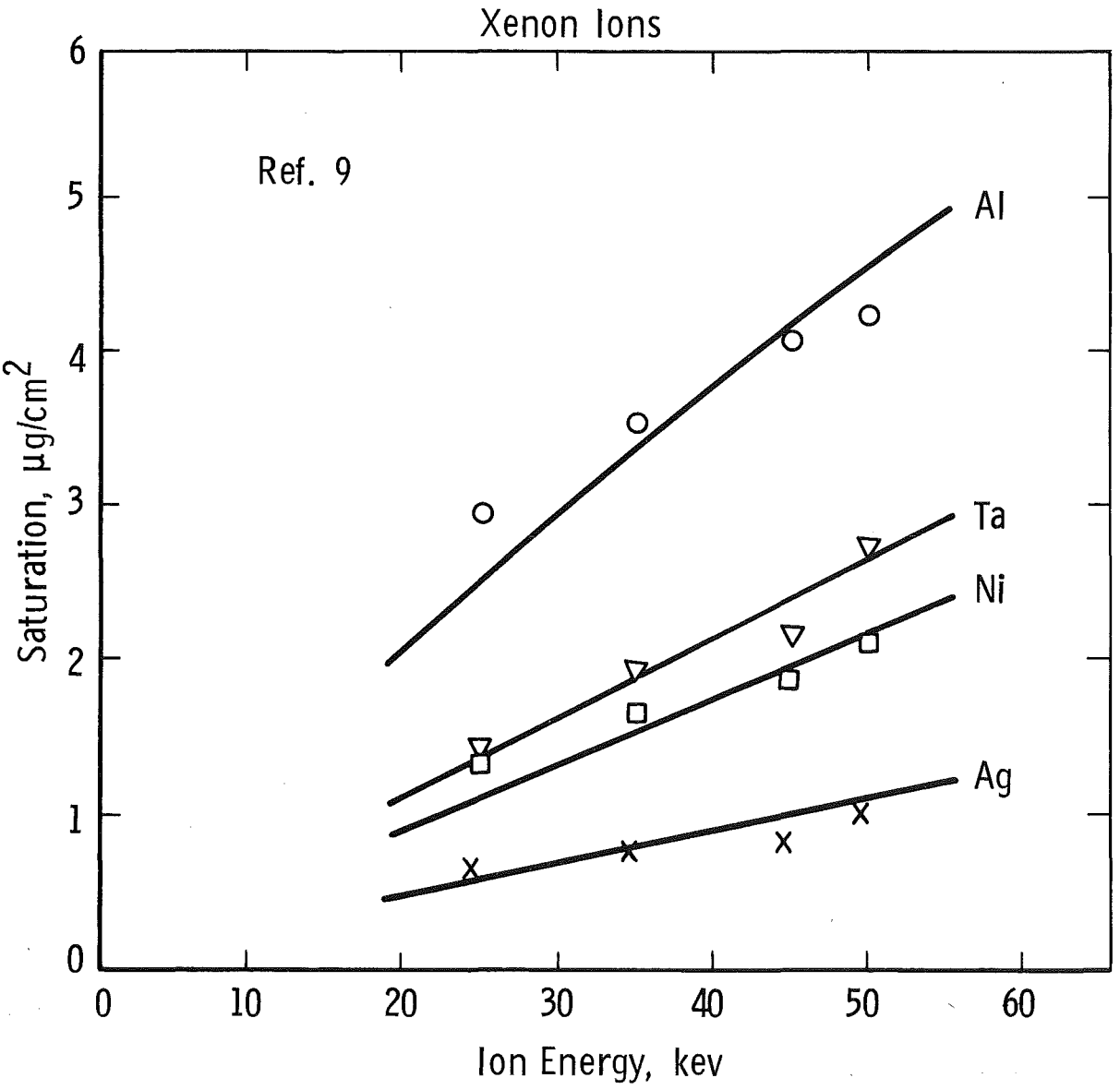

Fig. 23 Saturation Value vs Energy for Various Combinations

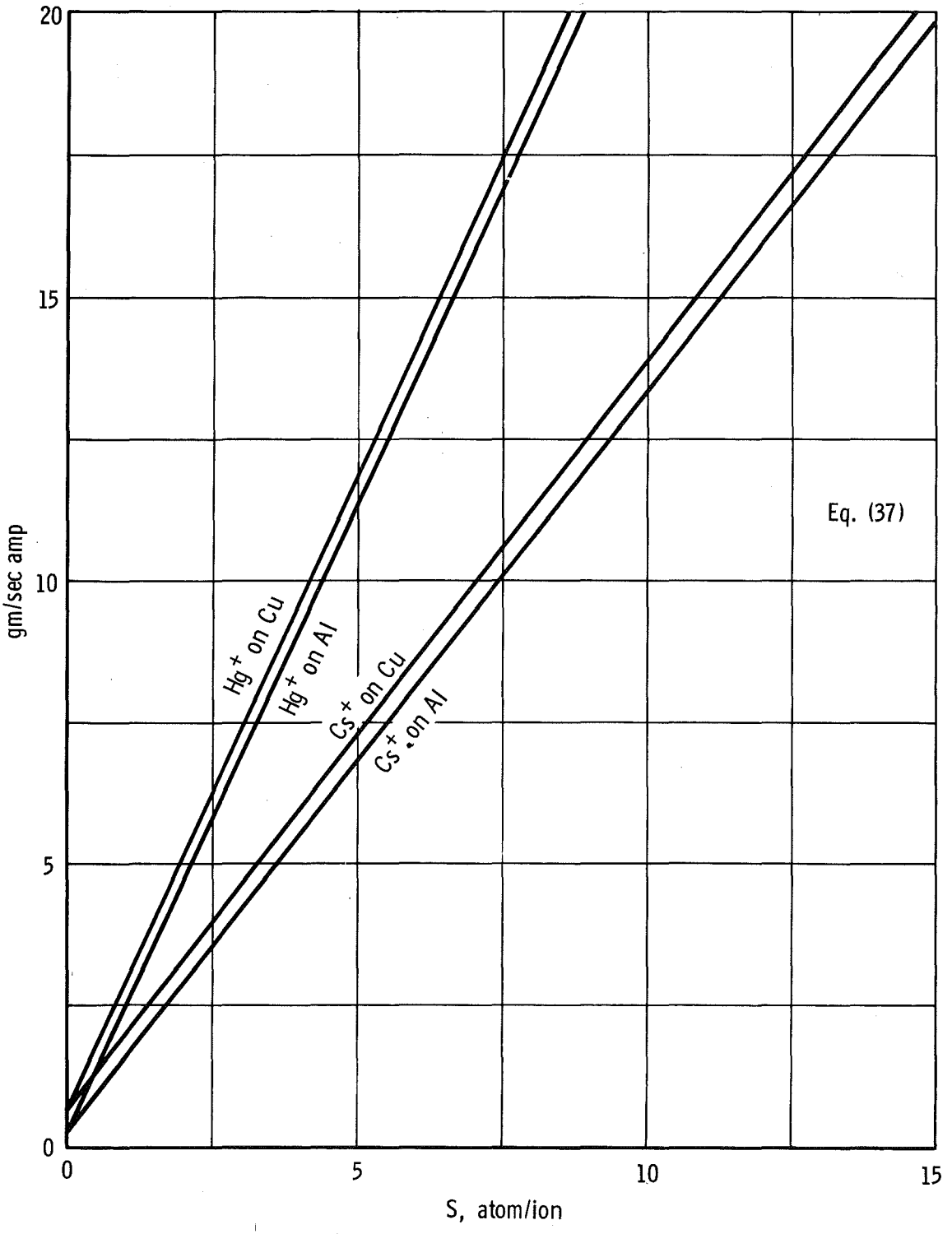

Fig. 24 Source of Material from Saturated Target vs Sputtering Ratio

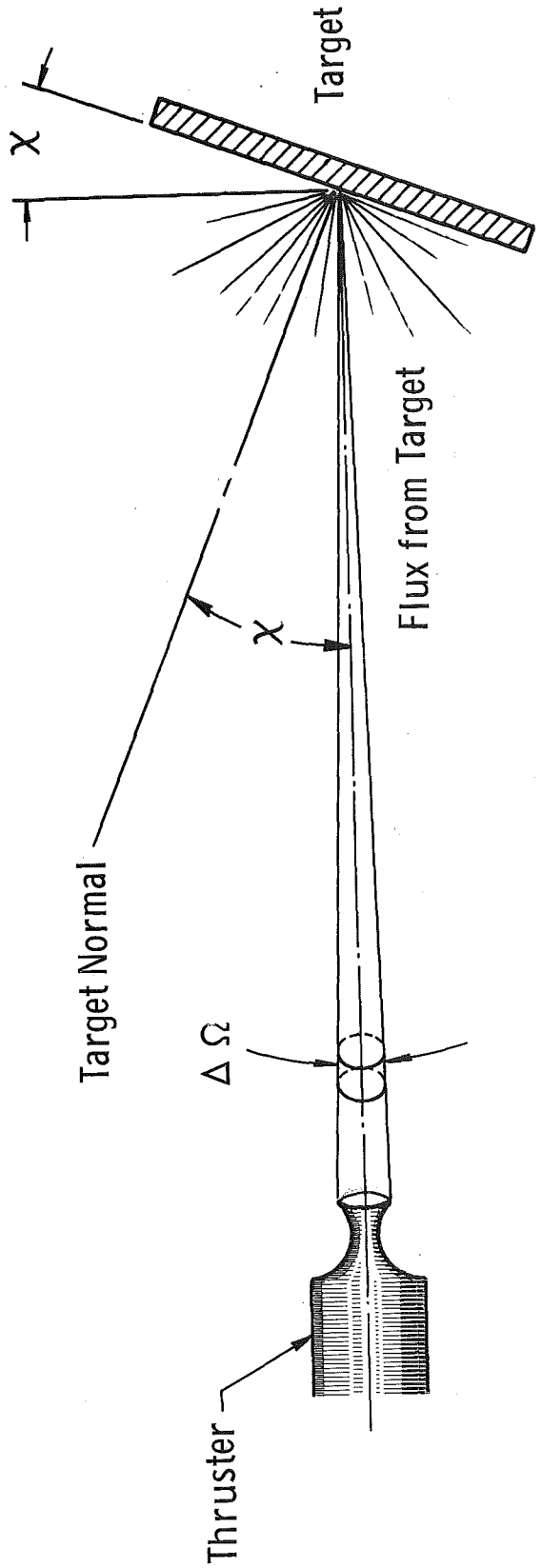

Fig. 25 Geometry for Eq. (40)

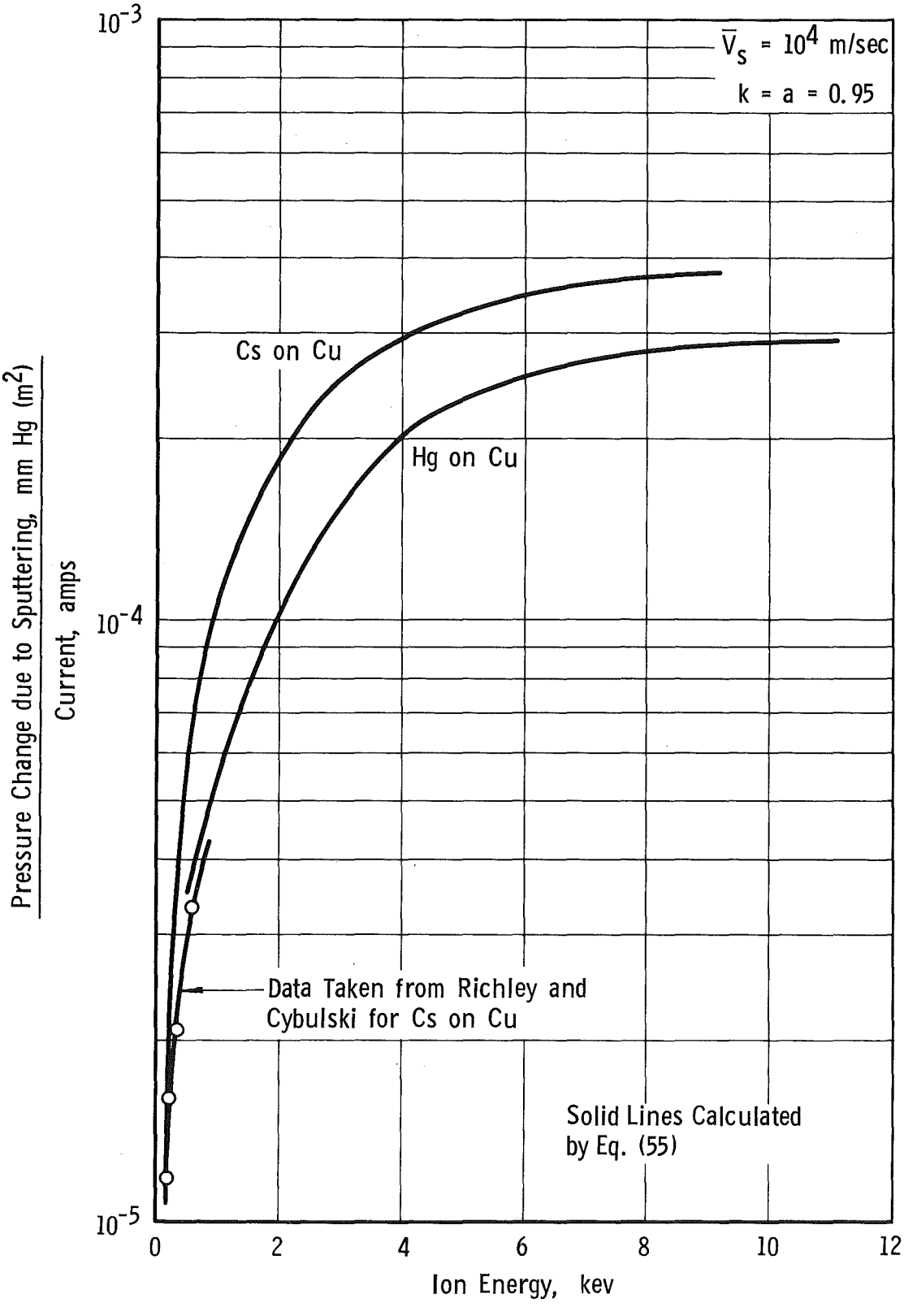

Fig. 26 Sputtered Particle Pressure Contribution vs Energy

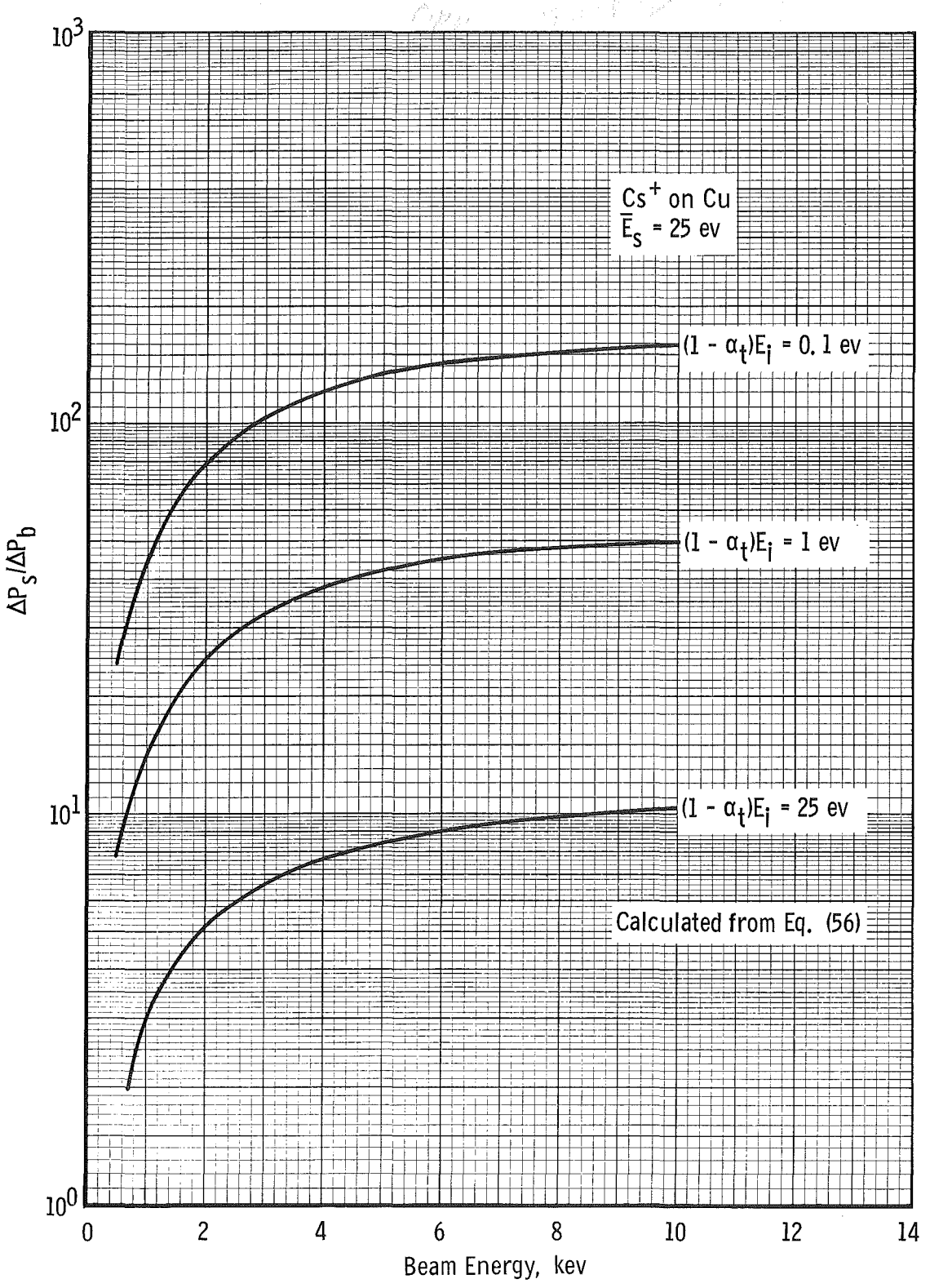

Fig. 27 Ratio of Sputtered Particle Pressure to Beam Pressure vs Ion Energy

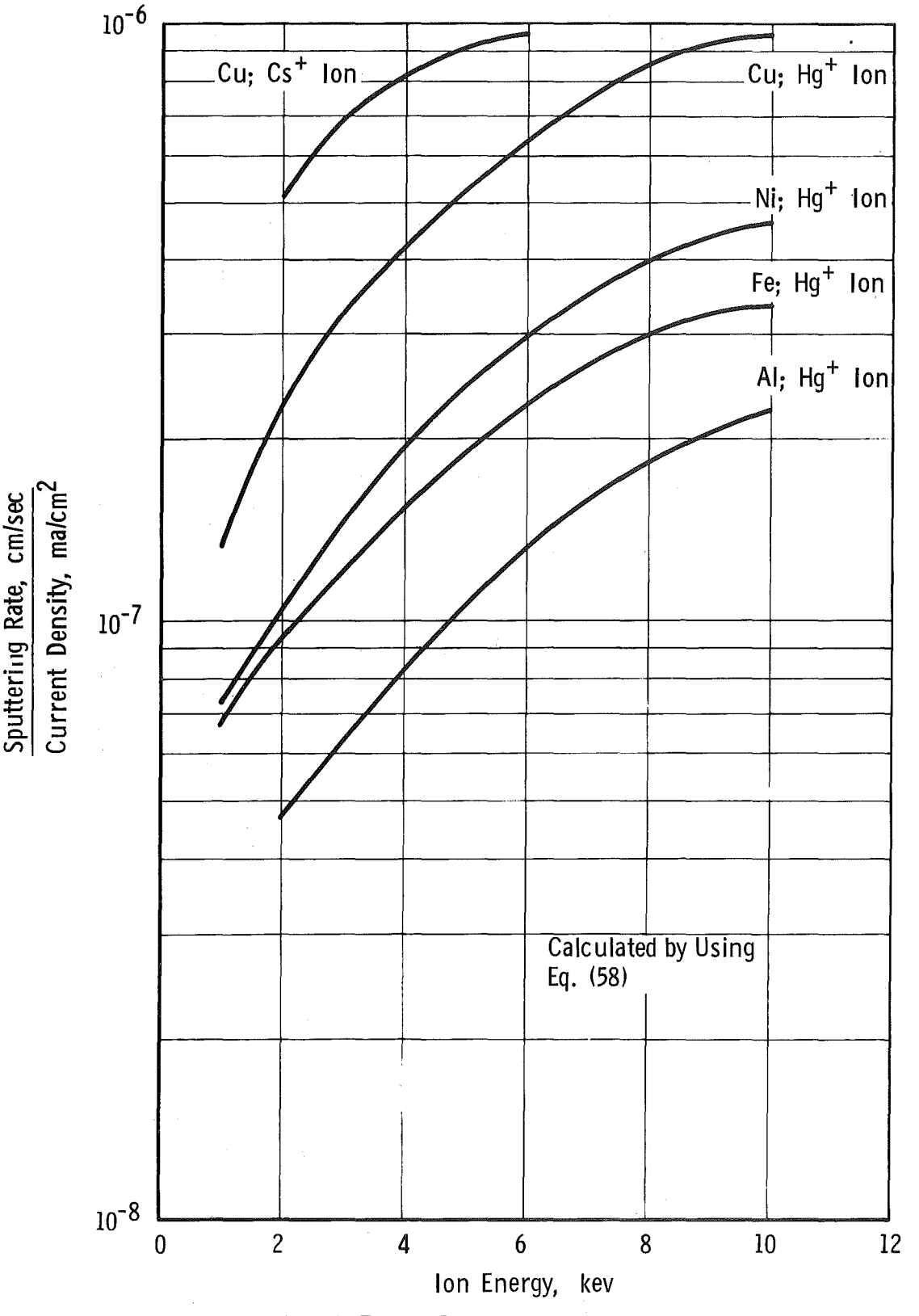

Fig. 28 Erosion Rate vs Ion Energy

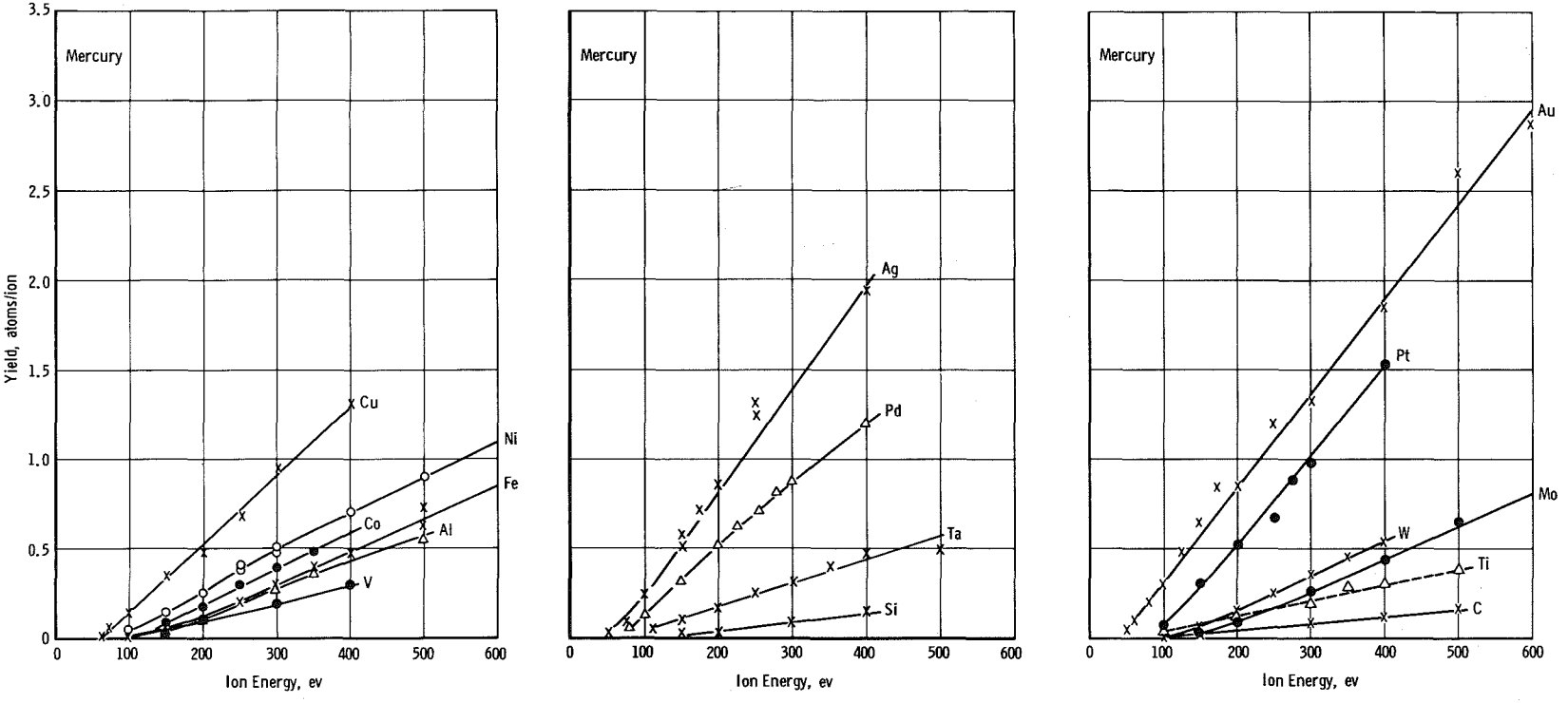

a. Hg^+

Fig. 29 Sputtering Yield vs Energy

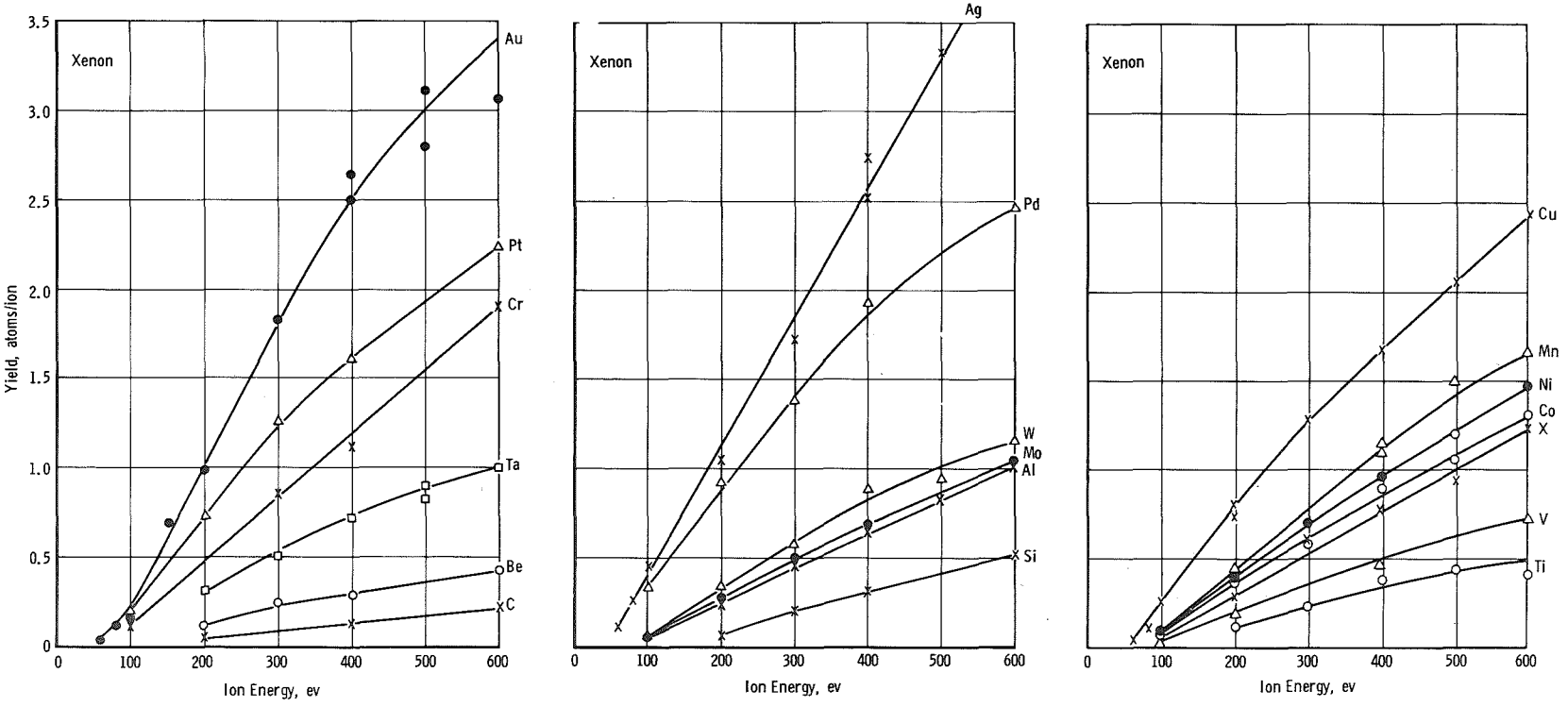

b. Xe^{+}

Fig. 29 Concluded

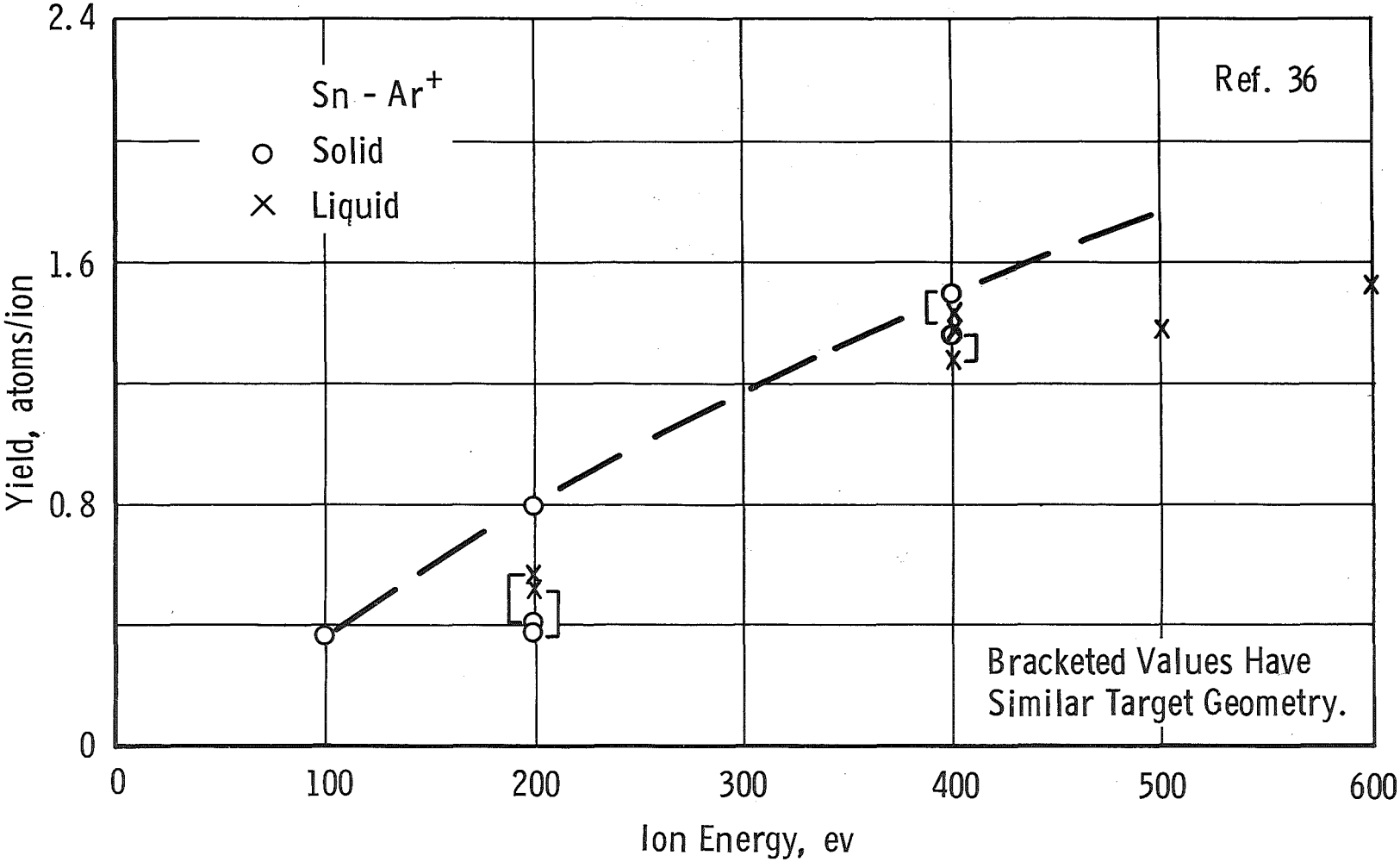

Fig. 30 Sputtering Yields for Liquid and Solid Tin (Ar^+)

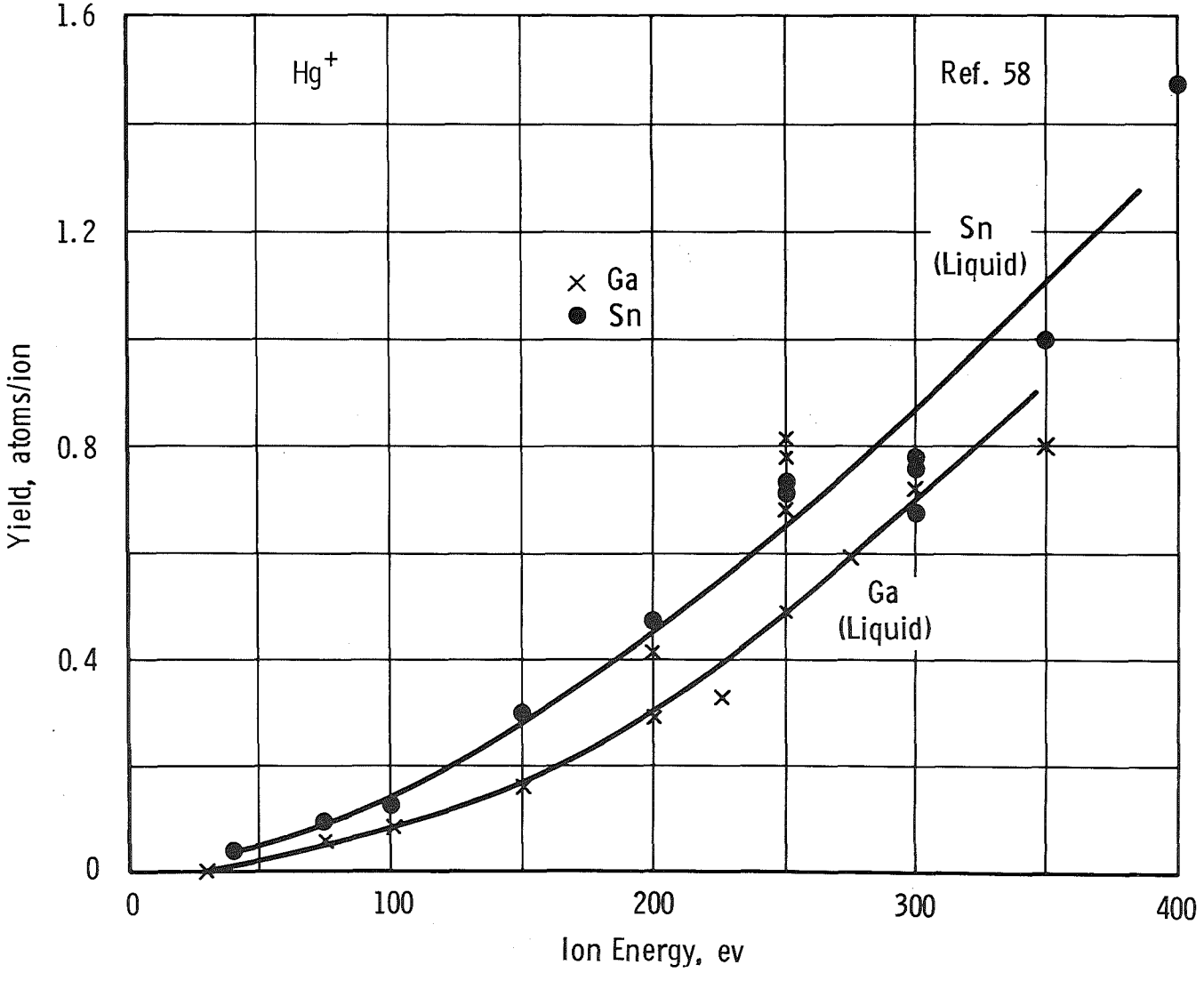

Fig. 31 Sputtering Yields for Liquid Tin and Gallium (Hg^+)

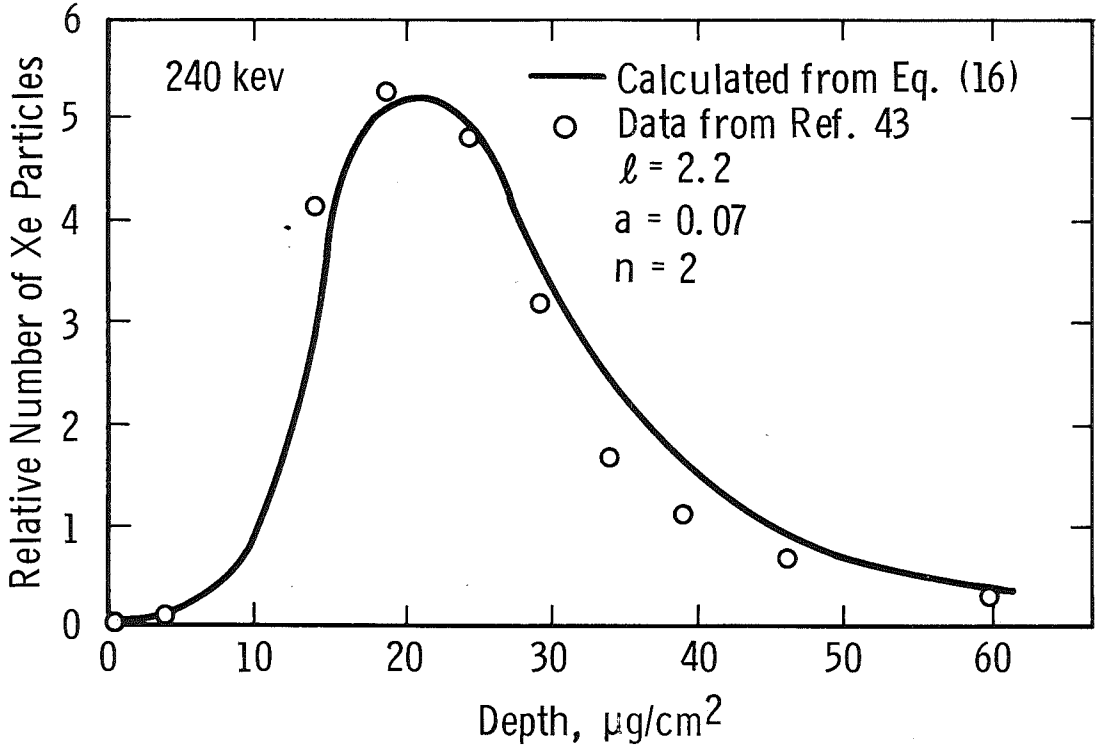

Fig. 32 Range Distribution of Xe^{133} in Al